

Radio over Fiber based Network Architecture

vorgelegt von
Master of Science
Hong Bong Kim
aus Berlin

von der Fakultät IV - Elektrotechnik und Informatik -
der Technischen Universität Berlin
zur Erlangung des akademischen Grades

Doktor der Ingenieurwissenschaften
- Dr.-Ing. -

genehmigte Dissertation

Promotionsausschuss:

Vorsitzender : Prof. Dr.-Ing. Klaus Petermann
Berichter : Prof. Dr.-Ing. Adam Wolisz
Berichter : Prof. Dr.-Ing. Ralf Lehnert

Tag der wissenschaftliche Aussprache: 4. Oktober 2005

Berlin 2005

D 83

To the memory of my father

Abstract

To meet the explosive demands of high-capacity and broadband wireless access, modern cell-based wireless networks have trends, i.e., continuous increase in the number of cells and utilization of higher frequency bands. It leads to a large amount of base stations (BSs) to be deployed; therefore, cost-effective BS development is a key to success in the market. In order to reduce the system cost, radio over fiber (RoF) technology has been proposed since it provides functionally simple BSs that are interconnected to a central control station (CS) via an optical fiber. It has the following main features: (1) it is transparent to bandwidth or modulation techniques, (2) simple and small BSs, (3) centralized operation is possible. Extensive research efforts have been devoted to the development of physical layer such as simple BS development and radio signal transport techniques over fiber, but few have been reported about upper layer and resource management issues for RoF networks. In this dissertation, we are concerned with RoF based network architecture that makes efficient use of its centralized control capability to address mobility management and bandwidth allocation. This work consists of three parts. In the first study, we consider RoF based wireless local area network (WLAN) operating at 60 GHz bands, which can provide high capacity wireless access; however, due to high propagation and penetration loss in the frequency bands a typical room in a building surrounded by walls must be supported by at least one BS. As a result, numerous BSs are required to cover the building. In such an environment slight movement of mobile hosts (MHs) could trigger handover, which is quite different situation compared to conventional WLAN systems; therefore, it is obvious that handover management becomes a significant issue. In the study, we propose a medium access control (MAC) protocol featuring fast and simple handover and quality of service support. It utilizes orthogonal frequency switching codes to avoid co-channel interference between adjacent cells and achieves fast handover at the cost of bandwidth. Six variants of the protocol are considered and evaluated by a simulation study. In the second study, RoF based network architecture for road vehicle communication (RVC) system at mm-wave bands is proposed. In this case handover management becomes even more significant and difficult due to small cell and high user mobility. An MAC protocol based on dynamic time division multiple access (TDMA) is proposed, which supports fast and simple handover as well as bandwidth allocation according to the movement of vehicles. Bandwidth management schemes maintaining high handover quality are also proposed and evaluated by a simulation study. An RoF based broadband wireless access network architecture for sparsely populated rural and remote areas is presented in the third study. In the architecture a CS has optical tunable-transmitter (TT) and tunable-receiver (TR) pairs and utilizes wavelength division multiplexing to access numerous

antenna base stations, each of which is fixed-tuned to a wavelength, for an efficient and flexible bandwidth allocation. Although its capacity is limited by the number of TT/TR pairs, it has simpler CS structure while maintaining trunking efficiency. Characteristics of the architecture, access protocol, and scheduling are discussed; in addition, capacity analysis based on multitraffic loss system is performed to show the properties of the proposed architecture.

Contents

Chapter 1 Introduction	1
1.1 Merging of the Wireless and Fiberoptic Worlds	1
1.2 Motivation and Scope	3
1.3 Organization of the Dissertation	4
Chapter 2 Background Material	7
2.1 Handover in Wireless Mobile Networks	7
2.1.1 Issues related to Handover	8
2.1.1.1 Architectural Issues	8
2.1.1.2 Handover Decision Algorithms	8
2.1.1.3 Handover-related Resource Management	11
2.1.2 Handover Architectures and Algorithms in Mobile Cellular Networks	13
2.1.2.1 Handover in GSM	13
2.1.2.2 Handover in IEEE 802.11 Wireless Local Area Networks	16
2.1.2.3 Comparison of Handover Procedures in IEEE 802.11 and GSM	17
2.2 Millimeter-wave Band Characteristics	17
2.2.1 Why Millimeter Waves?	17
2.2.2 60-GHz Band for Local Wireless Access	18
2.2.3 Millimeter-wave WLAN Systems	18
2.2.4 Handover Issue in Millimeter-band Wireless Networks	19
2.3 Summary	19
Chapter 3 Radio over Fiber Technologies	21
3.1 Introduction	21
3.2 Optical Transmission Link	22
3.2.1 Optical Fiber	22
3.2.1.1 Optical Transmission in Fiber	23
3.2.1.2 Multimode versus Single-Mode Fiber	24
3.2.1.3 Attenuation in Fiber	25
3.2.1.4 Dispersion in Fiber	25

3.2.1.5	Nonlinearities in Fiber	26
3.2.1.6	Couplers	26
3.2.2	Optical Transmitters	27
3.2.2.1	How a Laser Works	27
3.2.2.2	Semiconductor Diode Lasers	28
3.2.2.3	Optical Modulation	29
3.2.3	Optical Receivers	30
3.2.3.1	Photodetectors	30
3.2.4	Optical Amplifiers	30
3.2.4.1	Doped-Fiber Amplifier	31
3.3	Radio over Fiber Optical Links	31
3.3.1	Introduction to RoF Analog Optical Links	31
3.3.2	Basic Radio Signal Generation and Transportation Methods	31
3.3.3	RoF Link Configurations	32
3.3.4	State-of-the-Art Millimeter-wave Generation and Transport Technologies	34
3.3.4.1	Optical Heterodyning	34
3.3.4.2	External Modulation	36
3.3.4.3	Up- and Down-conversion	37
3.3.4.4	Optical Transceiver	37
3.3.4.5	Comparison of mm-wave Generation and Transport Techniques	37
3.3.5	RoF and Wavelength Division Multiplexing (WDM)	39
3.4	Summary	41
 Chapter 4 Chess Board Protocol: MAC protocol for WLAN at 60 GHz Band		43
4.1	Introduction	43
4.2	Network Architecture	44
4.3	Chess Board Protocol Description	45
4.3.1	System Setup	45
4.3.2	Basic Operations	45
4.3.3	Mobility Support	47
4.3.4	Initialization	49
4.4	Parameters of Chess Board Protocol	49
4.4.1	The Number of Channels	49
4.4.2	Slot length	51
4.4.3	Handover Latency	54
4.5	Delay-Throughput Analysis	54
4.5.1	System Model	55
4.5.2	Analysis	56

4.5.3	Numerical Results	59
4.6	Performance Evaluation	59
4.6.1	Simulation Setup	59
4.6.2	Six variants of Chess Board Protocol	63
4.6.3	Delay Performance of Group A MAC Protocols	64
4.6.4	Delay Performance of MAC A3	68
4.6.5	Delay Performance of Group B MAC Protocols	73
4.6.6	Delay Performance of MAC B3	79
4.6.7	Throughput Performance	84
4.7	Conclusion	86
Chapter 5 Radio over Fiber based Road Vehicle Communication System		89
5.1	Introduction	89
5.2	Related Works	90
5.3	System Description	90
5.3.1	Network Architecture	90
5.3.2	Basic Operations	92
5.4	Medium Access Control	93
5.4.1	Frame Structure	93
5.4.2	Initialization	94
5.5	Mobility Support	94
5.5.1	Types of handovers	94
5.5.2	Intra-VCZ Handover	95
5.5.3	Inter-VCZ Handover	95
5.5.4	Inter-CS Handover	95
5.5.5	Operation Example	96
5.6	Resource Allocation Issues	96
5.7	Bandwidth Management Schemes	97
5.7.1	Fixed-VCZ Schemes	98
5.7.2	Variable-VCZ Schemes	100
5.7.3	Inter-CS Handover Management	103
5.8	Performance Evaluation	104
5.8.1	Simulation Assumptions and Parameters	104
5.8.2	Numerical Results	105
5.8.2.1	Blocking Probabilities	105
5.8.2.2	Bandwidth Utilization	107
5.8.2.3	Cell Takeover Rate	111
5.8.2.4	The Effect of Speed	113

5.8.2.5	The Effect of Cell Size	113
5.8.2.6	The Influence of Threshold (Th) Parameter	118
5.8.2.7	Performance Evaluation Summary	119
5.9	Conclusions	119
Chapter 6 Radio over Fiber based Wireless Access Network Architecture for Rural and Remote Areas		121
6.1	Introduction	121
6.2	Network Architecture	122
6.2.1	Architecture Description	122
6.2.2	Basic Operations	123
6.3	Medium Access Protocol	124
6.3.1	Frame Structure	124
6.3.2	Scheduling	125
6.4	Capacity Analysis	126
6.5	Numerical Results	127
6.6	Discussion and Conclusion	129
Chapter 7 Conclusions and Future Works		131
7.1	Research Contributions	132
7.2	Future Research Directions	133
Appendix A Acronyms		135
Appendix B Selected Publications		139
Bibliography		141

List of Tables

2.1	Measured Penetration Losses and Results at 60 GHz Band [60]	19
3.1	Comparison of Millimeter-wave Generation and Transport Techniques	38
3.2	Millimeterwave-band RoF Experiments	39
4.1	Minimum slot length (bytes) when BW_{total} is 3 GHz, t_{prop} is 5 μsec and t_{proc} is 50 μsec	54
4.2	Summary of the Simulation Parameters	62
4.3	Six Variants of Chess Board Protocol	63
5.1	Bandwidth Management Schemes	98

List of Figures

2.1	Handover architectural issues [46].	9
2.2	Hard handover.	9
2.3	Handover decision.	10
2.4	Decision time algorithms in handover [46].	12
2.5	Handover-related resource management issues.	13
2.6	Handover types in GSM.	14
2.7	Intra-MSC handover in GSM.	15
2.8	Handover procedures in an IEEE 802.11 WLAN.	16
3.1	General radio over fiber system.	22
3.2	Optical transmission link.	22
3.3	Multimode (a) and single-mode (b) optical fibers (unit: μm).	24
3.4	Light traveling via total internal reflection within an optical fiber.	24
3.5	The general structure of a laser.	28
3.6	Structure of a semiconductor laser diode.	28
3.7	Intensity-modulation direct-detection (IMDD) analog optical link.	33
3.8	Representative RoF link configurations. (a) EOM, RF modulated signal. (b) EOM, IF modulated signal, (c) EOM, baseband modulated signal. (d) Direct modulation.	35
3.9	Optical heterodyning [20].	36
3.10	Electroabsorption transceiver (EAT).	38
3.11	Schematic illustration of a combination of DWDM and RoF transmission.	40
3.12	Optical spectra of DWDM mm-wave RoF signals of conventional optical (a) DSB and (b) SSB.	40
3.13	RoF ring architecture based on DWDM [38].	41
4.1	Radio over fiber network architecture.	44

4.2	System description. (a) An RoF WLAN system operating in the millimeter-wave band, (b) the total system bandwidth (BW_{total}) is subdivided into $2C$ channels, where BW_{ch} and BW_g are the channel bandwidth and the guard bandwidth, respectively, (c) and (d) show frequency switching patterns for downlink and uplink transmissions when the number of channels (C) is five. Note that the per user bandwidth (BW_{user}) is BW_{ch}/C .	46
4.3	Slot formats for the downlink and uplink data transmission.	48
4.4	Handover latency is defined as an interval between two time instants at which uplink packet transmissions are completed in the old and new picocells.	49
4.5	Handover example. MH using (f_1, f_{C+1}) moves from picocell 1 to picocell 2. (a) FS patterns used in each cell and (b) handover latency.	50
4.6	Bandwidth allocation.	52
4.7	The maximum number of channels (C_{max}) vs. per user data rate (BT_{user}). It is assumed that $BW_g = 0, BW_{down} = BW_{up} = BT_{user}$ and coding efficiency is 1 bit/Hz.	52
4.8	The minimum slot length vs. per user data rate with different BW_{total} values when the distance between the CS and BS is 1000 m and $t_{proc} = 50 \mu sec$.	53
4.9	The minimum handover latency vs. per user data rate with different BW_{total} values when the distance between the CS and BS is 1000 m and $t_{proc} = 50 \mu sec$.	55
4.10	System model for analysis. Successful requests from nodes are enqueued in the CS and served in FIFO mode, and assignment of uplink slot is informed through downlink slot. Uplink slot consists of one data slot and K minislots for requests.	56
4.11	Markov chain model with finite population for one channel which is shared by $M/C = M_c$ nodes.	57
4.12	Mean packet delay vs. packet arrival probability with different number of minislots (K) when C is five and σ is 0.3.	60
4.13	Mean packet delay vs. throughput with different number of minislots (K) when C is five and σ is 0.3.	60
4.14	Mean packet delay vs. packet arrival probability with different σ when C is five and K is three.	61
4.15	Indoor environment for simulation consists of four picocells and 40 MHs.	61
4.16	Mean packet delay of group A MACs when C is five and slot size is 1000 byte.	65
4.17	Mean packet delay of group A MACs when C is ten and slot size is 1000 byte.	65
4.18	Mean packet delay of group A MACs when C is 15 and slot size is 1000 byte.	66
4.19	Histogram of the packet delay of MAC A1 when C is five, slot size is 1000 byte, and traffic load per MH is 4 Mbps.	66
4.20	Histogram of the packet delay of MAC A2 when C is five, slot size is 1000 byte, and traffic load per MH is 4 Mbps.	67
4.21	Histogram of the packet delay of MAC A3 when C is five, slot size is 1000 byte, and traffic load per MH is 4 Mbps.	67

4.22	Mean packet delay of MAC A3 when slot size is 1000 byte.	69
4.23	Mean packet delay of MAC A3 when slot size is 500 byte.	70
4.24	Mean packet delay of MAC A3 when slot size is 1500 byte.	70
4.25	Mean packet delay of MAC A3 when slot size is 2000 byte.	71
4.26	Mean packet delay of MAC A3 with different number of channels and slot sizes when traffic load per MH is three Mbps.	71
4.27	Mean packet delay of MAC A3 with different number of channels when there are 20 MHs in the cluster.	72
4.28	Mean packet delay of MAC A3 with different number of channels when there are 30 MHs in the cluster.	72
4.29	Mean packet delay of MAC A3 when C is five.	73
4.30	Mean packet delay of MAC A3 when C is ten.	74
4.31	Mean packet delay of MAC A3 when C is 15.	74
4.32	Buffer length of MAC A3.	75
4.33	Mean packet delay of MAC A3.	75
4.34	Mean packet delay of group B MACs when C is five.	76
4.35	Mean packet delay of group B MACs when C is ten.	77
4.36	Mean packet delay of group B MACs when C is 15.	77
4.37	Histogram of the packet delay of MAC B1 when C is five, slot size is 1000 byte, and traffic load per MH is 7 Mbps	78
4.38	Histogram of the packet delay of MAC B2 when C is five, slot size is 1000 byte, and traffic load per MH is 7 Mbps	78
4.39	Histogram of the packet delay of MAC B3 when C is five, slot size is 1000 byte, and traffic load per MH is 7 Mbps	79
4.40	Mean packet delay of B3 when the slot size is 1000 bytes.	80
4.41	Mean packet delay of B3 when the slot size is 500 bytes.	80
4.42	Mean packet delay of B3 when the slot size is 1500 bytes.	81
4.43	Mean packet delay of B3 when the slot size is 2000 bytes.	81
4.44	Mean packet delay of B3 with different number of channels and slot sizes when traffic load per MH is five Mbps.	82
4.45	Mean packet delay of MAC B3 with different slot sizes when C is 5.	83
4.46	Mean packet delay of MAC B3 with different slot sizes when C is 10.	83
4.47	Mean packet delay of MAC B3 with different slot sizes when C is 15.	84
4.48	Buffer length of MAC B3.	85
4.49	Mean packet delay of MAC B3.	85
4.50	Throughput of MAC A3 with different number of channels when slot size is 1000 bytes.	86
4.51	Throughput of MAC B3 with different number of channels when slot size is 1000 bytes.	87
4.52	Throughput of MAC A3 with different number of channels and slot sizes.	87

4.53	Throughput of MAC B3 with different number of channels and slot sizes.	88
5.1	Road vehicle communication system based on radio over fiber technology.	91
5.2	An access network architecture for road vehicle communication system based on radio over fiber technology.	92
5.3	Frame allocation example.	93
5.4	Frame structure. For simplicity, guard time is not represented.	94
5.5	An example of the proposed architecture where cell 1,2,3 and 4,5 constitute two VCZs, respectively.	96
5.6	Frame allocation example for Fig. 5.5.	97
5.7	Pseudo code of bandwidth reservation scheme for inter-VCZ handover. R_q and B_H are initialized to zero from the beginning of the scheme. $\lceil x \rceil$ indicates the smallest integer greater than or equal to x	100
5.8	Pseudo code for part of step C2 to obtain the left set S_{left} and left empty bandwidth $B_{empty,left}$ for variable-VCZ scheme. $B_{take,left}$ and i are initialized to 0 and 1, respec- tively, and $B_{U,left}$ is the bandwidth being used in the left VCZ.	102
5.9	Pseudo code for part of step C2 to obtain the right set S_{right} and right empty bandwidth $B_{empty,right}$ for variable-VCZ scheme. $B_{take,right}$ and i are initialized to 0 and K , respectively, and $B_{U,right}$ is the bandwidth being used in the right VCZ.	102
5.10	Pseudo code for step C3 to give a set of cells over to an adjacent VCZ. $B_{empty,direction}$ are initialized to -1, respectively. Th is introduced to mitigate frequent takeover of cells between VCZs.	103
5.11	Simulation model comprises 50 cells and five VCZs that cover 5 km road. Each VCZ is initialized to cover ten contiguous cells and the cell size is 100 m. In fixed-VCZ schemes the configuration remains the same, while in the variable-VCZ schemes the number of cells covered by each VCZ can change with time.	105
5.12	P_{CB} and P_{HD} vs. offered load for FA1 when $R_v = 0.5$	105
5.13	P_{CB} and P_{HD} vs. offered load for FA2 when $R_v = 0.5$	106
5.14	P_{CB} and P_{HD} vs. offered load for FA2 when P_t is 0.01.	106
5.15	P_{CB} and P_{HD} vs. offered load for VA1 with $R_v = 0.5$	108
5.16	P_{CB} and P_{HD} vs. offered load for VA2 for different P_t values with $R_v = 0.5$ and $Th = 20$	108
5.17	P_{CB} and P_{HD} vs. offered load for VA2 for different R_v values when P_t is 0.01 and Th is 20.	109
5.18	B_U and B_H vs. offered load for FA1 when R_v is 0.5.	109
5.19	B_U and B_H vs. offered load for FA2 when R_v is 0.5.	110
5.20	B_U and B_H vs. offered load for FA2 when P_t is 0.01.	110
5.21	B_U and B_H vs. offered load for VA1 when R_v is 0.5.	111

5.22	B_U and B_H vs. offered load for VA2 when R_v is 0.5 and Th is 20.	112
5.23	B_U and B_H vs. offered load for VA2 when P_t is 0.01 and Th is 20.	112
5.24	Mean cell takeover rate (cells/sec/VCZ) and mean traffic takeover rate (BU s/sec/VCZ) for VA1 when R_v is 0.5.	113
5.25	Mean cell takeover rate (cells/sec/VCZ) and mean traffic takeover rate (BU s/sec/VCZ) for VA2 when R_v is 0.5 and Th is 20.	114
5.26	Mean cell takeover rate (cells/sec/VCZ) and mean traffic takeover rate (BU s/sec/VCZ) for VA2 when P_t is 0.01 and Th is 20.	114
5.27	P_{CB} and P_{HD} vs. offered load for VA2 when P_t is 0.01, Th is 20 and MH's speed is uniformly distributed between 40 and 60 km/h	115
5.28	B_U and B_H vs. offered load for VA2 when P_t is 0.01, Th is 20 and MH's speed is uniformly distributed between 40 and 60 km/h	115
5.29	Mean cell takeover rate (cells/sec/VCZ) and mean traffic takeover rate (BU s/sec/VCZ) for VA2 when P_t is 0.01, Th is 20 and MH's speed is uniformly distributed between 40 and 60 km/h	116
5.30	P_{CB} and P_{HD} vs. offered load for VA2 when P_t is 0.01, Th is 20 and cell size is 50 m	116
5.31	B_U and B_H vs. offered load for VA2 when P_t is 0.01, Th is 20 and cell size is 50 m	117
5.32	Mean cell takeover rate (cells/sec/VCZ) and mean traffic takeover rate (BU s/sec/VCZ) for VA2 when P_t is 0.01, Th is 20 and cell size is 50 m	117
5.33	P_{CB} and P_{HD} vs. offered load for VA2 when P_t is 0.01 and R_v is 0.5.	118
5.34	B_U and B_H vs. offered load for VA2 when P_t is 0.01 and R_v is 0.5.	118
5.35	Mean cell takeover rate (cells/sec/VCZ) and mean traffic takeover rate (BU s/sec/VCZ) for VA2 when P_t is 0.01 and R_v is 0.5.	119
6.1	A proposed radio over fiber access network architecture consisting of K transceivers (TRXs) and N base stations (BSs).	122
6.2	Frame structure. For simplicity, guard time is not shown.	124
6.3	Packing of five frames into two super-frames where frame three is fragmented in such a way that no wavelength collision occurs.	126
6.4	Blocking probabilities when $N = 10$ and $C = 20$	128
6.5	Blocking probabilities when $K = 3$, $N = 10$ and $C = 20$	129

Chapter 1

Introduction

1.1 Merging of the Wireless and Fiberoptic Worlds

For the future provision of broadband, interactive and multimedia services over wireless media, current trends in cellular networks - both mobile and fixed - are 1) to reduce cell size to accommodate more users and 2) to operate in the microwave/millimeter wave (mm-wave) frequency bands to avoid spectral congestion in lower frequency bands. It demands a large number of base stations (BSs) to cover a service area, and cost-effective BS is a key to success in the market. This requirement has led to the development of system architecture where functions such as signal routing/processing, handover and frequency allocation are carried out at a central control station (CS), rather than at the BS. Furthermore, such a centralized configuration allows sensitive equipment to be located in safer environment and enables the cost of expensive components to be shared among several BSs. An attractive alternative for linking a CS with BSs in such a radio network is via an optical fiber network, since fiber has low loss, is immune to EMI and has broad bandwidth. The transmission of radio signals over fiber, with simple optical-to-electrical conversion, followed by radiation at remote antennas, which are connected to a central CS, has been proposed as a method of minimizing costs. The reduction in cost can be brought about in two ways. Firstly, the remote antenna BS or radio distribution point needs to perform only simple functions, and it is small in size and low in cost. Secondly, the resources provided by the CS can be shared among many antenna BSs. This technique of modulating the radio frequency (RF) subcarrier onto an optical carrier for distribution over a fiber network is known as “*radio over fiber*”¹ (RoF) technology.

To be specific, the RoF network typically comprises a central CS, where all switching, routing, medium access control (MAC) and frequency management functions are performed, and an optical fiber network, which interconnects a large number of functionally simple and compact antenna BSs for wireless signal distribution. The BS has no processing function and its main function is to convert optical signal to wireless one and vice versa. Since RoF technology was first demonstrated for cordless or mobile telephone service in 1990 [5], a lot of research efforts have been made to investigate its

¹It is also called “radio on the fiber”, “radio on fiber”, “hybrid fiber radio”, and “fiber radio access” in the literature.

limitation and develop new, high performance RoF technologies. Their target applications range from mobile cellular networks [6],[7],[8], wireless local area network (WLAN) at mm-wave bands [9], broadband wireless access networks [30],[33],[34],[39] to road vehicle communication (RVC) networks for intelligent transportation system (ITS) [72],[73],[74]. Due to the simple BS structure, system cost for deploying infrastructure can be dramatically reduced compared to other wireline alternatives. In addition to the advantage of potential low cost, RoF technology has the further a benefit of transferring the RF signal to and from a CS that can allow flexible network resource management and rapid response to variations in traffic demand due to its centralized network architecture. In summary, some of its important characteristics are described below [13]:

- The system control functions, such as frequency allocation, modulation and demodulation scheme, are located within the CS, simplifying the design of the BS. The primary functions of the BSs are optical/RF conversion, RF amplification, and RF/optical conversion.
- This centralized network architecture allows a dynamic radio resource configuration and capacity allocation. Moreover, centralized upgrading is also possible.
- Due to simple BS structure, its reliability is higher and system maintenance becomes simple.
- In principle, optical fiber in RoF is transparent to radio interface format (modulation, radio frequency, bit rate and so on) and protocol. Thus, multiple services on a single fiber can be supported at the same time.
- Large distances between the CS and the BS are possible.

On the other hand, to meet the explosive demands of high-capacity and broadband wireless access, millimeter-wave (mm-wave) radio links (26–100 GHz) are being considered to overcome bandwidth congestion in microwave bands such as 2.4 or 5 GHz for application in broadband micro/picocellular systems, fixed wireless access, WLANs, and ITSs [1],[2],[3],[4]. The larger RF propagation losses at these bands reduce the cell size covered by a single BS and allow an increased frequency reuse factor to improve the spectrum utilization efficiency. Recently, considerable attention has been paid in order to merge RoF technologies with mm-wave band signal distribution [14],[20],[29],[30],[33],[34],[39],[72]. The system has a great potential to support cost-effective and high capacity wireless access. The distribution of radio signals to and from BSs can be either mm-wave modulated optical signals (RF-over-fiber) [33],[39], or lower frequency subcarriers (IF-over-fiber) [29],[30]. Signal distribution as RF-over-fiber has the advantage of a simplified BS design but is susceptible to fiber chromatic dispersion that severely limits the transmission distance [15]. In contrast, the effect of fiber chromatic dispersion on the distribution of intermediate-frequency (IF) signals is much less pronounced, although antenna BSs implemented for RoF system incorporating IF-over-fiber transport require additional electronic hardware such as a mm-wave frequency local oscillator (LO) for frequency up- and downconversion. These research activities fueled by rapid developments in both photonic and mm-wave technologies suggest simple BSs based

on RoF technologies will be available in the near future. However, while great efforts have been made in the physical layer, little attention has been paid to upper layer architecture. Specifically, centralized architecture of RoF networks implies the possibility that resource management issues in conventional wireless networks could be efficiently addressed. As a result, it is required to reconsider conventional resource management schemes in the context of RoF networks.

1.2 Motivation and Scope

In this dissertation, we are concerned with RoF based network architecture aimed at efficient mobility and bandwidth management using centralized control capability of the network. In particular, the focus is mainly placed on RoF networks operating at mm-wave bands. In indoor environments, the electromagnetic field at mm-wave tends to be confined by walls due to their electromagnetic properties at these frequencies. In outdoor environments, especially at frequencies around 60 GHz, an additional attenuation is necessary as oxygen absorption limits the transmission range [2],[4]. Both the cases result in very small cell as compared to microwave bands such as 2.4 or 5 GHz, requiring numerous BSs to be deployed to cover a broad service area. Thus, in such networks with a large number of small cells, we realize two important issues: (1) the system should be cost-effective and (2) mobility management is very significant.

One promising alternative to the first issue is an RoF based network since in this network functionally simple and cost-effective BSs are utilized in contrast to conventional wireless systems. However, the second issue is still challenging and difficult to realize as the conventional handover procedures cannot easily be applied to the system. In this dissertation, we consider first RoF network architecture operating at mm-wave bands with special emphasis on mobility management. Specifically, our concern is how to support fast and simple handover in such networks using RoF network's centralized control capability. In addition, an RoF based broadband wireless access network architecture is proposed, where wavelength division multiplexing (WDM) is utilized for bandwidth allocation.

The dissertation consists of three parts. In the first study, we propose an MAC protocol for an RoF based WLAN at 60 GHz band. Due to high propagation loss and penetration loss of the band a typical room enclosed by walls must be supported by at least one BS, leading to a situation that slight movement of users can trigger handover. The MAC protocol, called "*Chess Board protocol*", is based on frequency switching (FS) codes. Adjacent cells employ orthogonal FS codes to avoid possible co-channel interference. This mechanism allows a mobile host (MH) to stay tuned to its frequency during handover, which is a major characteristic feature of the proposed MAC protocol. Important parameters of the protocol are analyzed, and in order to investigate properties of the protocol in more realistic environments, six variants of it are considered and their performance is evaluated by a simulation study.

In the second study, an RVC system based on RoF at mm-wave bands is considered. An RVC system is an infrastructure network for future ITS, which will be deployed along the road. The design requirements are discussed in [78] for future RVC systems indicating the data rate of about 2–10 Mbps

per MH will be required. The system supports not only voice, data but also multimedia services such as realtime video under high mobility conditions. Since the current and upcoming mobile cellular systems (e.g., GSM, UMTS) at microwave bands cannot supply a high-speed user with such high data rate traffic [79],[80] mm-wave bands such as 36 or 60 GHz have been considered [72],[78],[81]. Thus, this system is characterized by very small cell and high user mobility. As a consequence, handover management becomes an even more significant and challenging issue. In this study we propose an RoF based RVC network architecture along with an MAC protocol featuring a support of fast handover and dynamic bandwidth allocation according to the movement of MHs using the centralized control capability of RoF networks. Bandwidth management schemes aiming at improving handover quality as well as efficient bandwidth usage are also proposed, and additionally a simulation study is carried out to evaluate them.

We put forward an RoF based broadband wireless access network architecture for rural and remote areas in the third study. The demand for broadband access has grown steadily as users experience the convenience of high-speed response combined with “*always-on*” connectivity. A broadband wireless access network (BWAN) is indeed a cost-effective alternative in providing users with such broadband services since it requires much less infrastructure compared to wireline access networks such as xDSL and cable modem networks [86]. Thus, these days the so-called “*wireless last mile*” has attracted much attention. However, it has been concerned mainly with densely populated urban areas. Recent survey shows that although penetration of personal computers in rural areas is significant in some countries most of the users still use low-speed dial-up modem for the Internet access [87][88]. Since in such case broadband services based on wireline networks are prohibitively expensive, wireless access network might be the best solution. It requires a large number of BSs to cover broad areas, while the traffic demand per BS is much lower compared to densely populated urban areas. In this study, we propose an RoF architecture for BWANs using WDM for efficient bandwidth allocation. Specifically, the CS has the smaller number of optical tunable transmitter (TT) and tunable receiver (TR) pairs than that of BSs resulting in simpler CS structure. The CS is interconnected to BSs, each of which is fixed-tuned to one of the available wavelengths, through broadcast-and-select type optical passive device. Although system capacity is limited by the number of TT-TR pairs it has simpler CS structure and flexibility in terms of bandwidth allocation. Thus, this system is suitable for BWANs where a number of BSs are required but the average traffic load per unit area is low, satisfying the requirements of rural and remote areas. Furthermore, a mathematical analysis to obtain blocking probabilities is also derived and discussed.

1.3 Organization of the Dissertation

The remaining part of this dissertation is divided into six chapters as detailed below:

- Chapter 2 describes the background material that is necessary to understand the dissertation. It deals with the handover issues in wireless mobile networks and millimeter-wave band characteristics.

- Chapter 3 covers the basic optical fiber communication link and surveys the state of the art on RoF technologies with a special emphasis devoted to RoF system operating at mm-wave bands.
- Chapter 4 presents the MAC protocol (Chess Board protocol) proposed for WLAN at 60 GHz band. Important parameters of the protocol are examined, and based on them, minimum handover latency is derived. A simple analysis is performed and a simulation study is carried out to examine the properties of the MAC protocol.
- In chapter 5 an RoF based network architecture and an MAC protocol for future RVC system are presented. It features a support of fast handover and dynamic bandwidth allocation according to the movement of MHs using the centralized control capability of the network. Mobility management and bandwidth management schemes are proposed and a simulation study is performed to show its capability to achieve higher handover quality and bandwidth utilization.
- Access network architecture based on RoF for BWANs suitable for rural areas is proposed in chapter 6. It depends on WDM to interconnect between the CS and BSs, and the CS has tunable optical devices to access BSs. A mathematical analysis based on multitraffic loss system model is derived and numerical results are described.
- Chapter 7 draws conclusions, summarizes the main contributions of this dissertation, and finally describes the possible future research directions.

Chapter 2

Background Material

This chapter deals with the handover issues in wireless mobile networks based on cellular architecture and mm-wave bands for short-range high capacity wireless communications. These two topics are essential to understand the contents of the dissertation.

2.1 Handover in Wireless Mobile Networks

In conventional mobile cellular networks and wireless LANs handover can be defined as the mechanism by which an ongoing connection between a mobile host (MH) and a corresponding terminal or host is transferred from one point of access to the fixed network to another [46]¹. When an MH moves away from a BS, the signal level degrades and it needs to switch communications to another BS. It is very important in any cellular-based wireless networks because ongoing connection should be maintained during handover. In cellular voice telephony and mobile data networks, such points of attachment are referred to as BSs and in wireless LANs, they are called access points (APs). In either case, such a point of attachment serves a coverage area called a “*cell*”. Handover, in the case of cellular telephony, involves the transfer of a voice call from one BS to another. In the case of WLANs, it involves transferring the connection from one AP to another. In hybrid networks, it will involve the transfer of a connection from one BS to another, from an AP to another, between a BS and an AP, or vice versa.

For a voice user, handover results in an audible click interrupting the conversation for each handover; and because of handover, data users may lose packets and unnecessary congestion control measures may come into play. Degradation of the signal level, however, is a random process, and simple decision mechanisms such as those based on signal strength measurements result in the *ping-pong effect*. The ping-pong effect refers to several handovers that occur back and forth between two BSs. This exerts severe burden on both the user’s quality perception and the network load. In the first part of this chapter, we discuss general handover-related issues, and handover procedures of representative conventional wireless networks. For excellent surveys on handover issues, see [44],[45],[46].

¹There is no exact definition for handover that can explain various kinds of handovers in a variety of modern wireless networks. However, we use this definition for our purpose throughout this dissertation.

2.1.1 Issues related to Handover

In this subsection we discuss general issues related to handover that should be taken into account in any kinds of wireless networks as long as they involve handover. In this dissertation handover issues are classified into three parts: (1) architectural issues, (2) handover decision algorithms, and (3) handover-related resource management. Architectural issues are those related to the methodology, control, and software/hardware elements involved in rerouting the connection. Issues related to the handover decision algorithms are the types of algorithms, metrics used by the algorithms, and performance evaluation methodologies. Handover-related resource management deals with the maintenance of quality of service (QoS) during handover.

2.1.1.1 Architectural Issues

The issues are concerned with handover procedures that involve a set of protocols to notify all the related entities of a particular connection that a handover has been executed and that the connection has to be redefined (Fig. 2.1) [46]. In data networks, the MH is usually registered with a particular point of attachment. In voice networks, an idle MH would have selected a particular BS that is serving the cell in which it is located. This is for the purpose of routing incoming data packets or voice calls appropriately. When the MH moves and executes a handover from one point of attachment to another, the old serving point of attachment has to be informed about the change. This is usually called “*dissociation*”. The MH will also have to reassociate itself with the new point of access to the fixed network. Other network entities involved in routing data packets to the MH or switching voice calls have to be aware of the handover in order to seamlessly continue the ongoing connection or call. Depending on whether a new connection is created before breaking the old one or not, handovers are classified into hard and seamless handovers. Fig. 2.2 illustrates hard handover between the MH and the BSs. A hard handover is essentially a “break before make” connection. The link to the prior BS is terminated before or as the user is transferred to the new cell’s BS; the MH is linked to no more than one BS at any given time. In CDMA, the existence of two simultaneous connections during handover results in soft handover. The decision mechanism or handover control may be located in a network entity (as in cellular voice) or in the MH itself (as in WLANs). These cases are called network controlled handover (NCHO) and mobile-controlled handover (MCHO), respectively. In global system for mobile communications (GSM), information sent by the MH can be employed by the network entity in making the handover decision. This is called mobile-assisted handover (MAHO). In any case, the entity that decides on the handover uses some metrics, algorithms, and performance measures in making the decision. These are discussed below.

2.1.1.2 Handover Decision Algorithms

Several algorithms are being employed or investigated to make the correct decision to handover. Traditional algorithms employ thresholds to compare the values of metrics from different points of attachment

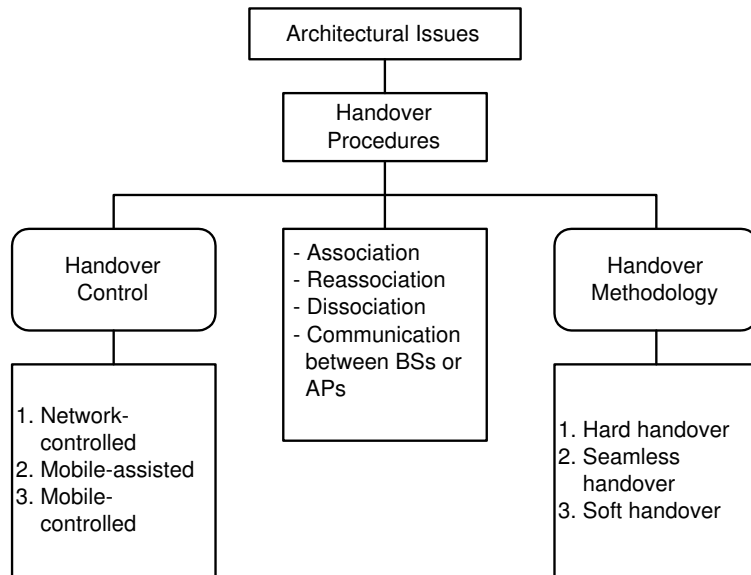


Figure 2.1: Handover architectural issues [46].

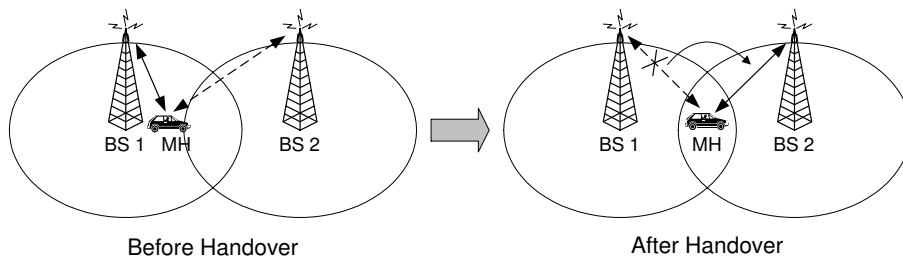


Figure 2.2: Hard handover.

and then decide on when to make the handover. A variety of metrics have been employed in mobile voice and data networks to decide on a handover. Primarily, the received signal strength (RSS) measurements from the serving point of attachment and neighboring points of attachment are used in most of these networks. Alternatively or in conjunction, the path loss, carrier-to-interference ratio (CIR), signal-to-interference ratio (SIR), bit error rate (BER), block error rate (BLER), symbol error rate (SER), power budgets, and cell ranking have been employed as metrics in certain mobile voice and data networks. In order to avoid the ping-pong effect, additional parameters are employed by the algorithms such as hysteresis margin, dwell timers, and averaging windows. Additional parameters (when available) may be employed to make more intelligent decisions. Some of these parameters also include the distance between the MH and the point of attachment, the velocity of the MH, and traffic characteristics in the serving cell. The performance of handover algorithms is determined by their effect on certain performance measures. Most of the performance measures that have been considered, such as call blocking probability, handover blocking probability, delay between handover request and execution, and call dropping probability, are related to voice connections. Handover rate (number of handovers per unit of time) is related to the ping-pong effect, and algorithms are usually designed to minimize the number of unnecessary handovers.

Traditional handover decision algorithms are all based on RSS or received power (P). Some of the traditional algorithms [44],[46] are as follows:

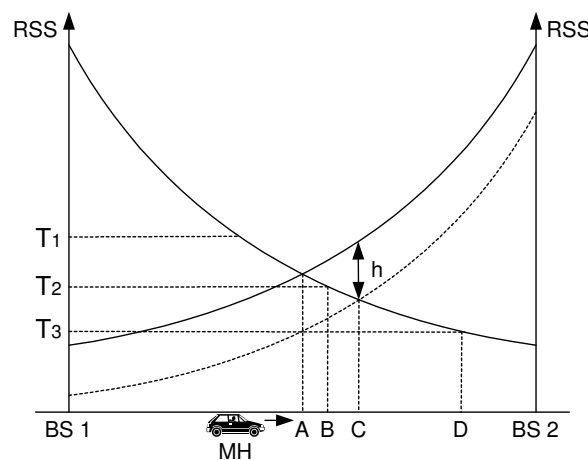


Figure 2.3: Handover decision.

- *RSS*: The BS whose signal is being received with the largest strength is selected (choose BS_{new} if $P_{new} > P_{old}$). In Fig. 2.3, the handover would occur at position A.
- *RSS plus Threshold*: A handover is made if the RSS of a new BS exceeds that of the current one and the signal strength of the current BS is below a threshold T (choose BS_{new} if $P_{new} > P_{old}$ and $P_{old} < T$). The effect of the threshold depends on its relative value as compared to the signal

strengths of the two BSs at the point at which they are equal. If the threshold is higher than this value, say T_1 in Fig. 2.3, this scheme performs exactly like the relative signal strength scheme, so the handover occurs at position A. If the threshold is lower than this value, say T_2 in Fig. 2.3, the MH would delay handover until the current signal level crosses the threshold at position B. In the case of T_3 , the delay may be so long that the MH drifts too far into the new cell. This reduces the quality of the communication link from BS 1 and may result in a dropped call. In addition, this results in additional interference to co-channel MHs. Thus, this scheme may create overlapping cell coverage areas.

- *RSS plus Hysteresis*: A handover is made if the RSS of a new BS is greater than that of the old BS by a hysteresis margin h (choose BS_{new} if $P_{new} > P_{old} + h$). In this case handover will occur at point C in Fig. 2.3. This technique prevents the so-called *ping-pong effect*.
- *RSS, Hysteresis plus Threshold*: A handover is made if the RSS of a new BS exceeds that of the current BS by a hysteresis margin h and the signal strength of the current BS is below a threshold T (choose BS_{new} if $P_{new} > P_{old} + h$ and $P_{old} < T$). In Fig. 2.3, the handover will occur at point C if the threshold is either T_1 or T_2 , and will occur at point D if the threshold is T_3 .
- *Algorithm plus Dwell Timer*: Sometimes a dwell timer is used with the above algorithms. A timer is started the instant the condition in the algorithm is true. If the condition continues to be true until the timer expires, a handover is performed.

Other techniques are emerging such as hypothesis testing [47], dynamic programming [48], and pattern recognition techniques based on neural networks or fuzzy logic systems [49].

2.1.1.3 Handover-related Resource Management

QoS guarantees during and after handover will become more significant and challenging in the near future since the current trends in cellular networks are 1) to reduce cell size to accommodate more MHs that will cause more frequent handovers, and 2) to support not only voice traffic but also data and multimedia traffic such as video. One of the issues is how to control (or reduce) handover drops due to lack of available bandwidth in the new cell, since MHs should be able to continue their ongoing sessions. Here, two connection-level QoS parameters are relevant: the probability (P_{CB}) of blocking new connection requests and the probability (P_{HD}) of dropping handovers. In ideal case, we would like to avoid handover drops so that ongoing connections may be preserved as in a QoS-guaranteed wired network. However, this is impossible in practice due to unpredictable fluctuations in handover traffic load.

Each cell can, instead, reserve fractional bandwidths of its capacity, and this reserved bandwidth can be used solely for handovers, not for new connection requests. The problem is then how much of bandwidth in each cell should be reserved for handovers. This concept of reserving bandwidth for handover was introduced in the mid-1980s [51]. In this scheme, a portion of bandwidth is permanently

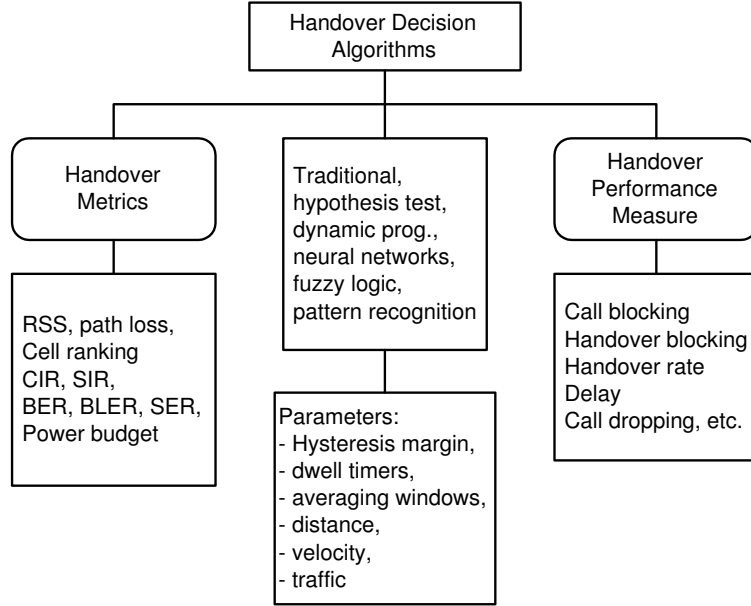


Figure 2.4: Decision time algorithms in handover [46].

reserved in advance for handovers. Since then intensive research efforts have been carried out for developing better schemes. Most existing bandwidth reservation schemes for handover assume that the handover connection arrivals are Poisson, and each connection requires an identical amount of bandwidth (e.g., voice call) with an exponentially distributed channel holding time in each cell [52]–[55]. But, it is known that the channel holding time of handed-over connections is not really exponentially distributed [56].

Recently, some schemes attempting to limit P_{HD} to a prespecified target value for multimedia mobile cellular networks have been proposed [57],[58],[85]. A probabilistic prediction of user mobility has been proposed in [57] based on the idea that mobility prediction is synonymous with data compression. From the observation that a connection originated from a cell follows a specific sequence of cells, rather than a random sequence of cells, the scheme utilizes character compression technique to predict future mobility of MHs. In [58], a handover probability at some future time has been derived using the aggregate history of handovers observed in each cell. These algorithms depend on the mobility history of users for statistical prediction to guarantee that P_{HD} is maintained below a prespecified target probability. Thus, they need a large amount of history data for proper operation. A much simpler scheme has been proposed in [85]. In this scheme each BS counts the number of handover successes and failures to adaptively change the reserved bandwidth for handover, and it does not depend on a large amount of handover history data unlike the above two schemes.

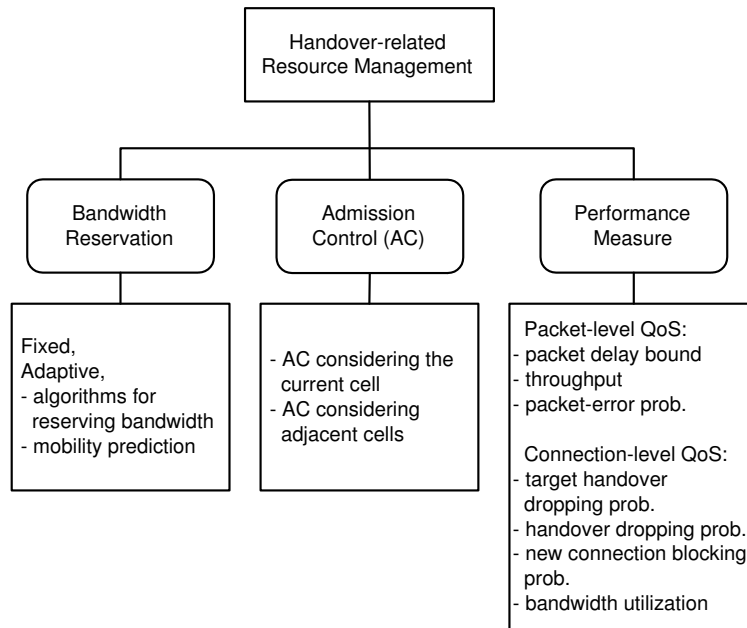


Figure 2.5: Handover-related resource management issues.

2.1.2 Handover Architectures and Algorithms in Mobile Cellular Networks

In this subsection we will see handover procedures for two typical conventional mobile networks, i.e., GSM and IEEE 802.11. The former is representative of mobile cellular networks, while the latter is WLAN. Focus is placed only on handover features, thus we don't refer to system architecture, operation and so on for the networks.

2.1.2.1 Handover in GSM

There are two basic reasons for a handover in GSM [50].

- when the MH moves out of the range of a base transceiver station (BTS) or a certain antenna of a BTS respectively, the received signal level becomes lower continuously until it falls underneath the minimal requirements for communication. Or the error rate may grow due to interference, the distance to the BTS may be too high (max. 35 km) etc. – all these effects may diminish the quality of the radio link and make radio transmission impossible.
- The wired infrastructure of GSM may decide that the traffic in one cell is too high and shift some MH to other cells with a lower load. Thus, handover may be due to load balancing.

There are four possible handover scenarios in GSM [50] as shown in Fig. 2.6.

- **Intra-cell handover:** Within a cell, narrow-band interference could make it impossible to transmit at a certain frequency. The base station controller (BSC) could then decide to change the carrier

frequency (scenario 1).

- **Inter-cell, intra-BSC handover:** This is a typical handover scenario. The MH moves from one cell to another, but stays within the control of the same BSC that performs a handover, assigns a new radio channel in the new cell and releases the old one (scenario 2).
- **Inter-BSC, intra-MSC handover:** As a BSC only controls a limited number of cells, GSM also has to perform handovers between cells controlled by different BSCs. This handover then has to be controlled by the mobile switching center (MSC) (scenario 3).
- **Inter MSC handover:** Finally, a handover could be required between two cells belonging to different mobile switching center (MSC). Now both MSCs perform the handover together (scenario 4).

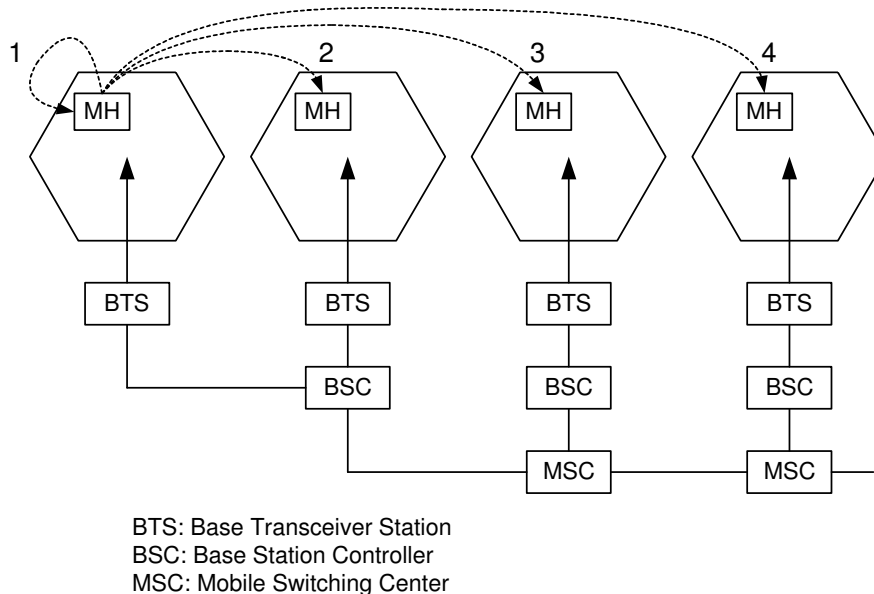


Figure 2.6: Handover types in GSM.

In order to provide all necessary information for a handover due to a weak signal level, both MH and BTS perform periodic measurements of the downlink and uplink quality, respectively (link quality comprises signal level and bit error rate). Measurement reports are sent by the MH about every half-second and contain the quality of the current link used for transmission as well as the quality of certain channels in neighboring cells.

While an MH moves away from one BTS closer to another one, the handover decision does not depend on the actual value of the received signal level, but on the average value. Therefore, the BSC collects all values (bit error rate and signal levels from uplink and downlink) from BTS and MH and

calculates average values. These values are then compared to threshold, i.e., the handover margin, which includes some hysteresis to avoid a ping-pong effect.

Fig. 2.7 shows the typical signal flow during an inter-BSC, intra-MS C handover (scenario 3 in Fig. 2.6). The MH sends its periodic measurements reports, the BTS_{old} forwards these reports to the BSC_{old} together with its own measurements. Based on these values and, e.g., on current traffic conditions, the BSC_{old} may decide to perform a handover and sends the message “HO required” to the MSC. The task of the MSC then comprises the request of the resources needed for the handover to the new BSC (BSC_{new}). This BSC checks if enough resources (typically frequencies or time slots) are available and activates a physical channel at the BTS_{new} to prepare for the arrival of the MH.

The BTS_{new} acknowledges the successful channel activation, and BSC_{new} acknowledges the handover request. The MSC then issues a handover command that is forwarded to the MH. The MH now breaks its old radio link and accesses the new BTS . The next steps include the establishment of the link. Basically, the MH has then finished the handover, but it is important to release the resources at the old BSC and BTS and to signal the successful handover using the handover and clear complete messages.

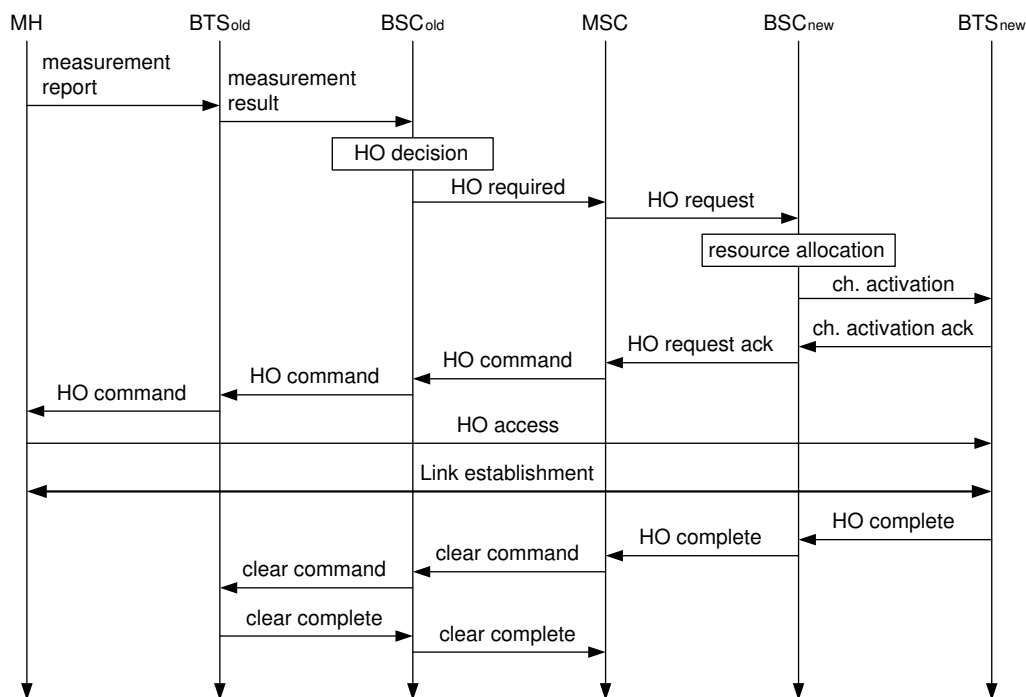


Figure 2.7: Intra-MS C handover in GSM.

2.1.2.2 Handover in IEEE 802.11 Wireless Local Area Networks

The IEEE 802.11 WLAN standard defines the coverage area of a single AP as a basic service set (BSS); to extend this, multiple BSSs are to be connected through a distribution system (usually the wired network) to form an extended service set (ESS). The 802.11 standard defines only the over-the-air interactions (communication between MHs and the AP). The internals of how the ESS should be formed are left to the AP management entity and are not defined by the 802.11 standard. Recently, a draft inter-access-point protocol (IAPP) has been specified to standardize the communication between APs over the wired interface (IEEE 802.11F) [59].

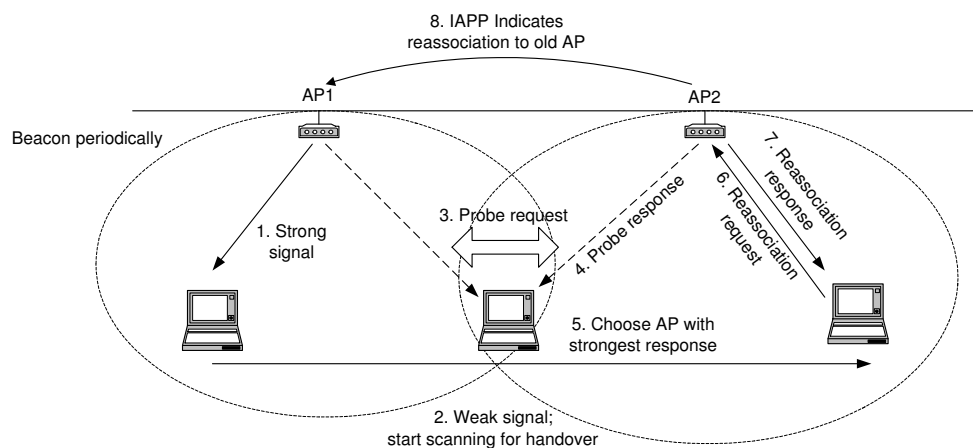


Figure 2.8: Handover procedures in an IEEE 802.11 WLAN.

The HO procedures in a WLAN are shown in Fig. 2.8 [46]. The AP broadcasts a beacon signal periodically (typically the period is around 100 ms). An MH that powers on scans the beacon signal and associates itself with the AP with the strongest beacon. The beacon contains information corresponding to the AP such as a time stamp, beacon interval, capabilities, ESS ID, and traffic indication map (TIM). The MH uses the information in the beacon to distinguish between different APs.

The MH keeps track of the RSS of the beacon of the AP with which it is associated; when the RSS becomes weak, it starts to scan for stronger beacons from neighboring APs. The scanning process can be either active or passive. In passive scanning, the MH simply listens to available beacons. In active scanning, the MH sends a probe request to a targeted set of APs that are capable of receiving its probe. Each AP that receives the probe responds with a probe response that contains the same information available in a regular beacon with the exception of the TIM. The probe response thus serves as a solicited beacon. The MH chooses the AP with the strongest beacon or probe response and sends a reassociation request to the new AP. The reassociation request contains information about the MH as well as the old AP. In response, the new AP sends a reassociation response that has information about the supported bit rates, station ID, and so on needed to resume communication. The old AP is not informed by the MH about the change of location. So far, each WLAN vendor had some form of proprietary implementation

of the emerging IAPP standard for completing the last stage of the HO procedure (intimating the old AP about the MH's change of location). The IAPP protocol employs two protocol data units (PDUs) to indicate that a handover has taken place. These PDUs are transferred over the wired network from the new AP to the old AP using UDP/IP.

2.1.2.3 Comparison of Handover Procedures in IEEE 802.11 and GSM

Even though the functionalities of IEEE 802.11, and GSM networks are different, the handover procedures have several similarities. The two networks use a separate signal (beacon, BCCH) with a constant transmit power in order to enable RSS measurements for handover decisions. While the beacon in 802.11 is on the same channel as data, it is on different physical channels in GSM. The primary difference is the fact that the circuit-switched voice networks have NCHO while data networks prefer MCHO. In both cases, channel monitoring is always performed at the terminal. When the handover control is with the network, the MH has to transmit the measured information to the decision entity.

2.2 Millimeter-wave Band Characteristics

Due to spectrum congestion in microwave bands and other reasons as will be described later, the interest of researchers and standardization bodies has indicated the mm-wave band as a candidate for some of the most challenging services to be provided in the future [1]. However, the use of the mm-wave band introduces some features that have to be taken into account in system design; these features are mainly related to the short wavelength and to the additional attenuation due to rain and oxygen absorption, when present.

2.2.1 Why Millimeter Waves?

The main advantages on the usage of mm-waves can be summarized as follows [1]:

- the high power level attenuation, due to the large value of frequency, in conjunction with oxygen and rain absorption, which leads to a high spatial filtering effect with the consequent frequent channel reuse;
- the small size of antennas and RF circuits;
- the large spectrum availability.

On the other hand, large values of signal attenuation become a fundamental drawback when long-distance communication links are to be managed. Hence, significant applications of the mm-wave can be found in the field of short-range communication systems, i.e., when link distances range from a few meters up to one kilometer.

Another useful consequence of the mm-wave band utilization, related to the large values of attenuation, is the low number of interfering signal sources that are usually present in the system. Both in indoor environments, due to walls, and in outdoor scenarios, due to high frequency, a number of interferers ranging from zero to two or three may be present. This represents a significant advantage in terms of capture probability when packet communications and narrow-band signaling are considered.

2.2.2 60-GHz Band for Local Wireless Access

For dense local communications, the 60 GHz band is of special interest because of the specific attenuation characteristic due to atmospheric oxygen of 10–15 dB/km [2]. The 10–15 dB/km regime makes the 60 GHz band unsuitable for long-range ($> 2 \text{ km}$) communications, so it can be dedicated entirely to short-range ($< 1 \text{ km}$) communications. For the small distances to be bridged in an indoor environment ($< 50 \text{ m}$) the 10–15 dB/km attenuation has no significant impact. The specific attenuation in excess of 10 dB/km occurs in a bandwidth of about 8 GHz centered around 60 GHz [2]. Thus, in principle there is about 8 GHz bandwidth available for dense wireless local communications. This makes the 60 GHz band of utmost interest for all kinds of short-range wireless communications. In the United States, the Federal Communications Commission (FCC) sets aside the 59–64 GHz frequency band for general unlicensed applications.

Indoor 60 GHz channel measurement results were reported in the literature [60],[61],[62],[63]. Spatial and temporal characteristics of 60 GHz indoor channels is reported in [60]. Specifically, it provides detailed angle-of-arrival and time-of-arrival parameters in a typical indoor environment for the 60 GHz channels. In [61], path loss measurements are reported for line-of-sight (LOS) and non-line-of-sight (NLOS) cases, fading statistics in a physically stationary environment are extracted and an investigation of the people movement effect on the temporal fading envelope is shown. The dynamic range of fading in a quiescent environment is 8.8 dB and increased to 35 dB when a person moves between the fixed terminals with the channel becoming extremely nonstationary. Rule-of-thumb penetration loss values at 60 GHz band are presented in Table 2.1 [60]. One should notice that when a typical office room is surrounded by normal concrete wall due to high penetration loss about 30 dB each room must be supported by at least one BS.

2.2.3 Millimeter-wave WLAN Systems

A series of mm-wave WLAN prototype systems have been developed at the Communications Research Laboratory in Japan since 1998 [64]-[67]. In the first prototype an ATM based WLAN was developed to support multimedia transmission at a data rate of 51.84 Mbps [64]. The second prototype is an IP based WLAN with a higher data transmission rate of 64 Mbps [65] [66]. The two prototype WLANs operate in the 60 GHz band and consist of one BS and several stationary stations, so handover procedure is not considered. In the third prototype WLAN 156 Mbps data transmission was demonstrated using 38 GHz band [67]. Two BSs, connected through fast Ethernet to each other, were developed, which forms two

Table 2.1: Measured Penetration Losses and Results at 60 GHz Band [60]

Material	Penetration loss
Composite wall with studs not in the path	8.8 dB
Composite wall with studs in the paths	35.5 dB
Glass door	2.5 dB
Concrete wall 1 week after concreting	73.6 dB
Concrete wall 5 months after concreting	46.5 dB
Concrete wall 14 months after concreting	28.1 dB
Plasterboard wall	5.4 to 8.1 dB
Partition of glass wool with plywood surfaces	9.2 to 10.1 dB
Partition of cloth-covered plywood	3.9 to 8.7 dB

BSSs. Handover procedure for a call moving from one BSS to the other BSS is considered. It is carried out by identifying BS address contained in the down-link frames. All the prototype systems operate in FDD mode using two fixed frequencies for up- and downlink transmissions, and utilize an MAC protocol called RS-ISMA (Reservation-based Slotted Idle Signal Multiple Access) [69], which is implemented in the BS. Therefore, the BS structure developed is not simple as assumed in this paper since it has processing function like MAC protocol. An RoF based WLAN prototype system using simple BS structure operating in the 60 GHz band was developed in [9]. The system utilizes wavelength division multiplexing (WDM) technology to assign different wavelength to each BS. Transmission experiments have been carried out with data rate of 50 Mbps.

2.2.4 Handover Issue in Millimeter-band Wireless Networks

In typical conventional wireless systems such as GSM and IEEE 802.11, there is a large overlapping area between cells with respect to MH's speed so that the entities involved in handover has enough time to make a decision on handover based on measurements. In contrast, in wireless networks based on mm-wave bands (either indoor or outdoor system) overlapping area, if any, can be very small. As a consequence, in indoor environment small movement of an MH might trigger handover, and in outdoor environment a fast MH will experience many handovers during its connection life time. This requires a totally different kind of approach to mobility management in mm-wave based wireless networks. In this dissertation, we are concerned with this particular issue in the context of RoF based networks.

2.3 Summary

In this chapter, we have described handover-related issues in conventional mobile wireless networks and mm-wave characteristics with a special emphasis on 60 GHz band. When mm-wave band is utilized in wireless networks having mobile users handover issues become very significant and challenging due to small cell size. This requires quite different approach as compared to conventional wireless networks. In

traditional mobile cellular networks, overlapping area between cells is so large that the entities involved in handover have enough time to monitor and trigger handover based on measurement data. On the other hand, in mm-wave wireless networks small movement of an MH may generate handover, necessitating very fast and simple handover procedure.

Chapter 3

Radio over Fiber Technologies

3.1 Introduction

Wireless networks based on RoF technologies have been proposed as a promising cost-effective solution to meet ever increasing user bandwidth and wireless demands. Since it was first demonstrated for cordless or mobile telephone service in 1990 [5], a lot of research has been carried out to investigate its limitation and develop new and high performance RoF technologies. In this network a CS is connected to numerous functionally simple BSs via an optic fiber. The main function of BS is to convert optical signal to wireless one and vice versa. Almost all processing including modulation, demodulation, coding, routing is performed at the CS. That means, RoF networks use highly linear optic fiber links to distribute RF signals between the CS and BSs.

Fig. 3.1 shows a general RoF architecture. At a minimum, an RoF link consists of all the hardware required to impose an RF signal on an optical carrier, the fiber-optic link, and the hardware required to recover the RF signal from the carrier. The optical carrier's wavelength is usually selected to coincide with either the $1.3 \mu m$ window, at which standard single-mode fiber has minimum dispersion, or the $1.55 \mu m$ window, at which its attenuation is minimum.

This chapter, constituting two major parts, briefly covers basic optical fiber transmission link and surveys state-of-the-art RoF technologies with an emphasis on RoF system operating at mm-wave bands. The first part is dedicated to a description of general optical transmission link, where digital signal transmission is assumed as current optical networks. The second part mainly deals with RoF technologies and is subdivided as follows: (1) RoF link characteristics, requirements, (2) RF signal generation and transportation techniques, and link configurations (3) the state of the art on mm-wave generation and transport technologies. In addition, RoF with wavelength division multiplexing (WDM) is described as it has been one of the hot topics in this area.

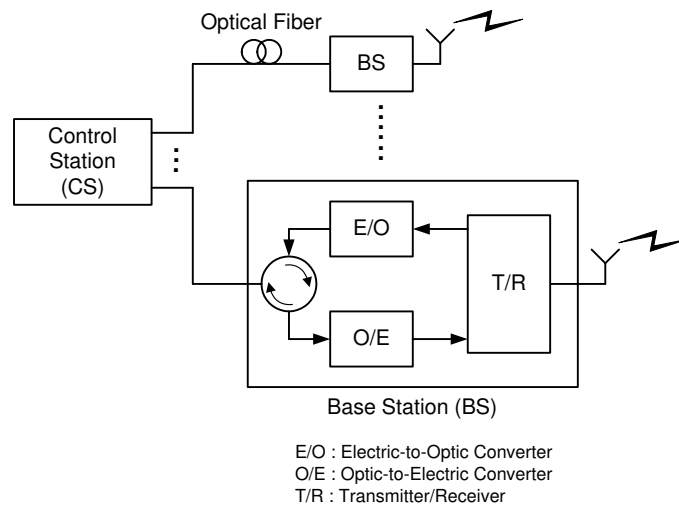


Figure 3.1: General radio over fiber system.

3.2 Optical Transmission Link

In the first part of this section, a general optical transmission link, shown in Fig. 3.2, is briefly described for which we assume that a digital pulse signal is transmitted over optical fiber unless otherwise specified. The optical link consists of an optical fiber, transmitter, receiver and amplifier, each of which is dealt with in the subsequent subsections.

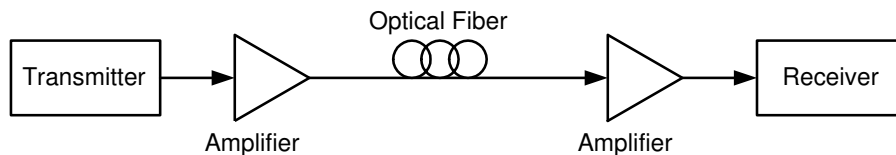


Figure 3.2: Optical transmission link.

3.2.1 Optical Fiber

Optical fiber is a dielectric medium for carrying information from one point to another in the form of light. Unlike the copper form of transmission, the optical fiber is not electrical in nature. To be more specific, fiber is essentially a thin filament of glass that acts as a waveguide. A waveguide is a physical medium or path that allows the propagation of electromagnetic waves, such as light. Due to the physical phenomenon of total internal reflection, light can propagate following the length of a fiber with little loss (Fig. 3.4).

Optical fiber has two low-attenuation regions [35]. Centered at approximately 1300 nm is a

range of 200 nm in which attenuation is less than 0.5 dB/km. The total bandwidth in this region is about 25 THz. Centered at 1550 nm is a region of similar size with attenuation as low as 0.2 dB/km. Combined, these two regions provide a theoretical upper bound of 50 THz of bandwidth. By using these large low-attenuation areas for data transmission, the signal loss for a set of one or more wavelengths can be made very small, thus reducing the number of amplifiers and repeaters actually needed. In single-channel long-distance experiments, optical signals have been sent over hundreds of kilometers without amplification. Besides its enormous bandwidth and low attenuation, fiber also offers low error rates. Communication systems using an optical fiber typically operate at BER's of less than 10^{-11} . The small size and thickness of fiber allows more fiber to occupy the same physical space as copper, a property that is desirable when installing local networks in buildings. Fiber is flexible, reliable in corrosive environments, and deployable at short notice. Also, fiber transmission is immune to electromagnetic interference and does not cause interference.

3.2.1.1 Optical Transmission in Fiber

Light can travel through any transparent material, but the speed of light will be slower in the material than in a vacuum. The ratio of the speed of light in a vacuum to that in a material is known as the material's *refractive index* (n) and is given by $n = c/v$, where c is the speed in a vacuum and v is the speed in the material. When light travels from one material of a given refractive index to another material of a different refractive index (i.e., when refraction occurs), the angle at which the light is transmitted in the second material depends on the refractive indices of the two materials as well as the angle at which light strikes the interface between the two materials. According to Snell's law, we have $n_a \sin \theta_a = n_b \sin \theta_b$, where n_a and n_b are the refractive indices of the first substance and the second substance, respectively; and θ_a and θ_b are the angles from the normal of the incident and refracted lights, respectively.

From Fig. 3.3, we see that the fiber consists of a core completely surrounded by a cladding (both of which consist of glass of different refractive indices). Let us first consider a step-index fiber, in which the change of refractive index at the core-cladding boundary is a step function. If the refractive index of the cladding is less than that of the core, then the *total internal reflection* can occur in the core and light can propagate through the fiber as shown in Fig. 3.4. The angle above which total internal reflection will take place is known as the *critical angle* and is given by θ_c .

$$\sin \theta_c = \frac{n_{clad}}{n_{core}}$$

where n_{clad} and n_{core} are the refractive indices of cladding and core, respectively. Thus, for a light to travel down a fiber, the light must be incident on the core-cladding surface at an angle greater than θ_c .

For the light to enter a fiber, the incoming light should be at an angle such that the refraction at the air-core boundary results in the transmitted light's being at an angle for which total internal reflection can take place at the core-cladding boundary. The maximum value of θ_{air} can be derived from

$$n_{air} \sin \theta_{air} = n_{core} \sin(90^\circ - \theta_c)$$

We can rewrite it as

$$n_{air} \sin \theta_{air} = \sqrt{n_{core}^2 - n_{clad}^2}$$

The quantity $n_{air} \sin \theta_{air}$ is referred to as the *numerical aperture* (NA) of the fiber and θ_{air} is the maximum angle with respect to the normal at the air-core boundary, so that the incident light that enters the core will experience total internal reflection inside the fiber.

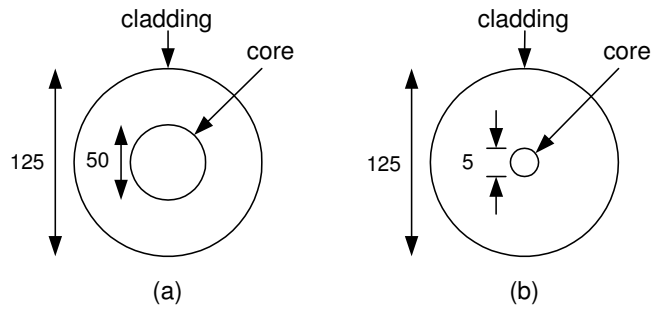


Figure 3.3: Multimode (a) and single-mode (b) optical fibers (unit: μm).

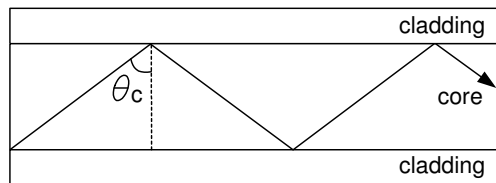


Figure 3.4: Light traveling via total internal reflection within an optical fiber.

3.2.1.2 Multimode versus Single-Mode Fiber

A mode in an optical fiber corresponds to one of the possible multiple ways in which a wave may propagate through the fiber. It can also be viewed as a standing wave in the transverse plane of the fiber. More formally, a mode corresponds to a solution of the wave equation that is derived from Maxwell's equations and subject to boundary conditions imposed by the optical fiber waveguide.

Although total internal reflection may occur for any angle θ that is greater than θ_c , light will not necessarily propagate for all of these angles. For some of these angles, light will not propagate due to destructive interference between the incident light and the reflected light at the core-cladding interface

within the fiber. For other angles of incidence, the incident wave and the reflected wave at the core-cladding interface constructively interfere in order to maintain the propagation of the wave. The angles for which waves do propagate correspond to *modes* in a fiber. If more than one mode propagates through a fiber, then the fiber is called *multimode*. In general, a larger core diameter or high operating frequency allows a greater number of modes to propagate.

The advantage of multimode fiber is that, its core diameter is relatively large; as a result, injection of light into the fiber with low coupling loss can be accomplished by using inexpensive, large-area light sources, such as light-emitting diodes (LED's). The disadvantage of multimode fiber is that it introduces the phenomenon of *intermodal dispersion*. In multimode fiber, each mode propagates at a different velocity due to different angles of incidence at the core-cladding boundary. This effect causes different rays of light from the same source to arrive at the other end of the fiber at different times, resulting in a pulse that is spread out in the time domain. Intermodal dispersion increases with the distance of propagation, so that it limits the bit rate of the transmitted signal and the distance that the signal can travel. Thus, in RoF networks multimode fiber is not utilized as much as possible, instead, single-mode fiber is widely used.

Single-mode fiber allows only one mode and usually has a core size of about $10\ \mu m$, while multimode fiber typically has a core size of $50\text{--}100\ \mu m$. It eliminates intermodal dispersion and hence can support transmission over much longer distances. However, it introduces the problem of concentrating enough power into a very small core. LED's cannot couple enough light into a single-mode fiber to facilitate long-distance communications. Such a high concentration of light energy may be provided by a semiconductor laser, which can generate a narrow beam of light.

3.2.1.3 Attenuation in Fiber

Attenuation in an optical fiber leads to a reduction of the signal power as the signal propagates over some distance. When determining the maximum distance that a signal can propagate for a given transmitter power and receiver sensitivity, one must consider attenuation. Let $P(L)$ be the power of the optical pulse at distance L km from the transmitter and A be the attenuation constant of the fiber (in dB/km). Attenuation is characterized by

$$P(L) = 10^{-AL/10} P(0)$$

where $P(0)$ is the optical power at the transmitter.

3.2.1.4 Dispersion in Fiber

Dispersion is the widening of a pulse duration as it travels through a fiber. As a pulse widens, it can broaden enough to interfere with neighboring pulses (bits) on the fiber, leading to intersymbol interference. Dispersion thus limits the bit spacing and the maximum transmission rate on a fiber-optic channel.

As described earlier, one form of the dispersion is an intermodal dispersion. This is caused when multiple modes of the same signal propagate at different velocities along the fiber. Intermodal dispersion does not occur in a single-mode fiber.

Another form of dispersion is *material* or *chromatic dispersion*. In a dispersive medium, the index of refraction is a function of the wavelength. Thus, if the transmitted signal consists of more than one wavelength, certain wavelengths will propagate faster than other wavelengths. Since no laser can create a signal consisting of an exact single wavelength, chromatic dispersion will occur in most systems.

A third type of dispersion is *waveguide dispersion*. Waveguide dispersion is caused as the propagation of different wavelengths depends on waveguide characteristics such as the indices and shape of the fiber core and cladding.

At 1300 nm, chromatic dispersion in a conventional single-mode fiber is nearly zero. Luckily, this is also a low-attenuation window (although loss is higher than 1550 nm). Through advanced techniques such as *dispersion shifting*, fibers with zero dispersion at a wavelength between 1300–1700 nm can be manufactured.

3.2.1.5 Nonlinearities in Fiber

Nonlinear effects in fiber may potentially have a significant impact on the performance of WDM optical communications systems. Nonlinearities in fiber may lead to attenuation, distortion, and cross-channel interference. In a WDM system, these effects place constraints on the spacing between adjacent wavelength channels, limit the maximum power on any channel, and may also limit the maximum bit rate. The details of the optical nonlinearities are very complex and beyond the scope of the dissertation. It should be emphasized that they are the major limiting factors in the available number of channels in a WDM system [35].

3.2.1.6 Couplers

A coupler is a general term that covers all devices that combine the light into or split the light out of a fiber. A splitter is a coupler that divides the optical signal on one fiber to two or more fibers. The most common splitter is a 1×2 splitter. The *splitting ratio*, α , is the amount of power that goes to each output. Combiners are the reverse of splitters, and when turned around, a combiner can be used as a splitter. In addition to the power split incurred in a coupler, a signal also experiences *return loss*. If the signal enters an input of the coupler, roughly half of the signal's power goes to each output of the coupler. However, a small amount of power is reflected in the opposite direction and is directed back to the inputs of the coupler. Another type of loss is *insertion loss*. One source of insertion loss is the loss incurred when the light is directed from a fiber into the coupler device; ideally, the axes of the fiber core and the coupler input port must be perfectly aligned, but full perfection may not be achievable due to the very small dimensions.

The passive star coupler (PSC) is a multiport device in which light coming into any input port is broadcast to every output port. The PSC is attractive because the optical power that each output receives P_{out} equals

$$P_{out} = \frac{P_{in}}{N}$$

where P_{in} is the optical power introduced into the star by a single node and N is the number of output ports of the star. Note that this expression ignores the excess loss, caused by flaws introduced in the manufacturing process.

3.2.2 Optical Transmitters

3.2.2.1 How a Laser Works

The word “*laser*” is an acronym for light amplification by stimulated emission of radiation. The key word is stimulated emission, which is what allows a laser to produce intense high-powered beams of coherent light (light that contains one or more distinct frequencies).

To understand stimulated emission, we must first acquaint ourselves with the energy levels of atoms. Atoms that are stable (in the ground state) have electrons in the lowest possible energy levels. In each atom, there are a number of discrete levels of energy that an electron can have, which are referred to as “*states*”. To change the level of an atom in the ground state, the atom must absorb energy. When an atom absorbs energy, it becomes excited and moves to a higher energy level. At this point, the atom is unstable and usually moves quickly back to the ground state by releasing a “*photon*”, a particle of light.

There are certain substances, however, whose states are *quasi-stable*, which means that the substances are likely to stay in the excited state for longer periods of time without constant excitation. By applying enough energy (in the form of either an optical pump or an electrical current) to a substance with quasi-stable states for a long enough period of time, *population inversion* occurs, which means that there are more electrons in the excited state than in the ground state. This inversion allows the substance to emit more light than it absorbs.

Fig. 3.5 shows a general representation of the structure of a laser. The laser consists of two mirrors that form a cavity (the space between the mirrors), a lasing medium, which occupies the cavity, and an excitation device. The excitation device applies current to the lasing medium, which is made of a quasi-stable substance. The applied current excites electrons in the lasing medium, and when an electron in the lasing medium drops back to the ground state, it emits a photon of light. The photon will reflect off the mirrors at each end of the cavity and will pass through the medium again.

Stimulated emission occurs when a photon passes very close to an excited electron. The photon may cause the electron to release its energy and return to the ground state. In the process of doing so, the electron releases another photon, which will have the same direction and coherency (frequency) as the stimulating photon. Photons for which the frequency is an integral fraction of the cavity length

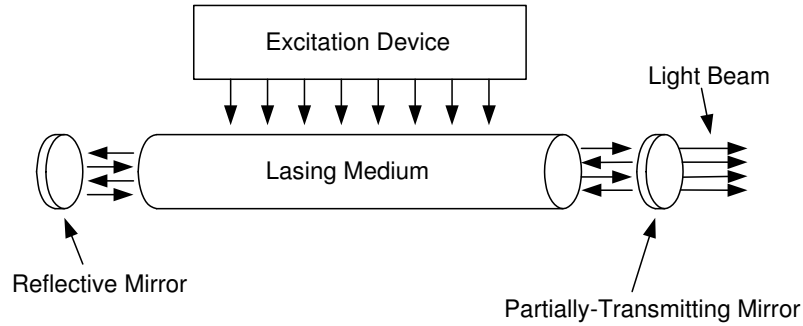


Figure 3.5: The general structure of a laser.

will coherently combine to build up light at the given frequency within the cavity. Between normal and stimulated emission, the light at the selected frequency builds in intensity until energy is being removed from the medium as fast as it is being inserted. The mirrors feed the photons back and forth, so further stimulated emission can occur and higher intensities of light can be produced. One of the mirrors is partially transmitting, so that some photons will escape the cavity in the form of a narrowly focused beam of light. By changing the length of the cavity, the frequency of the emitted light can be adjusted.

The frequency of the photon emitted depends on its change in energy levels. The frequency is determined by the equation

$$f = \frac{E_i - E_f}{h} \quad (3.1)$$

where f is the frequency of the photon, E_i is the initial (quasi-stable) state of the electron, E_f is the final (ground) state of the electron, and h is Planck's constant ($= 6.626 \times 10^{-34} \text{ J} \cdot \text{s}$).

3.2.2.2 Semiconductor Diode Lasers

The most useful type of a laser for optical networks is the semiconductor diode laser. The simplest implementation of a semiconductor laser is the bulk laser diode, which is a p-n junction with mirrored edges perpendicular to the junction (see Fig. 3.6).

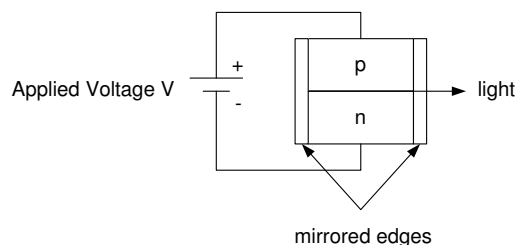


Figure 3.6: Structure of a semiconductor laser diode.

In semiconductor materials, electrons may occupy either the valence band or the conduction band. The valence band and conduction band are analogous to the ground state and excited state of an electron mentioned above. The valence band corresponds to an energy level at which an electron is not free from an atom. The conduction band corresponds to an energy level at which an electron has become a free electron and may move freely to create current flow. The region of energy between the valence band and the conduction band is known as the “*band gap*”. An electron may not occupy any energy levels in the bandgap region. When an electron moves from the valence band to the conduction band, it leaves a vacancy, or “*hole*”, in the valence band. When the electron moves from the conduction band to the valence band, it recombines with the hole and may produce the spontaneous emission of a photon. The frequency of the photon is given by Eq. (3.1), where $E_i - E_f$ is the band-gap energy.

A semiconductor may be doped with impurities to increase either the number of electrons or the number of holes. An n-type semiconductor is doped with impurities that provide extra electrons. These electrons will remain in the conduction band. A p-type semiconductor is doped with impurities that increase the number of holes in the valence band. A p-n junction is formed by layering p-type semiconductor material over n-type semiconductor material.

In order to produce stimulated emission, voltage is applied across the p-n junction to forward bias the device and cause electrons in the “n” region to combine with holes in the “p” region, resulting in light energy being released at a frequency related to the band gap of the device. By using different types of semiconductor materials, light with various ranges of frequencies may be released. The actual frequency of light emitted by the laser is determined by the length of the cavity formed by mirrored edges perpendicular to the p-n junction.

3.2.2.3 Optical Modulation

To transmit data across an optical fiber, the information must first be encoded, or modulated, onto the laser signal. Analog techniques include amplitude modulation (AM), frequency modulation (FM), and phase modulation (PM). Digital techniques include amplitude shift keying (ASK), frequency shift keying (FSK), and phase shift keying (PSK). Of all these techniques, binary ASK currently is the preferred method of digital modulation because of its simplicity. In binary ASK, also known as on-off keying (OOK), the signal is switched between two power levels. The lower power level represents a 0 bit, while the higher power level represents a 1 bit.

In systems employing OOK, modulation of the signal can be achieved by simply turning the laser on and off (direct modulation). In general, however, this can lead to chirp, or variations in the laser’s amplitude and frequency, when the laser is turned on. A preferred approach for high bit rates (≥ 10 Gb/s) is to have an external modulator that modulates the light coming out of the laser. To this end, the Mach Zehnder interferometer or electroabsorption modulation are widely utilized [10][13].

3.2.3 Optical Receivers

3.2.3.1 Photodetectors

In receivers employing direct detection, a photodetector converts the incoming photonic stream into a stream of electrons. The electron stream is then amplified and passed through a threshold device. Whether a bit is a logical zero or one depends on whether the stream is above or below a certain threshold for a bit duration. In other words, the decision is made based on whether or not light is present during the bit duration. The basic detection devices for direct-detection optical networks are the PN photodiode (a p-n junction) and the PIN photodiode (an intrinsic material is placed between p- and n- type material). In its simplest form, the photodiode is basically a reverse-biased p-n junction. Through the photoelectric effect, light incident on the junction will create electron-hole pairs in both the “n” and the “p” regions of the photodiode. The electrons released in the “p” region will cross over to the “n” region, and the holes created in the “n” region will cross over to the “p” region, thereby resulting in a current flow.

3.2.4 Optical Amplifiers

Although an optical signal can propagate a long distance before it needs amplification, both long-haul and local lightwave networks can benefit from optical amplifiers. All-optical amplification may differ from optoelectronic amplification in that it may act only to boost the power of a signal, not to restore the shape or timing of the signal. This type of amplification is known as 1R (regeneration), and provides total data transparency (the amplification process is independent of the signal’s modulation format). 1R amplification is emerging as the choice for the transparent all-optical networks of tomorrow. Today’s digital networks [e.g., Synchronous Optical Network (SONET) and Synchronous Digital Hierarchy (SDH)], however, use the optical fiber only as a transmission medium, the optical signals are amplified by first converting the information stream into an electronic data signal and then retransmitting the signal optically. Such amplification is referred to as 3R (regeneration, reshaping, and reclocking). The reshaping of the signal reproduces the original pulse shape of each bit, eliminating much of the noise. Reshaping applies primarily to digitally modulated signals but in some cases it may also be applied to analog signals. The reclocking of the signal synchronizes the signal to its original bit timing pattern and bit rate. Reclocking applies only to digitally modulated signals. Another approach to amplification is 2R (regeneration and reshaping), in which the optical signal is converted to an electronic signal, which is then used to modulate a laser directly. The 3R and 2R techniques provide less transparency than the 1R technique, and in future optical networks, the aggregate bit rate of even just a few channels might make 3R and 2R techniques less practical.

Optical amplification uses the principle of stimulated emission, similar to the approach used in a laser. The two basic types of optical amplifiers are semiconductor laser amplifiers and rare-earth-doped-fiber amplifiers.

3.2.4.1 Doped-Fiber Amplifier

Optical doped-fiber amplifiers are lengths of fiber doped with an element (rare earth) that can amplify light. The most common doping element is erbium, which provides gain for wavelengths of 1525–1560 *nm*. At the end of the length of fiber, a laser transmits a strong signal at a lower wavelength (referred to as the pump wavelength) back up the fiber. This pump signal excites the dopant atoms into a higher energy level. This allows the data signal to stimulate the excited atoms to release photons. Most erbium-doped fiber amplifiers (EDFA's) are pumped by lasers with a wavelength of either 980 or 1480 *nm*.

A limitation to optical amplification is the unequal gain spectrum of optical amplifiers. While an optical amplifier may provide gain across a range of wavelengths, it will not necessarily amplify all wavelengths equally. This characteristic – accompanied by the fact that optical amplifiers amplify noise as well as signal and the fact that the active region of the amplifier can spontaneously emit photons, which also cause noise – limits the performance of optical amplifiers. Thus, a multiwavelength optical signal passing through a series of amplifiers will eventually result in the power of the wavelengths' being uneven.

3.3 Radio over Fiber Optical Links

3.3.1 Introduction to RoF Analog Optical Links

Unlike conventional optical networks where digital signal is mainly transmitted, RoF is fundamentally an analog transmission system because it distributes the radio waveform, directly at the radio carrier frequency, from a CS to a BS. Actually, the analog signal that is transmitted over the optical fiber can either be RF signal, IF signal or baseband (BB) signal. For IF and BB transmission case, additional hardware for upconverting it to RF band is required at the BS. At the optical transmitter, the RF/IF/BB signal can be imposed on the optical carrier by using direct or external modulation of the laser light. In an ideal case, the output signal from the optical link will be a copy of the input signal. However, there are some limitations because of non-linearity and frequency response limits in the laser and modulation device as well as dispersion in the fiber. The transmission of analog signals puts certain requirements on the linearity and dynamic range of the optical link. These demands are different and more exact than requirements on digital transmission systems [10].

3.3.2 Basic Radio Signal Generation and Transportation Methods

In this section, a brief overview of how to generate and transport radio signal over an optical fiber in RoF networks is given. Virtually all of the optical links transmitting microwave/mm-wave signals apply intensity modulation of light [13]. Essentially, three different methods exist for the transmission of microwave/mm-wave signals over optical links with intensity modulation: (1) direct intensity modulation, (2) external modulation, and (3) remote heterodyning [13]. In direct intensity modulation an

electrical parameter of the light source is modulated by the information-bearing RF signal ¹. In practical links, this is the current of the laser diode, serving as the optical transmitter. The second method applies an unmodulated light source and an external light intensity modulator. This technique is called “*external modulation*”. In a third method, RF signals are optically generated via *remote heterodyning*, that is, a method in which more than one optical signal is generated by the light source, one of which is modulated by the information-bearing signal and these are mixed or heterodyned by the photodetector or by an external mixer to form the output RF signal. The external modulation and heterodyne methods are discussed in more detail in subsection 3.3.4. In this subsection, we consider only direct intensity modulation.

Direct intensity modulation is the simplest of the three solutions. So it is used everywhere that it can be used. When it is combined with direct detection using PD, it is frequently referred to as intensity-modulation direct-detection (IMDD) (Fig. 3.7). A direct-modulation link is so named because a semiconductor laser directly converts a small-signal modulation (around a bias point set by a dc current) into a corresponding small-signal modulation of the intensity of photons emitted (around the average intensity at the bias point). Thus, a single device serves as both the optical source and the RF/optical modulator (Fig. 3.7). One limiting phenomenon to its use is the modulation bandwidth of the laser. Relatively simple lasers can be modulated to frequencies of several gigahertz, say, 5–10 GHz. Although there are reports of direct intensity modulation lasers operating at up to 40 GHz or even higher, these diodes are rather expensive or nonexistent in commercial form. That is why at higher frequencies, say, above 10 GHz, external modulation rather than direct modulation is applied. In entering into the millimeter band a new adverse effect, such as the nonconvenient transfer function of the transmission medium, is observed. It turns out that the fiber dispersion and coherent mixing of the sidebands of modulated light may cause transmission zeros, even in the case of rather moderate lengths of fiber. For example, a standard fiber having a one *km* length has a transmission zero at 60 GHz if 1.55 μm wavelength light is intensity modulated. Due to this phenomenon, optical generation rather than transmission of the RF signal is preferable.

Because the number of BSs is high in RoF networks, simple and cost-effective components must be utilized. Therefore, in the uplink of an RoF network system, it is convenient to use direct intensity modulation with cheap lasers; this may require downconversion of the uplink RF signal received at the BS. In the downlink either lasers or external modulators can be used.

3.3.3 RoF Link Configurations

In this section we discuss a typical RoF link configuration, which is classified based on the kinds of frequency bands (baseband (BB), IF, RF bands) transmitted over an optical fiber link. Representative RoF link configurations are schematically shown in Fig. 3.8 [72]. Here, we assume that a BS has its own light source for explanation purpose, however, as will be seen in section 3.3.4 BS can be configured

¹Not only RF but also IF or baseband signal can be used to modulate LD, which is discussed in section 3.3.3.

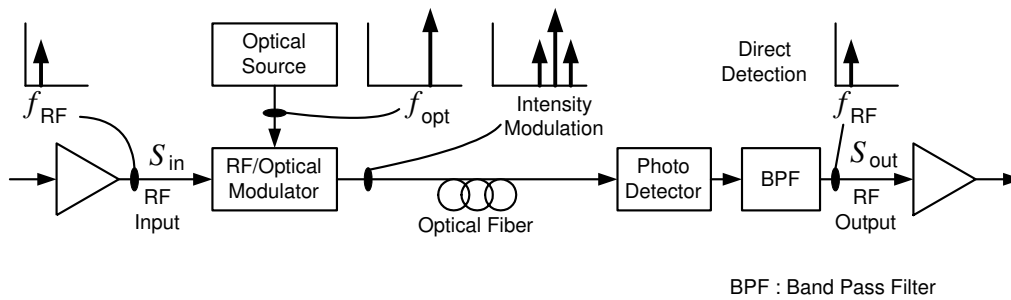


Figure 3.7: Intensity-modulation direct-detection (IMDD) analog optical link.

without light source for uplink transmission. In each configuration of the figure, BSs do not have any equipment for modulation and demodulation, only the CS has such equipment.

In the downlink from the CS to the BSs, the information signal from a public switched telephone network (PSTN), the Internet, or other CS is fed into the modem in the CS. The signal that is either RF, IF or BB bands modulates optical signal from LD. As described earlier, if the RF band is low, we can modulate the LD signal by the signal of the RF band directly. If the RF band is high, such as the mm-wave band, we sometimes need to use external optical modulators (EOMs), like electroabsorption ones. The modulated optical signal is transmitted to the BSs via optical fiber. At the BSs, the RF/IF/BB band signal is recovered to detect the modulated optical signal by using a PD. The recovered signal, which needs to be upconverted to RF band if IF or BB signal is transmitted, is transmitted to the MHs via the antennas of the BSs.

In the configuration shown in Fig. 3.8 (a), the modulated signal is generated at the CS in an RF band and directly transmitted to the BSs by an EOM, which is called “*RF-over-Fiber*”. At each BS, the modulated signal is recovered by detecting the modulated optical signal with a PD and directly transmitted to the MHs. Signal distribution as *RF-over-Fiber* has the advantage of a simplified BS design but is susceptible to fiber chromatic dispersion that severely limits the transmission distance [15]. In the configuration shown in Fig. 3.8 (b), the modulated signal is generated at the CS in an IF band and transmitted to the BSs by an EOM, which is called “*IF-over-Fiber*”. At each BS, the modulated signal is recovered by detecting the modulated optical signal with a PD, upconverted to an RF band, and transmitted to the MHs. In this scheme, the effect of fiber chromatic dispersion on the distribution of IF signals is much reduced, although antenna BSs implemented for RoF system incorporating *IF-over-Fiber* transport require additional electronic hardware such as a mm-wave frequency LO for frequency up- and downconversion. In the configuration (c) of the figure, the modulated signal is generated at the CS in baseband and transmitted to the BSs by an EOM, which is referred to as “*BB-over-Fiber*”. At each BS, the modulated signal is recovered by detecting the modulated optical signal with a PD, upconverted to an RF band through an IF band or directly, and transmitted to the MHs. In the baseband transmission, influence of the fiber dispersion effect is negligible, but the BS configuration is the most

complex. Since, without a subcarrier frequency, it has no choice but to adopt time-division or code-division multiplexing. In the configuration shown in Fig. 3.8 (d), the modulated signal is generated at the CS in a baseband or an IF band and transmitted to the BSs by modulating a LD directly. At each BS, the modulated signal is recovered by detecting the modulated optical signal with a PD, upconverted to an RF band, and transmitted to the MHs. This is feasible for relatively low frequencies, say, less than 10 GHz.

By reducing the frequency band used to generate the modulated signal at the CS such as IF-over-Fiber or BB-over-Fiber, the bandwidth required for optical modulation can greatly be reduced. This is especially important when RoF at mm-wave bands is combined with dense wavelength division multiplexing (DWDM) as will be discussed in section 3.3.5. However, this increases the amount of equipment at the BSs because an upconverter for the downlink and a downconverter for the uplink are required. In the RF subcarrier transmission, the BS configuration can be simplified only if a mm-wave optical external modulator and a high-frequency PD are respectively applied to the electric-to-optic (E/O) and the optic-to-electric (O/E) converters.

For the uplink from an MH to the CS, the reverse process is performed. In the configuration shown in Fig. 3.8 (a), the signals received at a BS are amplified and directly transmitted to the CS by modulating an optical signal from a LD by using an EOM. In the configuration (b) and (c), the signals received at a BS are amplified and downconverted to an IF or a baseband frequency and transmitted to the CS by modulating an optical signal from a LD by using an EOM. In the configuration (d), the signals received at a BS are amplified and downconverted to an IF or a baseband frequency and transmitted to the CS by directly modulating an optical signal from a LD.

3.3.4 State-of-the-Art Millimeter-wave Generation and Transport Technologies

Recently, a lot of research has been carried out to develop mm-wave generation and transport techniques, which include the optical generation of low phase noise wireless signals and their transport overcoming the chromatic dispersion in fiber. Several state-of-the-art techniques that have been investigated so far are described in this section, which are classified into the following four categories [11]:

1. optical heterodyning [16] [17] [18] [19] [20] [21]
2. external modulation [22][23] [24] [25]
3. up- and down-conversion [26] [27] [28] [29] [30]
4. optical transceiver [31] [32] [33] [34] [75]

3.3.4.1 Optical Heterodyning

In optical heterodyning technique, two or more optical signals are simultaneously transmitted and are heterodyned in the receiver. One or more of the heterodyning products is the required RF signal. For

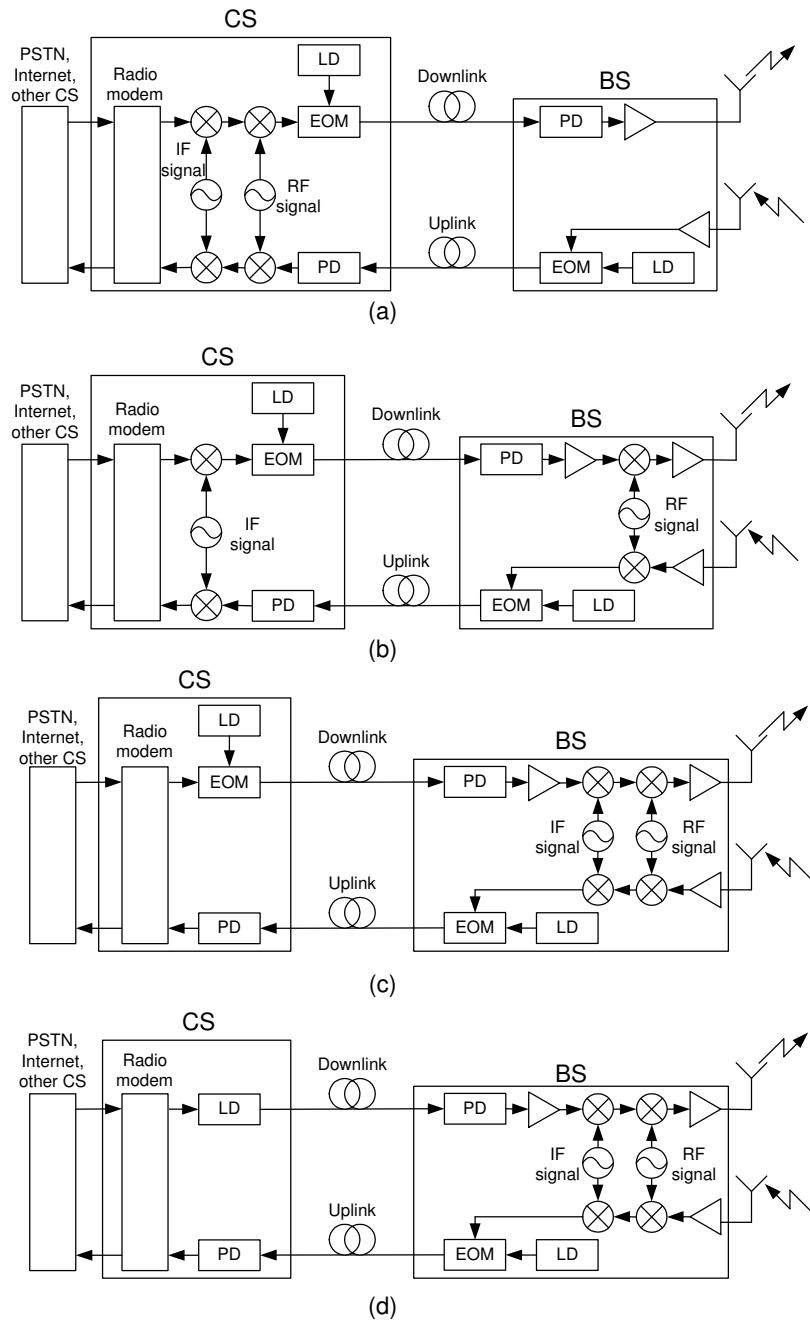


Figure 3.8: Representative RoF link configurations. (a) EOM, RF modulated signal. (b) EOM, IF modulated signal, (c) EOM, baseband modulated signal. (d) Direct modulation.

example, two optical signals with a wavelength separation of 0.5 nm at 1550 nm will generate a beat frequency of around 60 GHz. Heterodyning can be realized by the PD itself or the optical signals can be detected separately and then converted in an electrical (RF) mixer. In a complete (duplex) system, the PD can be replaced by an electroabsorption transceiver.

Because phase noise is a key problem in digital microwave/mm-wave transmission, care must be taken to produce a small phase noise only by the heterodyned signals. This can be achieved if the two (or more) optical signals are phase coherent; in turn, this can be realized if the different frequency optical signals are somehow deduced from a common source or they are phase-locked to one master source. Benefits of this approach are that (1) it overcomes chromatic dispersion effect and (2) it offers a flexibility in frequency since frequencies from some megahertz up to the terahertz-region is possible. However, it uses either a precisely biased electrooptic modulator [17] or sophisticated lasers [18][19][20].

Fig. 3.9 shows a typical design of optical heterodyning [20]. The master laser's intensity is modulated by the unmodulated RF reference signal; several harmonics of the reference signal and consequently several sidebands are generated. The reference laser is injection locked by one of these and the signal laser by another one in such a way that the difference of their frequencies corresponds to the mm-wave local oscillator frequency. And, as seen, the optical field generated by the signal laser is also modulated by the information-bearing IF signal.

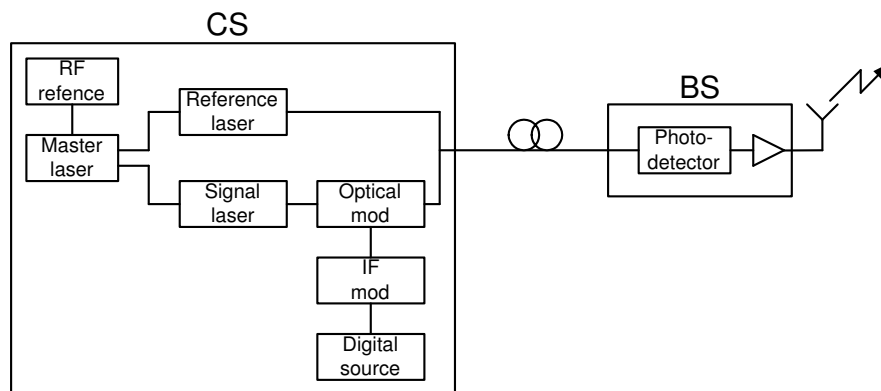


Figure 3.9: Optical heterodyning [20].

3.3.4.2 External Modulation

Although direct intensity modulation is by far the simplest, due to the limited modulation bandwidth of the laser this is not suitable for mm-wave bands. This is the reason why at higher frequencies, say, above 10 GHz, external modulation rather than direct modulation is applied. External modulation is done by a high speed external modulator such as electro-absorption modulator (EAM). Its configuration is simple, but it has some disadvantages such as fiber dispersion effect and high insertion loss. Representative configurations are shown in Fig. 3.8 (a)–(c), where intensity modulation is employed.

In conventional intensity modulation, the optical carrier is modulated to generate an optical field with the carrier and double sidebands (DSB). When the signal is sent over fiber, chromatic dispersion causes each spectral component to experience different phase shifts depending on the fiber link distance, modulation frequency, and the fiber dispersion parameter. If the relative phase between these two components is 180° , the components destructively interfere and the mm-wave electrical signal disappears. To reduce such dispersion effects, optical single-sideband (SSB) is widely used [23][24][25]. Specially designed EAM was developed and experimented at 60 GHz band RoF system in [22][23], while a Mach-Zehnder modulator (MZM) and a fiber Bragg grating filter were used in [24] and [25], respectively, to produce single-sideband optical modulation.

3.3.4.3 Up- and Down-conversion

In this technique IF band signal is transported over optical fiber instead of RF band signal. The transport of the IF-band optical signal is almost free from the fiber dispersion effect, however, the electrical frequency conversion between the IF-band and mm-wave requires frequency mixers and a mm-wave LO, resulting in the additional cost to the BS. Another advantage of this technique is the fact that it occupies small amount of bandwidth, which is especially beneficial when the system is combined with DWDM as is described in section 3.3.5. A representative configuration is shown in Fig. 3.8 (b).

3.3.4.4 Optical Transceiver

The simplest BS structure can be implemented with an optical transceiver such as electro-absorption transceiver (EAT). It serves both as an O/E converter for the downlink and an E/O converter for the uplink at the same time. Two wavelengths are transmitted over an optical fiber from the CS to BS. One of them for downlink transmission is modulated by user data while the other for uplink transmission is unmodulated (Fig. 3.10). The unmodulated wavelength is modulated by uplink data at the BS and returns to the CS. That is, an EAT is used as the photodiode for the data path and also as a modulator to provide a return path for the data, thereby removing the need for a laser at the remote site. This device has been shown to be capable of full duplex operation in several experiments at mm-wave bands [31] [32] [33] [34]. A drawback is that it suffers from chromatic dispersion problem. Fig. 3.10 shows an RoF system based on EAT developed in [34]. Note that two wavelengths are always needed for up- and downlink communication, and full-duplex operation is possible.

3.3.4.5 Comparison of mm-wave Generation and Transport Techniques

Table 3.1 summarizes the advantages and the disadvantages of the four techniques described above [11]. In addition, Table 3.2 shows some experimental results reported in the literature. It suggests that at mm-wave bands very high bit rate up to 155 Mbps is easily feasible. This implies that together with small cell size (picocell) RoF technology can provide much higher capacity than conventional wireless networks at microwave bands such as 2.4 or 5 GHz.

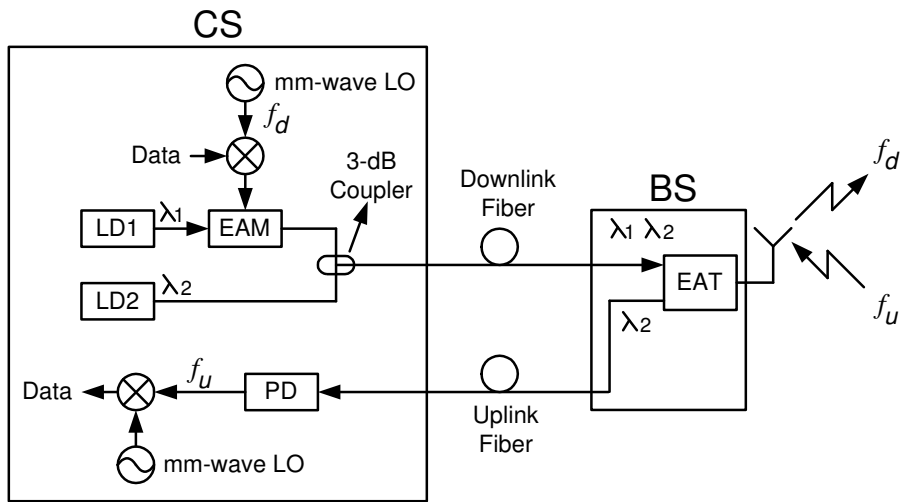


Figure 3.10: Electroabsorption transceiver (EAT).

Table 3.1: Comparison of Millimeter-wave Generation and Transport Techniques

Techniques	Advantages	Disadvantages
Optical Heterodyning	Full modulation depth Fiber dispersion effect free No mm-wave OSC	Complicated light source
External Modulation	Simple configuration DFB LD	Fiber dispersion effect High insertion loss Nonlinear response High-freq. EAM
Up- and down-conversion	Direct IF modulation Fiber dispersion effect free	mm-wave OSC High-freq. EAM
Optical Transceiver	Modulator/Photodetector	High-freq. EAM WDM

Table 3.2: Millimeterwave-band RoF Experiments

Techniques	RF band (GHz)	IF Band (GHz)	Bit Rate (Mbps)	Modulation	Fiber length (km)	Ref.
Optical Heterodyning	64	–	155	OQPSK	12.8	[20]
	60	–	155.52	DPSK	25	[21]
External Modulation	59.6	2.6	156	DPSK	50	[22]
	60.0,59.6	3.0,2.6	156	DPSK	85	[23]
Up- and down-Conversion	40	3.0	156	DPSK	50	[30]
	40	3.0	155(down) 51.8(up)	BPSK	40	[29]
Optical Transceiver	60	–	120	QPSK	13	[31]
	60,59.6	3.0,2.6	155.52	DPSK	27.5	[33]

3.3.5 RoF and Wavelength Division Multiplexing (WDM)

The application of WDM in RoF networks has many advantages including simplification of the network topology by allocating different wavelengths to individual BSs, enabling easier network and service upgrades and providing simpler network management. Thus, WDM in combination with optical mm-wave transport has been widely studied [36]–[43]. A schematic arrangement is illustrated in Fig. 3.11, where for simplicity, only downlink transmission is depicted. Optical mm-wave signals from multiple sources are multiplexed and the composite signal is optically amplified, transported over a single fiber, and demultiplexed to address each BS. Furthermore, there have been several reports on dense WDM (DWDM) applied to RoF networks [36][37][43]. Though a large number of wavelengths is available in the modern DWDM technologies, since mm-wave bands RoF networks may require even more BSs wavelength resources should be efficiently utilized.

A challenging issue is that the optical spectral width of a single optical mm-wave source may approach or exceed WDM channel spacing. For example, Fig. 3.12 shows an optical spectrum of DWDM mm-wave RoF signals with optical DSB modulation (a) and SSB modulation (b), where we assume that the carrier frequency of the mm-wave signal is 60 GHz. Fig. 3.12 (a) indicates that to transmit single data channel at 60 GHz band, more than 120 GHz bandwidth is necessary for DSB modulation. In addition, from a viewpoint of cost reduction, it is preferable to use the channel allocation in accordance with ITU grid because of the availability of optical components. Then, the minimum channel spacing in this case is 200 GHz [43]. In case of SSB modulation, this is 100 GHz as shown in Fig. 3.12 (b). To increase the spectral efficiency of the system, the concept of optical frequency interleaving has been proposed [41][43].

Another issue is related to the number of wavelengths required per BS. It is desirable to use one wavelength to support full-duplex operation. In [40], a wavelength reuse technique has been proposed, which is based on recovering the optical carrier used in downstream signal transmission and reusing the same wavelength for upstream signal transmission.

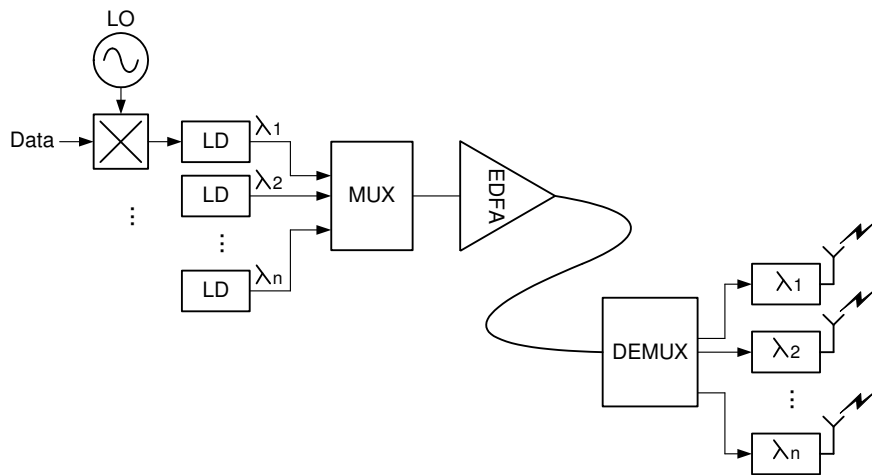


Figure 3.11: Schematic illustration of a combination of DWDM and RoF transmission.

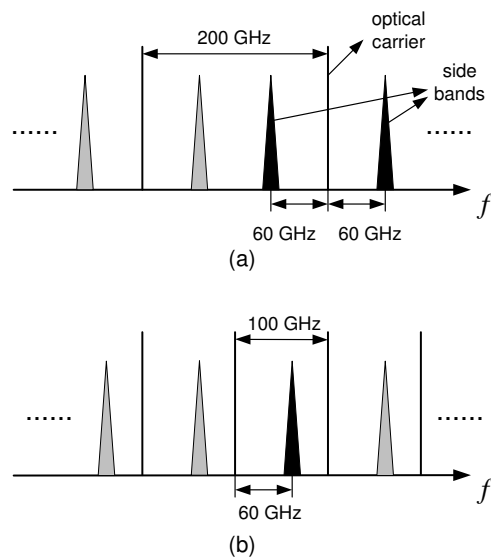


Figure 3.12: Optical spectra of DWDM mm-wave RoF signals of conventional optical (a) DSB and (b) SSB.

Fig. 3.13 shows a typical unidirectional fiber ring architecture that can be used for the delivery of broadband wireless services [38][77]. In the CS, all down- and uplink light sources are multiplexed and amplified. The modulated downlink channels and the unmodulated uplink channels are fed into the fiber backbone of the ring network. At each BS, a pair of down- and uplink wavelengths is dropped through an OADM to the EAT, which simultaneously detects and modulates the down- and uplink channel, respectively. The modulated uplink channels are added to the backbone again, looped back to the CS, where they are demultiplexed and detected. The major advantage of this point-to-multipoint WDM ring network is the centralization of all required light sources in the CS, allowing for a simple BS configuration.

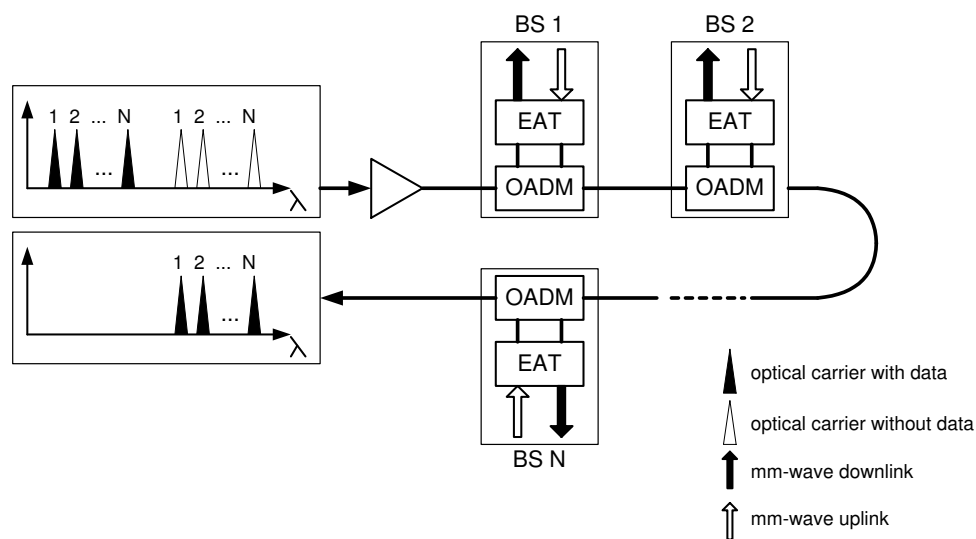


Figure 3.13: RoF ring architecture based on DWDM [38].

3.4 Summary

In this chapter a brief description of conventional optical transmission link and basic optical components was given, and RoF technologies have been described including typical RoF link configurations, state-of-the-art mm-wave generation and transport techniques, and RoF system combined with WDM. Due to its potentiality to support broadband service with little infrastructure and many advantages such as cost-effectiveness, easy deployment, maintenance RoF networks will be a promising alternative to future wireless networks.

Chapter 4

Chess Board Protocol: MAC protocol for WLAN at 60 GHz Band

4.1 Introduction

Millimeter-wave access technology is being proposed for the future distribution of broadband services as mm-wave band offers a large transmission bandwidth and overcomes spectral congestion in the lower microwave frequency regions. Of all the mm-wave bands, especially, the 60 GHz band is of much interest since a massive amount of license-free spectrum has been allocated with a worldwide overlap of 3 GHz (59–62 GHz) [2]. However, due to its high propagation loss and penetration loss cell size becomes very small. In indoor environment, every room should have at least one BS; therefore, simple and cost-effective BS will be a key to the success of the system.

RoF based WLAN is a promising alternative to the system, since in this network functionally simple BSs are used that are interconnected to a CS via an optical fiber, while signal routing and processing functions are centralized at the CS. Recent research activities in this field suggest that cost-effective and simple BSs are expected to be available in the near future [9],[10],[12],[21],[23],[30]. However, in this system small movement of an MH can cause handover request, suggesting a challenging problem that is quite different from conventional WLAN systems at microwave bands. In this chapter, we propose an MAC protocol called “*Chess Board protocol*” for RoF based WLAN operating at 60 GHz band, featuring fast and easy handover and QoS support. Using the capability of centralized control of RoF networks it depends on frequency switching (FS) codes for providing simple handover, and adjacent picocells employ orthogonal FS codes to avoid possible co-channel interference. This mechanism allows an MH to stay tuned to its frequency during handover, which is a major characteristic of the Chess Board protocol. Important parameters of the protocol are analyzed and minimum handover latency derived from them is discussed. Simple delay-throughput analysis without user mobility as well as a more realistic simulation study are performed to investigate the properties of the protocol.

The chapter begins with a description of the RoF network architecture on which the proposed

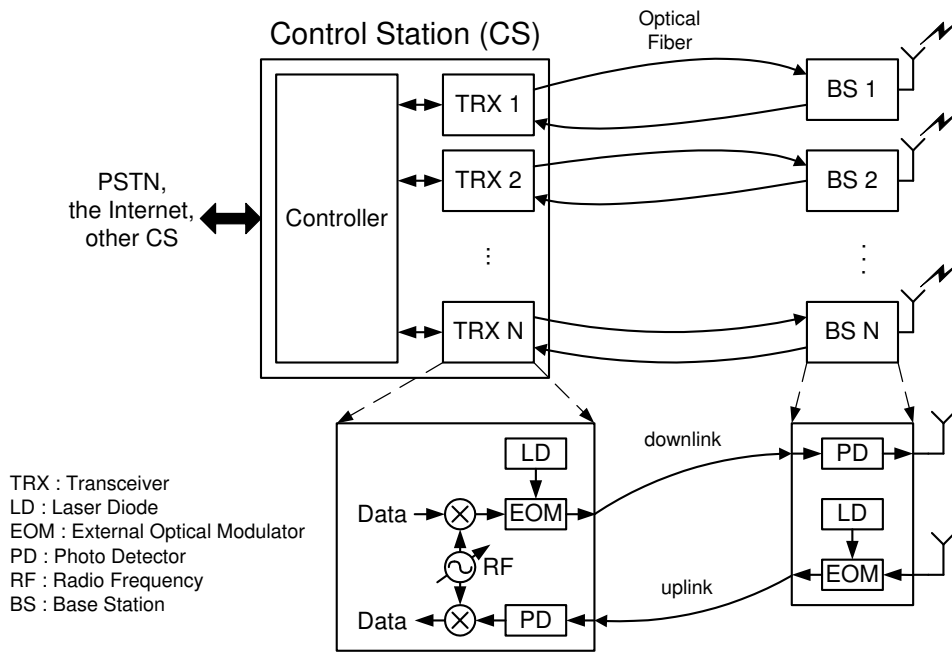


Figure 4.1: Radio over fiber network architecture.

WLAN is based in section 4.2. In section 4.3 Chess Board protocol along with system setup, basic operation, and mobility support is described. The important parameters of the protocol are considered in section 4.4, which is followed by simple delay-throughput analysis in section 4.5. Performance evaluation is reported in section 4.6. Finally, the chapter ends up with conclusion in section 4.7.

4.2 Network Architecture

The RoF network assumed in this study must have the following capabilities: (1) frequency division duplexing (FDD) and (2) dynamic RF channel change. Fig. 4.1 shows an example RoF architecture having such capability. It utilizes subcarrier modulation technique that is widely used in RoF networks [13]. In the technique for downlink transmission (from CS to MH) user data first modulates RF source (called “subcarrier”) which, in turn, modulates optical carrier (called “main carrier”) from light source. This signal is carried over the downlink optical fiber to a BS, where the optical signal is converted into wireless signal which is emitted from the BS. For uplink transmission (from MH to CS), the wireless signal received at the BS is changed into optical signal by modulating light source. It is then transported over uplink optical fiber to the CS, where a PD first demodulates optical signal to obtain electrical signal which is again demodulated using oscillator to acquire user data. In this architecture the CS has as many transceivers (TRXs) as BSs, and each transceiver contains at least 1) a light source such as LD and an EOM for downlink transmission, 2) a PD for uplink reception, and 3) a modem to transmit and receive user data in the RF domain. The BS is basically composed of a PD, an LD, and an EOM, and it has no processing functions. When RF is high (e.g., > 10 GHz), external modulation technique is usual that is

depicted in the figure since we are concerned with RoF networks at 60 GHz band in this study [10]. For flexibility in RF channel change, we assume each transceiver is equipped with a tunable oscillator.

4.3 Chess Board Protocol Description

4.3.1 System Setup

Due to 60 GHz wave characteristics every room in a building is covered by at least one picocell, each having its own BS (Fig. 4.2 (a)). It becomes immediately obvious that in such system with high number of very small cells, the issue of efficient mobility management has a very special significance.

We assume that the system works in FDD mode, since most optic-wireless converters developed thus far support this mode [29],[33],[34]. By subdividing the total system bandwidth (BW_{total}), $2C$ (frequency) channels are obtained, where C channels (f_1, f_2, \dots, f_C) are used for downlink transmission and the other C channels ($f_{C+1}, f_{C+2}, \dots, f_{2C}$) for uplink transmission (Fig. 4.2 (b)). Note that the bandwidth – i.e., the frequency spectrum – assigned to the uplink and to the downlink does not have to be identical, making it possible to support asymmetric traffic. In addition, the time axis is also subdivided into time slots of equal length and C time slots are grouped into a frame (Fig. 4.2 (d)).

4.3.2 Basic Operations

The MH is assigned a pair of channels (f_i, f_{C+i}), $i = 1, 2, \dots, C$ and a pair of time slots ($t_{k \bmod C}, t_{k+1 \bmod C}$), $k = 1, 2, \dots$ for downlink and uplink communication, respectively. Only after having received a permit from the downlink channel f_i during the time slot $t_{k \bmod C}$, the MH may transmit uplink packets over the uplink channel f_{C+i} during the next time slot $t_{k+1 \bmod C}$. Every BS supports all channels, but each of them is used in the proper time slot. Fig. 4.2 shows an example of FS patterns for downlink and uplink, respectively, when C is five. During every frame time, each of the C time slots and C channels is utilized once and only once. Adjacent picocells must not use the identical FS pattern to avoid possible co-channel interference. One FS pattern used by one picocell can be reused by another picocell if they are sufficiently spaced from one another to avoid interference. For proper operations using FS patterns, we assume that the system is synchronous, i.e., all system components especially the CS and MHs have the same notion of time slots. The synchronous operation of all cells, however, is enabled by the centralized architecture. A sketch of the operation may be the following. Since the CS may initially measure the round-trip time (RTT) to any BS, it is then possible to transmit downlink slots towards that BS $RTT/2$ in advance. This leads to a fully slotted system.

Notice that this frequency switching concept in Chess Board protocol is not new. Indeed, this is widely used in frequency hopping system, e.g., in Bluetooth. The differences between conventional frequency hopping system and Chess Board protocol are: (1) in conventional frequency hopping system, BS as well as MHs are changing frequency channels according to prespecified (normally pseudo random pattern) frequency hopping pattern, on the other hand in Chess Board protocol only BS changes

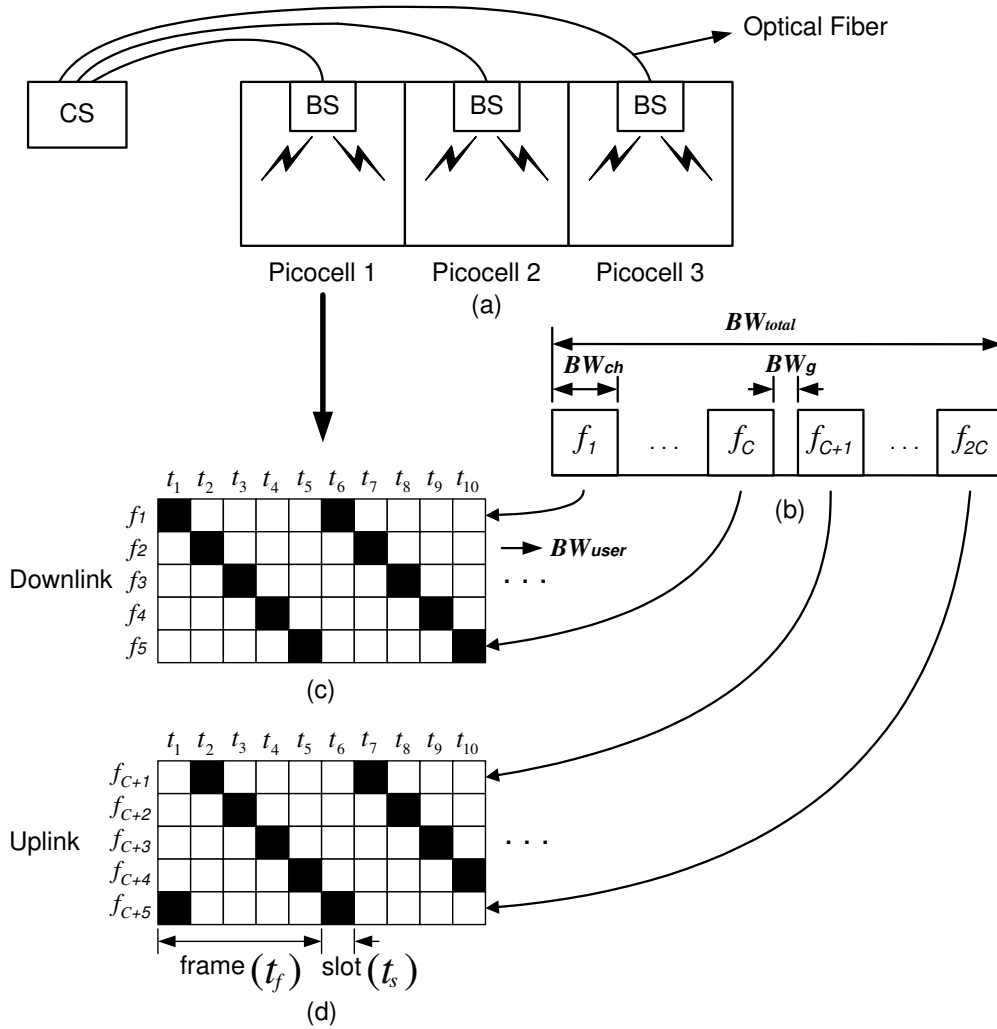


Figure 4.2: System description. (a) An RoF WLAN system operating in the millimeter-wave band, (b) the total system bandwidth (BW_{total}) is subdivided into $2C$ channels, where BW_{ch} and BW_g are the channel bandwidth and the guard bandwidth, respectively, (c) and (d) show frequency switching patterns for downlink and uplink transmissions when the number of channels (C) is five. Note that the per user bandwidth (BW_{user}) is BW_{ch}/C .

frequency channels while MHs staying tuned to a pair of channels, (2) due to centralized network architecture, Chess Board protocol can support synchronous operation to avoid co-channel interference, resulting in zero hitting probability between two frequency switching patterns used in adjacent picocells. Whereas in conventional frequency hopping system, normally asynchronous operation is assumed between two frequency hopping patterns. Thus, it has non-zero hitting probability between two frequency hopping patterns. In order to differentiate the Chess Board protocol from conventional frequency hopping system, we refer to frequency switching instead of frequency hopping.

Fig. 4.3 shows downlink and uplink slot formats and essentially, they have the same format. The downlink slot begins with an MAC address indicating the destination of the slot. This MAC address is followed by a permission field, which authorizes transmission of the MH specified in the MAC address in the following uplink slot. The next field is for downlink payload, destined to the MH specified by the MAC address. The last field consists of another MAC address and reservation result, which indicates whether the request for bandwidth from the addressed MH is successfully confirmed or not.

The uplink slot constitutes two parts. The first one is used for uplink data transmission consisting of MH's MAC address, piggyback field, and payload field. The second part is used for reservation only by MHs that have not yet succeeded in reservation. If the piggyback field is set, it means that MH still has more data to send and requests assignment of one more slot. Non-setting this field indicates that its transmit buffer is empty. Each payload field (both uplink and downlink) allows packing several small packets or fragmentation for a large size packet. To request a permit for uplink transmission on some channel, the MH sends a request to the CS using the reservation field in any slot in this channel (Fig. 4.3). Note that the slot formats in the figure is an example that has minimum fields necessary for the protocol to work properly. Different slot formats is possible while keeping the basic operation rule of Chess Board protocol. For instance, more than one minislots can be assigned to reduce reservation time, or multiple MAC addresses may be contained in the downlink slot to transport multiple downlink packets to MHs specified by the MAC addresses. In addition, a variety of QoS requirements for each communication session can be met using different scheduling algorithm. Scheduling issue is not our concern and will not be treated any more in this study. Instead, simple six variants of Chess Board protocol will be considered in section 4.6.

4.3.3 Mobility Support

As long as an MH remains tuned to a certain frequency channel pair and time slot pair it can expect the time instants at which downlink slots arrive. However, when it moves into an adjacent picocell using a different FS pattern, the MH will receive the downlink slot in an unexpected time instant. Thus, the MH can easily realize within at most a single frame time ($t_f = C \cdot t_s$) that it moved into another picocell (i.e., the number of channels (C) and the slot size (t_s) determines the minimum handover latency). Furthermore, using the following slot for the uplink transmission the MH can and should make a reservation in the new pair of time slots. Note that the CS knows that the MH with this MAC address has been transmitting previously in a different picocell, so it is possible a) to treat such request

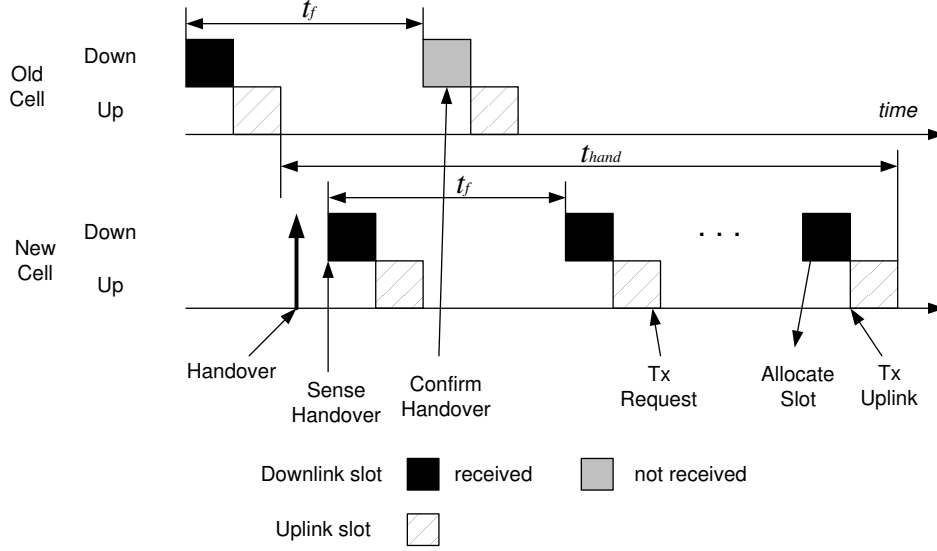


Figure 4.4: Handover latency is defined as an interval between two time instants at which uplink packet transmissions are completed in the old and new picocells.

the link to the old BS is not valid any more, the MH sends a request to the new picocell to be allocated bandwidth. If the request is successful and uplink slot is allocated to the MH in the next frame, the minimum handover latency will be $2C + 1$ slots.

4.3.4 Initialization

When a new MH comes into the system, the first action it has to take is to select a channel randomly if it has the capability to change channels or to use the prespecified channel if it has no ability to change channels, and keep listening on the downlink channel. Within at most t_f , it will receive a downlink packet. After having done that it can send in a following slot on an uplink channel a first reservation request for uplink transmission permits.

4.4 Parameters of Chess Board Protocol

The proposed MAC protocol has two major parameters: (1) the number of channels C and (2) the slot length L_s . Some constraints on the two parameters and minimum handover latency derived from them are discussed in this section.

4.4.1 The Number of Channels

If we assume that the total system bandwidth (BW_{total}) is fixed, guard bandwidth (BW_g) is zero, and downlink and uplink channel bandwidths are of the same size ($BW_{down} = BW_{up} \triangleq BW_{ch}$), the sum of all channel bandwidth ($2C \cdot BW_{ch}$) must be less than or equal to BW_{total} (see Fig. 4.6). That is,

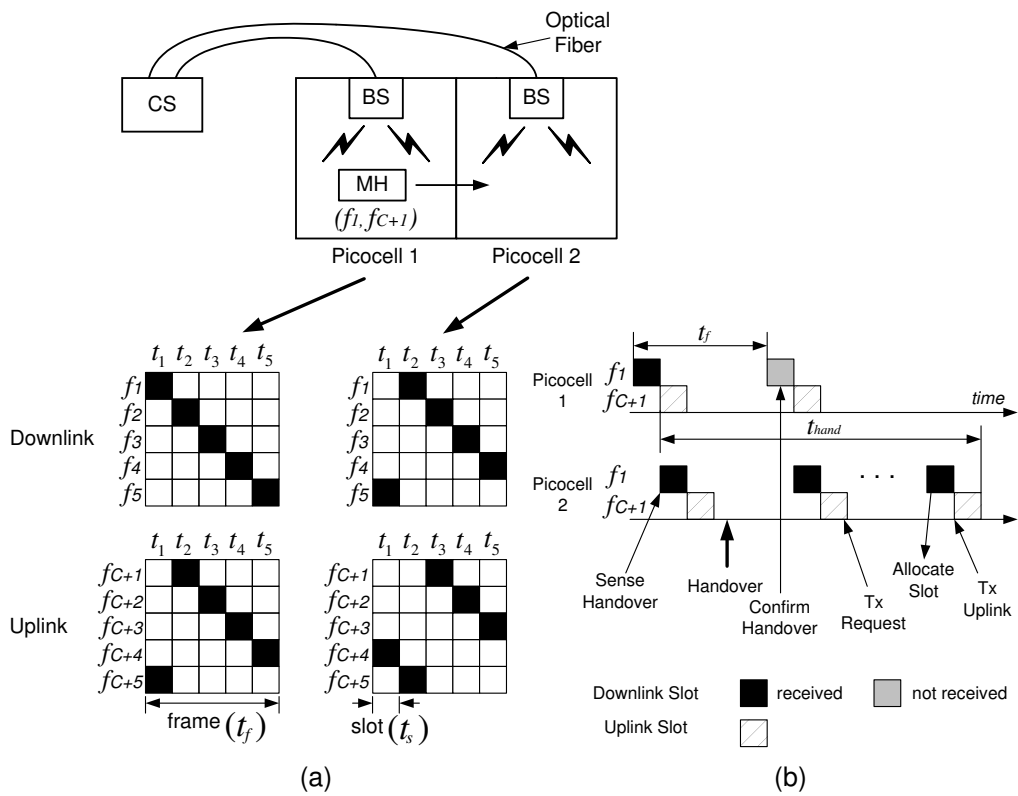


Figure 4.5: Handover example. MH using (f_1, f_{C+1}) moves from picocell 1 to picocell 2. (a) FS patterns used in each cell and (b) handover latency.

$$2C \cdot BW_{ch} \leq BW_{total}$$

Moreover, since the per user bandwidth BW_{user} is obtained by dividing the channel bandwidth (BW_{ch}) by C (see Fig. 4.2) we have

$$2C^2 \cdot BW_{user} \leq BW_{total}$$

As C must be an integer value, we have

$$C \leq \left\lfloor \sqrt{\frac{BW_{total}}{2 \cdot BW_{user}}} \right\rfloor$$

where $\lfloor x \rfloor$ is the largest integer less than or equal to x . Thus, the maximum number of channels is given by

$$C_{max} = \left\lfloor \sqrt{\frac{BW_{total}}{2 \cdot BW_{user}}} \right\rfloor$$

Since BW_{ch} consists of uplink, downlink bandwidth and two guard bandwidths, the relationship is represented by

$$C \leq \left\lfloor \sqrt{\frac{BW_{total}}{BW_{up} + BW_{down} + 2 \cdot BW_g}} \right\rfloor$$

As an example when a given total system bandwidth is 3 GHz with a desired per user data rate (BT_{user}) of 20 Mbps (assuming a 1 bit/Hz coding efficiency, $BW_{up} = BW_{down}$, $BW_g = 0$ and $2BT_{user} = BW_{up} + BW_{down}$), C is less than or equal to eight. In this case the above equation becomes

$$C \leq \left\lfloor \sqrt{\frac{BW_{total}}{2 \cdot BT_{user}}} \right\rfloor \quad (4.2)$$

Note here that by $BT_{user} = 20$ Mbps we mean that an MH can carry out uplink and downlink communication at a rate of 20 Mbps, respectively. Fig. 4.7 shows the maximum number of channels vs. per user data rate with different total bandwidths. As will be explained, the minimum number of channels is three that is also depicted in the figure.

4.4.2 Slot length

From the assumption that an MH receives the reservation result in the next frame after it sends a request in the current frame, we can derive a simple relation for the slot length given by

$$L_s \geq \left\lceil \frac{(2 t_{prop} + t_{proc}) \cdot C \cdot BT_{user}}{C - 2} \right\rceil, \quad C \geq 3 \quad (4.3)$$

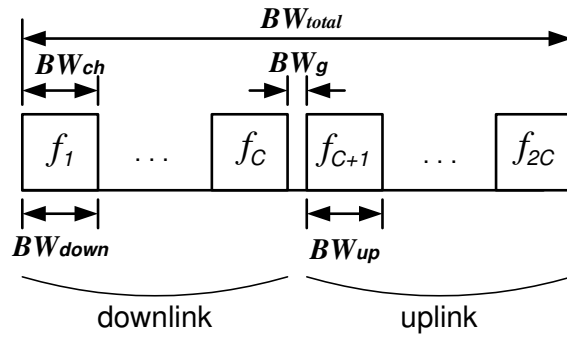


Figure 4.6: Bandwidth allocation.

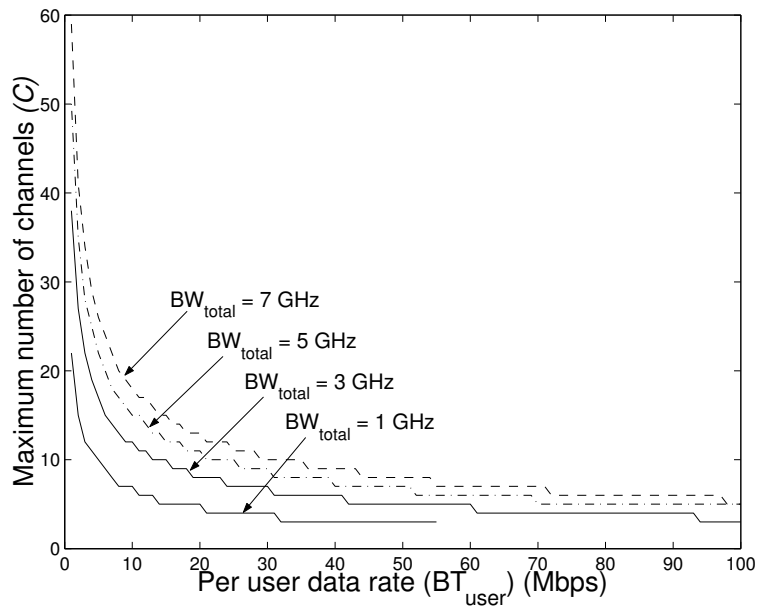


Figure 4.7: The maximum number of channels (C_{max}) vs. per user data rate (BT_{user}). It is assumed that $BW_g = 0$, $BW_{down} = BW_{up} = BT_{user}$ and coding efficiency is 1 bit/Hz.

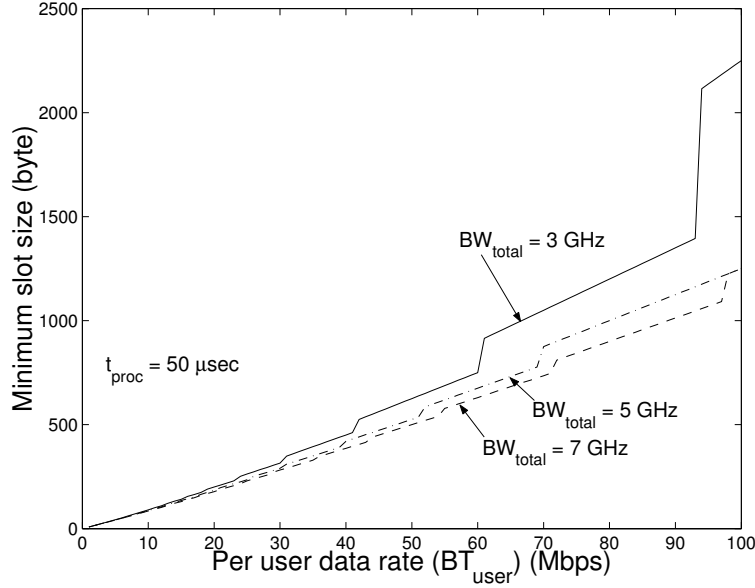


Figure 4.8: The minimum slot length vs. per user data rate with different BW_{total} values when the distance between the CS and BS is 1000 m and $t_{proc} = 50\ \mu\text{sec}$.

where L_s is the slot length in bits, t_{prop} is the propagation delay in seconds including the delay over an optical fiber as well as in the air, t_{proc} is the processing time spent by the CS to process reservation request, and $\lceil x \rceil$ is the smallest integer greater than or equal to x .

Given the number of channels (C), the derivation procedure of Eq. (4.3) is as follows. Suppose an MH sends a request at the end of an uplink slot to the CS at time $t = 0$, then the CS receives the whole packet at time $t = t_{prop}$ assuming reservation slot size is negligible when compared to the whole uplink slot. Note here that the reservation result must be available at the MH before the rest $(C - 1)$ packets are transmitted. After processing for reservation (t_{proc}), the CS transmits downlink packet including the reservation result, which will be received completely at time $t = 2 \cdot t_{prop} + t_{proc} + t_s$ by the MH. This value must be smaller than or equal to $(C - 1) \cdot t_s$, which results in Eq. (4.3).

From the equation we see two important facts. First, the minimum slot length is obtained when C is the maximum value that can be derived from Eq. (4.2). Second, the number of channels must be greater than or equal to three (see the denominator of the equation), which is a lower bound of the number of channels C . Fig. 4.8 shows the minimum slot length in bytes vs. per user data rate when the distance between the CS and BS is 1000 m and t_{proc} is $50\ \mu\text{sec}$ with the assumption that the signal transmission speed over an optical fiber is $2.0 \times 10^8\text{ m/s}$. The minimum slot length depends on the propagation delay (t_{prop}), i.e. the distance between the CS and the BS, processing time at the CS and total system bandwidth. Since the maximum number of channels increases as the total system bandwidth grows the minimum slot size in turn decreases provided the per user data rate, propagation and processing delay remain the same. Table 4.1 presents the minimum slot length in bytes when BW_{total} is 3 GHz , t_{prop} is $5\ \mu\text{sec}$ and t_{proc} is $50\ \mu\text{sec}$.

Table 4.1: Minimum slot length (bytes) when BW_{total} is 3 GHz, t_{prop} is 5 μsec and t_{proc} is 50 μsec

BT_{user} (Mbps)	The number of channels										max ch.
	3	4	5	6	7	8	9	10	11	12	
10	225	150	125	113	105	100	97	94	92	90	12
20	450	300	250	225	210	200					8
30	675	450	375	338	315						7
40	900	600	500	450							6
50	1125	750	625								5
60	1350	900	750								5
70	1575	1050									4
80	1800	1200									4
90	2025	1350									4
100	2250										3
110	2475										3
120	2700										3
130	2925										3
140	3150										3
150	3375										3
160	3600										3

4.4.3 Handover Latency

Since the minimum slot time t_s is $(2 \cdot t_{prop} + t_{proc}) / (C - 2)$, Eq. (4.1) can be rephrased as follows.

$$(2C + 1) \cdot \left(\frac{2 \cdot t_{prop} + t_{proc}}{C - 2} \right) \leq \min(t_{hand}) \leq (3C - 1) \cdot \left(\frac{2 \cdot t_{prop} + t_{proc}}{C - 2} \right) \quad (4.4)$$

where $3 \leq C \leq \left\lfloor \sqrt{\frac{BW_{total}}{2 \cdot BT_{user}}} \right\rfloor$ assuming a 1 bit/Hz coding efficiency, $BW_{up} = BW_{down}$, $BW_g = 0$ and $2BT_{user} = BW_{up} + BW_{down}$. It is obvious that the minimum handover latency is also acquired when the number of channels has the maximum value.

Fig. 4.9 shows the minimum handover latency vs. the per user data rate with the above assumptions when the distance between the CS and BS is 1000 m and t_{proc} is 50 μsec , where the left part of Eq. (4.4) was used with $C = \left\lfloor \sqrt{\frac{BW_{total}}{2 \cdot BT_{user}}} \right\rfloor$. Although the minimum handover latency increases with BT_{user} , it is less than 0.5 msec when BT_{user} is smaller than 100 Mbps. From the figure it is clear that as the total system bandwidth increases since the maximum number of channels also grows the minimum handover latency becomes smaller. This implies that Chess Board protocol potentially has far smaller handover latency compared to other conventional wireless systems.

4.5 Delay-Throughput Analysis

In this section an analytic model using two-dimensional Markov chain for Chess Board protocol is developed to investigate delay-throughput characteristics.

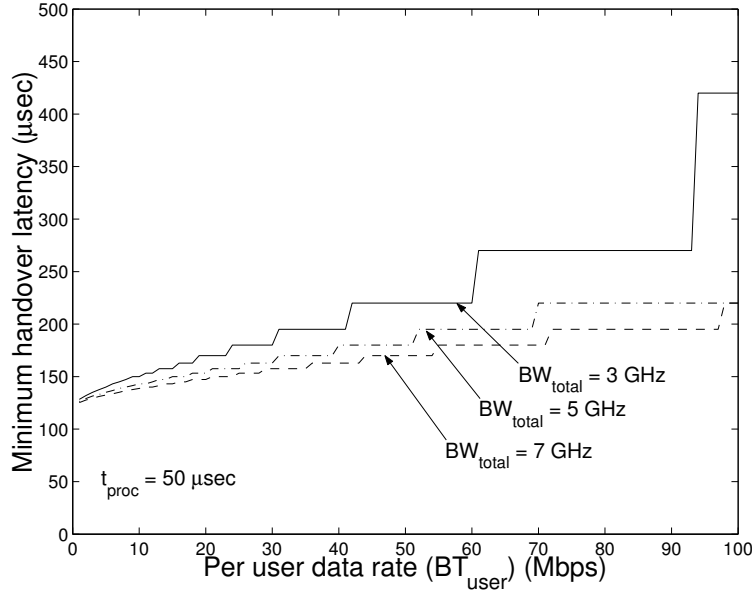


Figure 4.9: The minimum handover latency vs. per user data rate with different BW_{total} values when the distance between the CS and BS is 1000 m and $t_{proc} = 50 \mu sec$.

4.5.1 System Model

Only one picocell without mobile users is considered, i.e., there is no MHs coming in and going out of the picocell. Thus, we use a term “node” instead of MH in this section. Fig. 4.10 demonstrates a system model for analysis, where downlink slot contains information about downlink data, assignment of uplink slot and result of requests that have been transmitted in the previous frame, while uplink slot constitutes one data slot and K minislots for uplink requests. When a node has the data to transmit, it must first send a request with probability σ using one of the K minislots chosen at random. If the request is successful, the CS enqueues it and the requests in the queue are served in first-in-first-out (FIFO) fashion. When the request collides with other requests, the node retransmits the request with probability σ in the next uplink slot. After having received a permission from the CS, i.e., from the corresponding downlink channel, the node can send its uplink packet using data slot. Data slot is used on a reservation basis, free of conflict. Since downlink communication is simple, only uplink performance is considered. When there are M nodes and C (uplink) channels in a cell, we assume that one channel is shared by $M_c = M/C$ nodes. Furthermore, for simplicity, M is assumed to be divisible by C .

For analysis the following assumptions are made:

- A node generates a fixed-size packet according to Bernoulli process with blocked calls lost, i.e., an input buffer consists of one message and a node generates a new message with probability p during a frame time.
- Transmission of reservation packets have random access to the K minislots without retransmission discrimination, i.e., a reservation packet is transmitted into one of the minislots with probability σ

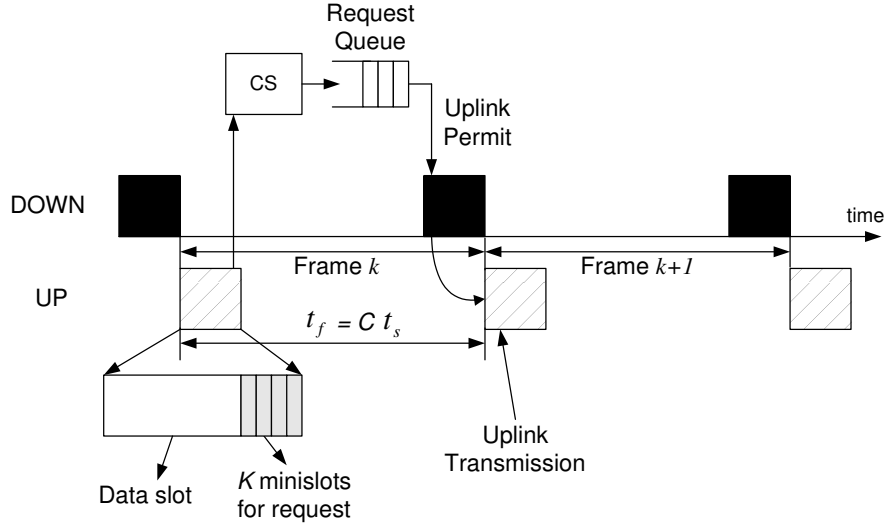


Figure 4.10: System model for analysis. Successful requests from nodes are enqueued in the CS and served in FIFO mode, and assignment of uplink slot is informed through downlink slot. Uplink slot consists of one data slot and K minislots for requests.

regardless of whether it is a new or a retransmitted packet.

- Messages generated by nodes consist of one data packet.
- Each uplink slot has one data slot and K minislots for uplink requests and the size of minislot is negligible relative to data slot.
- The result of uplink requests is broadcast in the next downlink slot.
- The queuing discipline in the request queue at the CS is FIFO.

From the above assumptions system analysis becomes simple that only one channel is considered with a population of M/C for which one uplink slot is available every frame time.

4.5.2 Analysis

Define the system state at the beginning of frame k by a two-dimensional vector,

$$S_k = (N_1^k, N_2^k) \in \mathbf{S}$$

where

$$\begin{aligned} N_1^k &\in \{0, \dots, M_c\} \\ N_2^k &\in \{0, \dots, M_c - N_1^k\} \end{aligned}$$

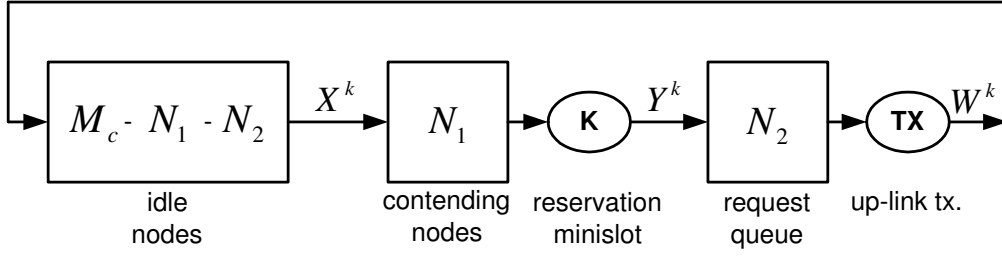


Figure 4.11: Markov chain model with finite population for one channel which is shared by $M/C = M_c$ nodes.

represent the number of nodes in contention mode and in the request queue at the CS, respectively, at the beginning of frame k and M_c is the number of nodes using the channel as described in Fig. 4.11. Thus, the dimension of the state space is

$$|\mathbf{S}| = \frac{(M_c + 2)(M_c + 1)}{2} \quad (4.5)$$

Now we define the dynamic equations of the system that dictate the system state transitions. Let X^k be the number of new packets generated from idle nodes (see Fig. 4.11) in frame k , Y^k be the number of successful reservation requests sent in frame k , and W^k be the number of packet transmissions that are successfully completed in frame k . Then, the set of dynamic equations can be written by

$$\begin{aligned} N_1^{k+1} &= N_1^k + X^k - Y^k \\ N_2^{k+1} &= N_2^k + Y^k - W^k \end{aligned}$$

In order to derive the probability distribution of Y^k , we need the following expression. It describes the probability, as derived in [70], that v minislots have exactly one request, given that u requests are placed and there are K minislots for reservation requests.

$$\begin{aligned} B(u, v|K) &\triangleq Pr[u \text{ successful requests} | v \text{ requests were transmitted in } K \text{ minislots}], \\ &= Pr[Y^k = u | v \text{ requests were transmitted in } K \text{ minislots}], \\ &= \frac{(-1)^u K! v!}{u! K^v} \sum_{x=u}^{\min(K, v)} (-1)^x \frac{(K-x)^{v-x}}{(x-u)!(K-x)!(v-x)!} \end{aligned} \quad (4.6)$$

Then, the probability distribution of Y^k given (N_1, N_2) is represented by

$$Pr[Y^k = u | N_1^k, N_2^k] = \sum_{v=0}^{N_1^k} \binom{N_1^k}{v} \sigma^v (1-\sigma)^{N_1^k-v} B(u, v|K)$$

where σ is the probability of transmitting requests. If we assume that the idle nodes generate packets according to Bernoulli distribution with a packet generation probability of p , the probability distribution of X^k is obtained from

$$Pr[X^k = x | N_1^k, N_2^k] = \binom{M_c - N_1^k - N_2^k}{x} p^x (1-p)^{M_c - N_1^k - N_2^k - x}$$

As uplink slot has one data slot, W^k is

$$W^k = \min(N_2^k, 1)$$

Then, the state transition probability is expressed as

$$\begin{aligned} Pr[N_1^{k+1}, N_2^{k+1} | N_1^k, N_2^k] &= Pr[Y^k = N_2^{k+1} - N_2^k + W^k | N_1^k, N_2^k] \\ &\times Pr[X^k = N_1^{k+1} - N_1^k + N_2^{k+1} - N_2^k + W^k | N_1^k, N_2^k] \end{aligned}$$

Using two-dimensional Markov chain model with finite population, we can obtain steady state probabilities.

$$\Pi = \{\pi_1, \pi_2, \dots, \pi_{|S|}; \pi_i = \lim_{k \rightarrow \infty} Pr(S_k = i)\}$$

which satisfy the following expressions.

$$\begin{aligned} \pi &\geq 0, \quad \sum_j \pi_j = 1, \quad \text{and} \\ \pi_i &= \sum_j \pi_j Pr[S_{k+1} = i | S_k = j] \end{aligned}$$

Then, the expected number of packets sent in a data slot (throughput) is

$$\eta = \sum_{n_1=0}^{M_c} \sum_{n_2=0}^{M_c - n_1} \pi_{n_1, n_2} W(n_1, n_2)$$

where

$$W(n_1, n_2) = \min(n_2, 1)$$

The expected packet delay for the system is the sum of the reservation request packet delay D_1 , and the data packet delay D_2 . Obtaining the stationary state expectations as follows,

$$\begin{aligned} E[N_1] &= \sum_{n_1=0}^{M_c} \left\{ n_1 \sum_{n_2=0}^{M_c - n_1} \pi_{n_1, n_2} \right\} \\ E[N_2] &= \sum_{n_2=0}^{M_c} \left\{ n_2 \sum_{n_1=0}^{M_c - n_2} \pi_{n_1, n_2} \right\} \end{aligned}$$

Little's formula may then be used to determine the delays to be

$$D_1 = \frac{F E[N_1]}{\eta} \text{ (slots)}$$

$$D_2 = \frac{F E[N_2]}{\eta} \text{ (slots)}$$

The overall expected packet delay is therefore given by

$$D = F \left(\frac{E[N_1] + E[N_2]}{\eta} \right) \text{ (slots)} \quad (4.7)$$

4.5.3 Numerical Results

In this subsection, throughput and delay as functions of traffic load is investigated using the model developed in the previous subsection. A population size of 60 and $C = 5$ are assumed for all results. Fig. 4.12 shows mean packet delay vs. packet arrival probability (traffic load) with different K when σ is 0.3. This figure suggests that under this condition one request slot ($K = 1$) is not enough, but rather at least two request slots are necessary.

Delay-throughput performance is indicated in Fig. 4.13 with different number of minislots. When $K = 1$ maximum throughput is slightly over 30 %. The figure shows that throughput performance is dramatically enhanced as K increases. Fig. 4.14 shows that just as in slotted-ALOHA the mean packet delay and throughput are influenced by the probability of transmitting reservation request.

Note that the results in this section represent the worst case in Chess Board protocol in the sense that every node is allowed to have only one packet to transmit. In other words, each node must make a reservation for every packet. In the next section, we perform a simulation study based on more realistic situation, where a node is able to buffer multiple packets so that after having succeeded in reservation it can transmit several packets sequentially by setting piggyback bit.

4.6 Performance Evaluation

As described in section 4.4 Chess Board protocol has two major parameters: the number of channels and slot size. In this section, we present performance evaluation results of Chess Board protocol, where focus is placed on the effect of the two parameters on mean packet delay and throughput.

4.6.1 Simulation Setup

Fig. 4.15 shows the indoor environment for our simulation study consisting of four picocells and 40 MHs. MHs move the four picocells according to random waypoint mobility model. They can cross boundaries between picocells without any constraints and it is assumed that handover takes place as soon as they cross the boundary. Different FS satisfying orthogonality requirements are employed in each picocell.

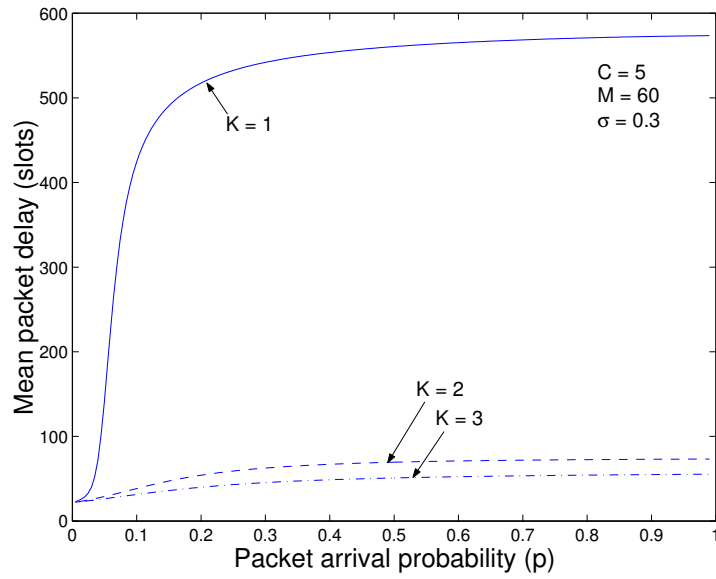


Figure 4.12: Mean packet delay vs. packet arrival probability with different number of minislots (K) when C is five and σ is 0.3.

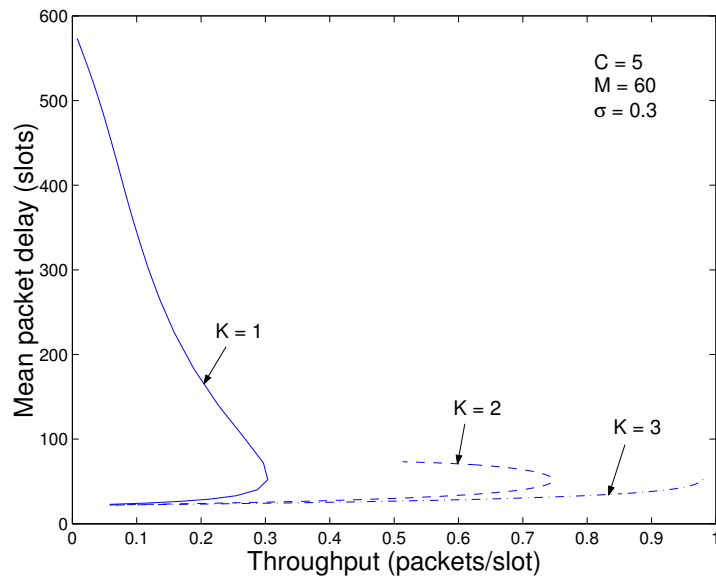


Figure 4.13: Mean packet delay vs. throughput with different number of minislots (K) when C is five and σ is 0.3.

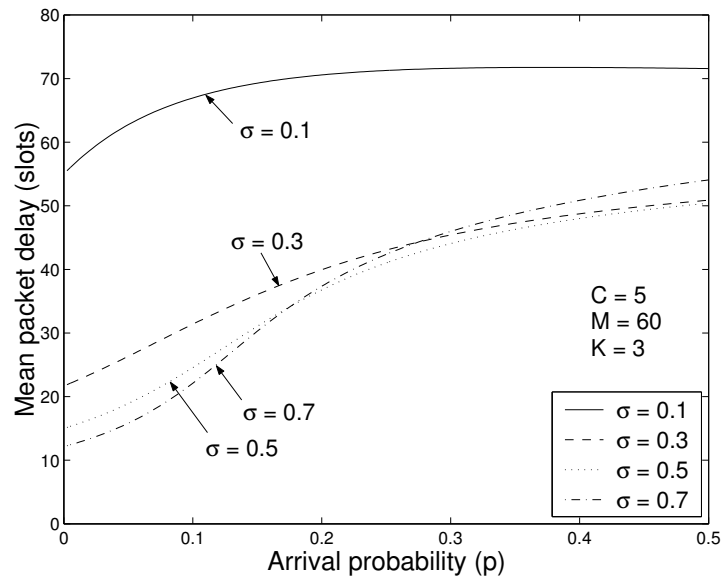


Figure 4.14: Mean packet delay vs. packet arrival probability with different σ when C is five and K is three.

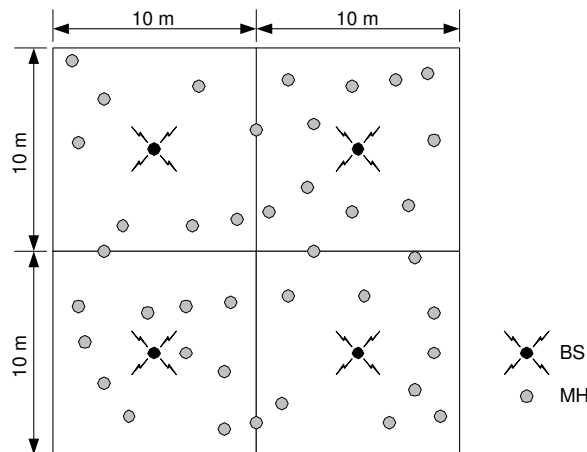


Figure 4.15: Indoor environment for simulation consists of four picocells and 40 MHs.

Table 4.2: Summary of the Simulation Parameters

Picocells	4	Guard time	32 bytes
MHs	40	FCS	4 bytes
BS Capacity	155 Mbps	Buffer Length	10 Mbytes
MAC adrs	6 bytes	Mobility Model	Random Waypoint
Permit field	1 byte	Speed of MH	1.5 m/s
Reservation slot	16 bytes	Simulated Time	≥ 3000 sec
Flag	8 bytes	Statistics Collection	after 300 sec

Table 4.2 summarizes the parameters for simulation. Unless otherwise specified, these values are assumed for all the simulation results. Picocell capacity of 155 Mbps is assumed since a lot of experimental studies demonstrate successful data transmission at this rate [20],[21],[23],[29], [30],[33],[34], [76]. Some overheads are taken into account, which include MAC address, permit field, reservation slot, flag, guard time, and frame check sequence (FCS). MHs are moving at human walking speed of 1.5 m/s . Notice that in order to evaluate mean packet delay a relatively large amount of buffer size (10 Mbytes) is assumed. As will be cleared later on, using random waypoint model a large portion of the MHs could aggregate in a picocell, causing longer packet delay. If the buffer size is not large enough, packet loss is observed to begin with moderate traffic load. Each simulation was run for at least 3000 seconds (simulated time). It continues to run until the confidence interval of 95 % falls within 3.0 %.

Other assumptions for simulation are as follows:

- After having sent a request an MH receives the reservation result in the next frame time from the corresponding downlink channel.
- The capacity of a BS (BT_{BS}) is 155 Mbps. The channel data rate (BT_{ch}) is defined as $BT_{BS}/C - O$, where C is the number of channels and O is overhead normalized with regard to BT_{BS} including MAC address, permit field, reservation field and guard time.
- Message traffic consists of three packets: 41 bytes (45%), 576 bytes (35%), and 1500 bytes (20%). Since Chess Board protocol allows for packing small packets into a data slot or fragmenting a large packet into several data slots, different size of packets frequently found in wide-area Internet traffic are used to investigate the effect of the slot size on system performance [71].
- Interarrival time between packets is exponentially distributed.
- Channel is perfect (error-free).
- p -persistent algorithm is used for sending a request packet.

Table 4.3: Six Variants of Chess Board Protocol

MAC	Channel change during operation	Request when the channel is used	Group
A1	NO	blocked	A
A2		queued	
A3		shared	
B1	YES	assigned if any, blocked if not	B
B2		assigned if any, queued if not	
B3		assigned if any, shared if not	

- MHs use harmonic backoff algorithm (attempting probabilities 1, 1/2, 1/3, . . .) in computing their probabilities to transmit a request.
- Initial channel distribution by MHs is uniform. For example, if C is five each channel is shared by eight MHs ($= 40/5$). Sometimes, this assumption does not hold when 40 is not divisible by C . In that case channel distribution among MHs is such that the variance of it is minimized. For example, when the number of channels is 19 since 40 MHs is not divided by 19 channels, each of the 17 channels is shared by two MHs and the rest two channels are shared by three MHs, respectively.

4.6.2 Six variants of Chess Board Protocol

Six variants of Chess Board protocol, classified into two groups, are considered in this study as shown in Table 4.3. In the first group (group A), MHs are assumed not to have the capability to change channels during operation, whereas MHs in group B are assumed to be able to change channels. Channel change operation in group B, however, is limited to the case when the CS requests MHs to do for some reason. That might include free channel allocation, load balancing, and so on.

MAC A1 is the simplest among six variants, in which the CS allows a single channel to be used by only one MH, and it has no queue for requests. When the channel is being used, further requests are blocked. In particular, if an MH moves into another picocell where “its” channel is already used, there is no way to continue transmission. MAC A2 is also similar but the only difference is that the CS does enqueue requests for “busy” channels rather than rejecting the request. When the channel is released the CS assigns it to the MH at the head of the queue. In MAC A3, interleaved usage of slots in a single channel by several MHs is performed. That is, if multiple MHs want to use the same channel and their requests have been successfully received by the CS, the channel (i.e., uplink slot) is then assigned to them in a round-robin fashion, thereby assuring equal portion of the channel capacity to each candidate

MH.

In group B protocols, MHs are assumed to be able to change channels. So the CS attempts to find capacity not only in the channel on which the request has been issued but also in other channels. In MAC B1 when a request from an MH arrives at the BS, the CS investigates each channel whether it is reserved or not. If a channel is released, it assigns the channel to the MH. Furthermore, if the free channel is different from that of used one when the MH has sent the request, the MH must change channels according to the channel number received from the CS. When all the channels are reserved, the request is rejected. A queue for requesting MHs is maintained in MAC B2, so if there is no free channel when a request arrives at the CS, it is enqueued. As soon as a channel is released it is allocated to the MH at the head of the queue. Channel change operation is required if necessary when the free channel and the channel used by the MH at the head of the queue are different. MAC B3 is similar to MAC B2 with an exception that when the number of requesting MHs is greater than the number of channels, all the channels are shared by the MHs in a round-robin fashion. In this case whenever the CS transmits a permit to an MH, it must also inform the MH of the next channel number in the permit field of downlink slot (see Fig. 4.3).

Note that in the MAC protocols A2 and B2, when an MH in the queue moves into another picocell without being assigned a channel, it must resend a request to the CS in the new picocell. Then, the CS enqueues the request in the queue for the new picocell and dequeues it from the queue for the old picocell. Similar operation is carried out by the CS for MAC A3 and B3. It can be expected that group B protocols will outperform group A protocols at the expense of increased complexity.

4.6.3 Delay Performance of Group A MAC Protocols

The mean packet delay is defined as the average time spent by a packet from the instant it is generated till its transmission is completed. Fig. 4.16 shows the mean packet delay of group A MAC protocols when C is five and the packet size is 1000 bytes. MAC A2 and A3 indicate similar performance with traffic load while MAC A1 exhibits longer packet delay. When the traffic load is less than or equal to 4.5 Mbps per MH, MAC A2 and A3 display almost constant mean packet delay. After that, it grows exponentially.

Fig. 4.17 and 4.18 indicate the mean packet delay when C is 10 and 15, respectively. MAC A2 and A3 again show similar performance as in the previous case, while MAC A1 illustrates longer delay. Note that in MAC A2, the CS has a queue for requests for uplink transmission, while in MAC A3 one channel is shared by multiple MHs in a round-robin fashion. The three figures above imply that with this simulation scenario, there is no great difference between the two schemes. In addition, from the figures we notice that the small number of channels is beneficial in terms of the mean packet delay. Alternatively, with fixed total system bandwidth, small number of channels means larger channel bandwidth, leading to better performance. In particular, in our simulation scenario the number of MHs sharing the same channel is $40/C$ provided 40 is divisible by C . When C is five, the number of MHs using a channel (say, channel one) in the cluster is eight, since we have assumed that the channel distribution among

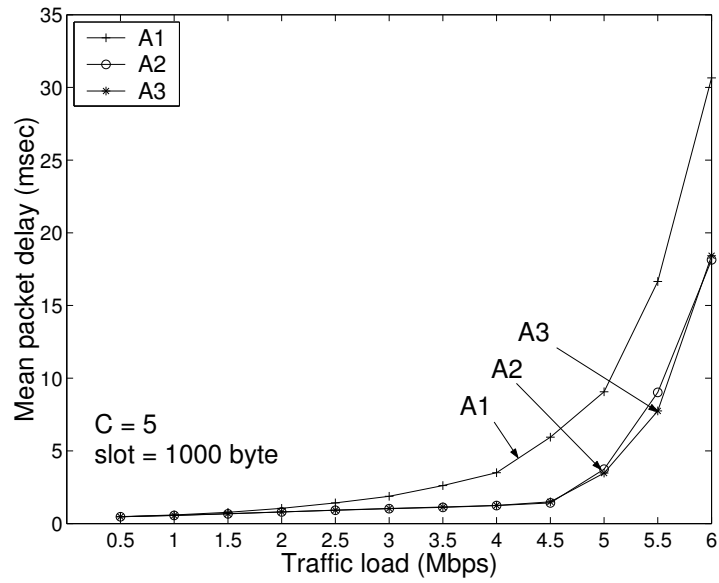


Figure 4.16: Mean packet delay of group A MACs when C is five and slot size is 1000 byte.

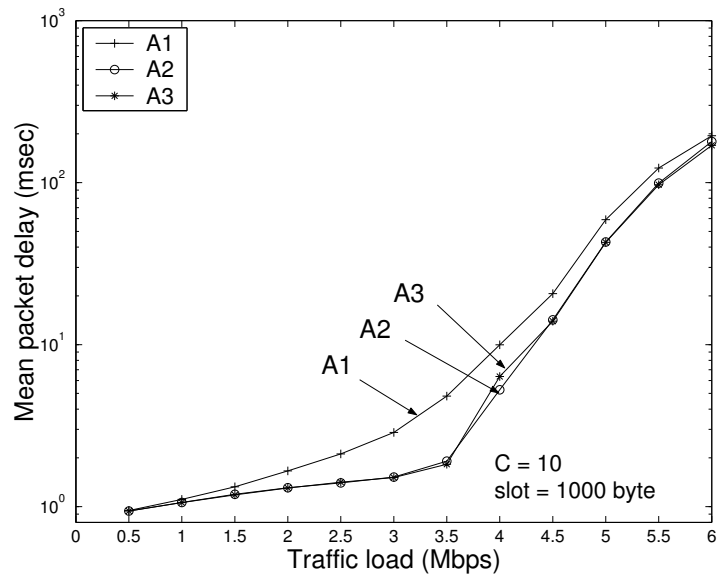


Figure 4.17: Mean packet delay of group A MACs when C is ten and slot size is 1000 byte.

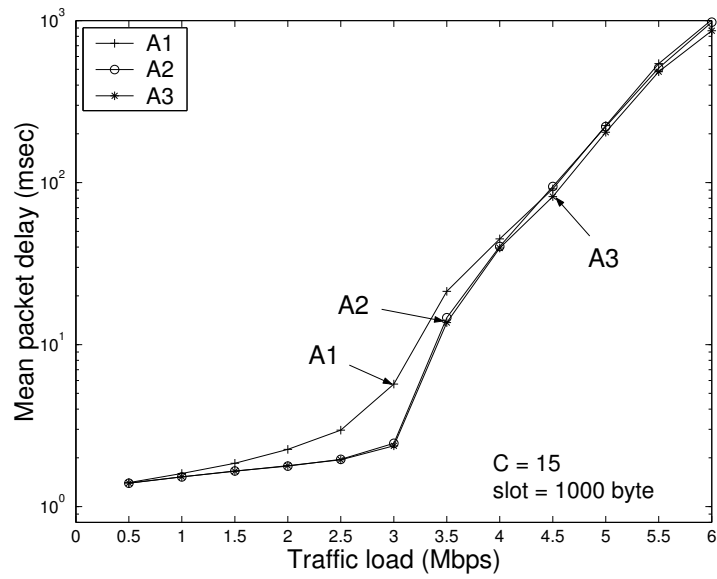


Figure 4.18: Mean packet delay of group A MACs when C is 15 and slot size is 1000 byte.

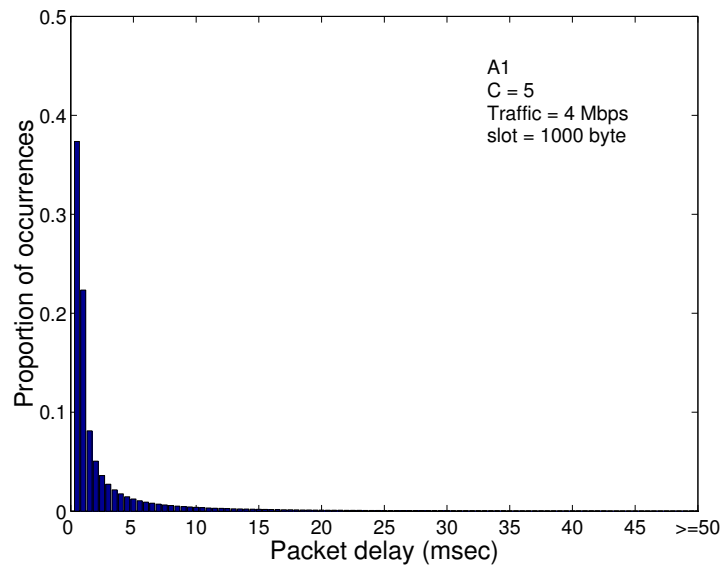


Figure 4.19: Histogram of the packet delay of MAC A1 when C is five, slot size is 1000 byte, and traffic load per MH is 4 Mbps.

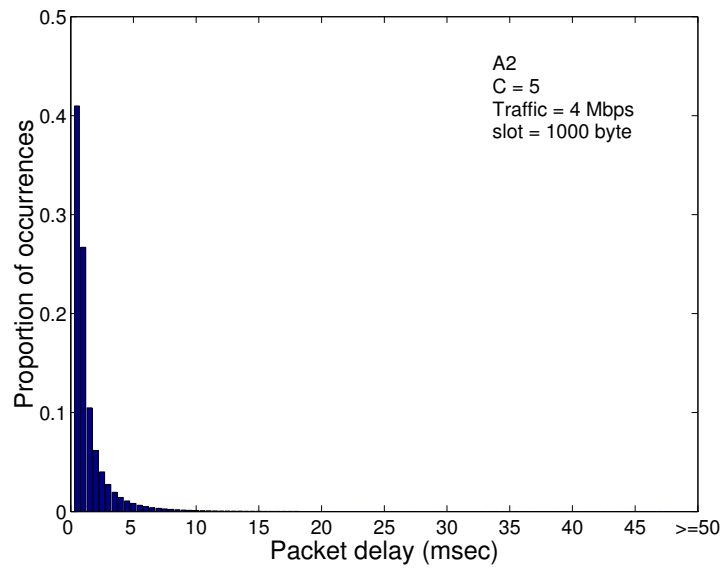


Figure 4.20: Histogram of the packet delay of MAC A2 when C is five, slot size is 1000 byte, and traffic load per MH is 4 Mbps.

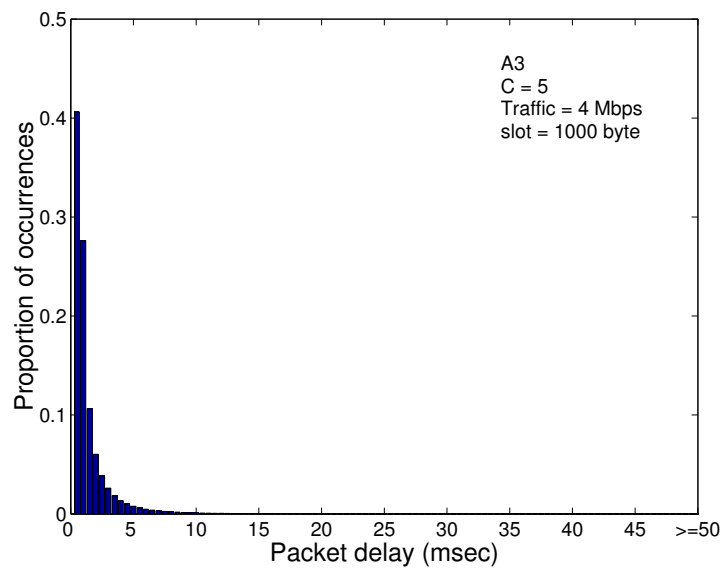


Figure 4.21: Histogram of the packet delay of MAC A3 when C is five, slot size is 1000 byte, and traffic load per MH is 4 Mbps.

MHs is uniform if 40 is divisible by C . In this case, channel bandwidth is 31 Mbps ($= 155/5$). On the other hand, when C is ten, four MHs are utilizing the same channel in the cluster, and the channel bandwidth is 15.5 Mbps ($= 155/10$). When C is 15, the channel bandwidth is approximately 10.3 Mbps ($\approx 155/15$). Fig. 4.16, 4.17, and 4.18 imply that the sharing a larger capacity channel among multiple MHs is better in terms of the mean packet delay.

Fig. 4.19 shows packet delay histogram when C is five, slot size is 1000 bytes, and traffic load per MH is four Mbps. Histograms for MAC A2 and A3 with the same simulation conditions are shown in Fig. 4.20 and 4.21, respectively. We observe from these figures that MAC A2 and A3 have almost the same performance, and it is obvious that MAC A2 and A3 are much better than MAC A1 in terms of the mean packet delay. In particular, in MAC A1 the proportion of packet delay exceeding 5.0 ms is 14.0 %, while it is 3.44 % and 3.7 % for MAC A2 and A3, respectively. From now onward, we concentrate only on the properties of MAC A3 in more detail.

4.6.4 Delay Performance of MAC A3

Fig. 4.22 portrays the effect of the number of channels on the mean packet delay of MAC A3, when the slot size is 1000 bytes. With light traffic load (1 and 2 Mbps), smaller number of channels is beneficial in terms of the mean packet delay, due to the fact that the frame time is directly proportional to the number of channels ($t_f = C \cdot t_s$). An interesting effect is observed when the traffic load is 3 Mbps. When C is 19, each of the 17 channels is shared by two MHs and the other two channels are shared by three MHs, respectively. If the three MHs come together in the same picocell, which are using the same channel, their total traffic load (9 Mbps) becomes greater than the channel data rate (8.1 Mbps $\approx 155/19$), thus resulting in high mean packet delay. Similar arguments can be applied for $C=17,18$. Whereas each channel is shared by only two MHs when C is 20. Thus, if two MHs using the same channel stay in the same picocell, their total traffic load (6 Mbps) is smaller than the channel data rate (7.75 Mbps $\approx 155/20$). That is the reason why the mean packet delay is lower when C is 20 than when C is 19. Therefore, one can notice that the mean packet delay in A3 depends not only on the number of channels and slot size but also on the channel distribution of MHs. We call this effect as “*nonuniform channel distribution effect*” in this study. Notice that if the time duration that the three MHs stay in the same picocell is so long that MH’s buffer is not enough to store overflowed packets, there must be packet loss. However, as the MH has enough buffer in our simulation scenario compared to the time duration, no packet loss is observed when the traffic load per MH is less than or equal to 4 Mbps for MAC A3.

The effect of the number of channels on the mean packet delay of MAC A3 are shown in Fig. 4.23, 4.24, and 4.25 with different slot sizes of 500, 1000, and 1500 bytes, respectively. The “*nonuniform channel distribution effect*” is again observed in each figure; moreover, it becomes severe when the slot size is small. Fig. 4.26 exhibits that the effect is alleviated with larger slot size. Due to the overhead considered in our simulation scenario, channel bandwidth becomes small as the slot size decreases. Smaller bandwidth is, in turn, more sensitive to the traffic load. The figures show that for some number of channels, e.g. 19, although it is much larger than the average number of MHs ($=10$) in a

picocell, excessive mean packet delay can be occurred due to nonuniform channel distribution of MHs. Notice that the distribution of 19 channels among MHs is allocated in such a way that the variance of the average number of MHs per channel is minimized. Otherwise, for instance, when each of the ten channels is shared by four MHs and the rest of nine channels are unused, much larger mean packet delay will be observed.

Fig. 4.27 shows the mean packet delay vs. traffic load of MAC A3 when the number of MHs is 20. The “*nonuniform channel distribution effect*” begins to occur with an average traffic load of 4 Mbps and becomes clearer when the traffic load per MH is 5 Mbps. Fig. 4.28 indicates the same performance when the number of MHs is 30. The mean packet delay is observed to be larger when C is 13 than when C is 15 due to the “*nonuniform channel distribution effect*” when the traffic load is 4 Mbps.

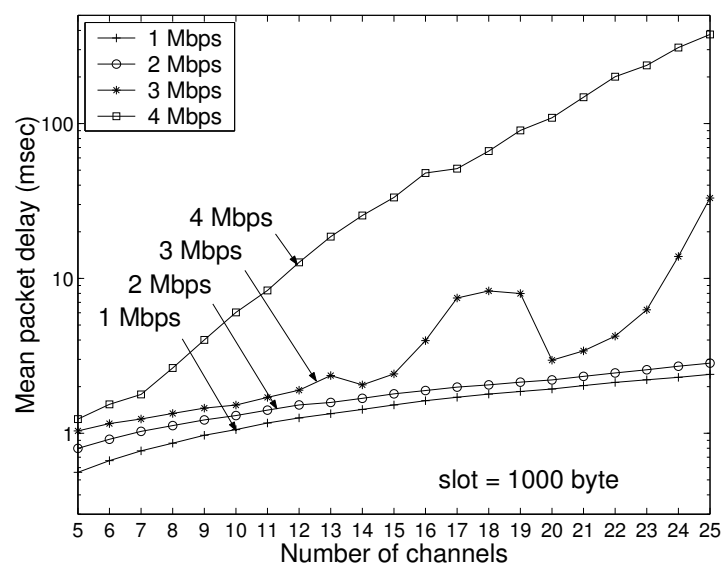


Figure 4.22: Mean packet delay of MAC A3 when slot size is 1000 byte.

The impact of the slot size in MAC A3 is presented in Fig. 4.29 indicating smaller slot size is better than larger one when C is five. This is because frame time is proportional to slot size when C is fixed. However, due to the fixed size overhead, too small size slot may cause larger delay under heavy traffic load. When the slot size is large and traffic load is light, a small portion of the slot will be used for transmitting user data. In this case, mean packet delay is linearly proportional to the slot size, e.g., when the traffic load is one or two Mbps in the figure. As traffic load increases an MH packs many packets in one uplink slot if the slot is large enough and it has many packets in the buffer. Thus, the mean packet delay with traffic loads of three and four Mbps in the figure show similar performance when the slot size is large. In some cases, four Mbps shows shorter mean packet delay than three Mbps with larger slot size.

Fig. 4.30 illustrates the effect of the slot size on the mean packet delay of MAC A3 when C is ten. As each channel is shared by four MHs and channel bandwidth is about 15.5 Mbps when the four

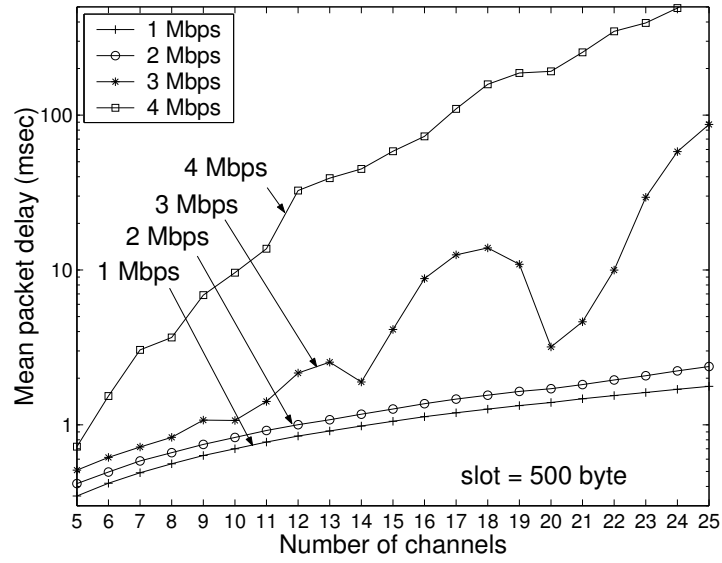


Figure 4.23: Mean packet delay of MAC A3 when slot size is 500 byte.

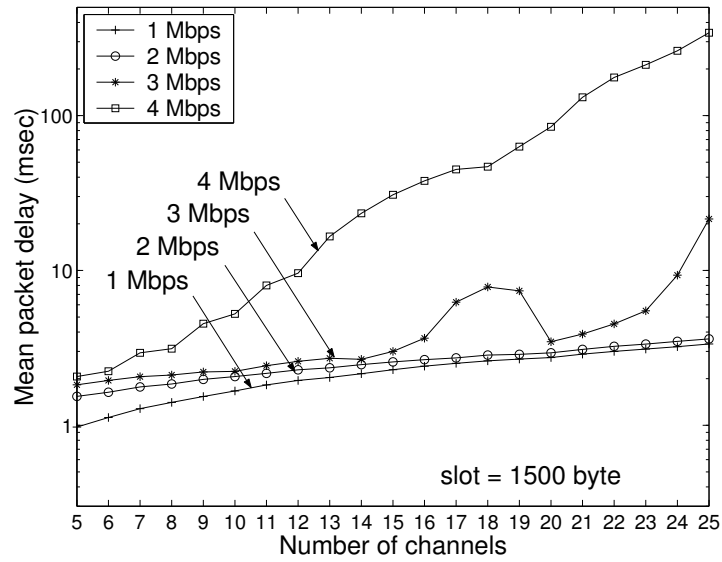


Figure 4.24: Mean packet delay of MAC A3 when slot size is 1500 byte.

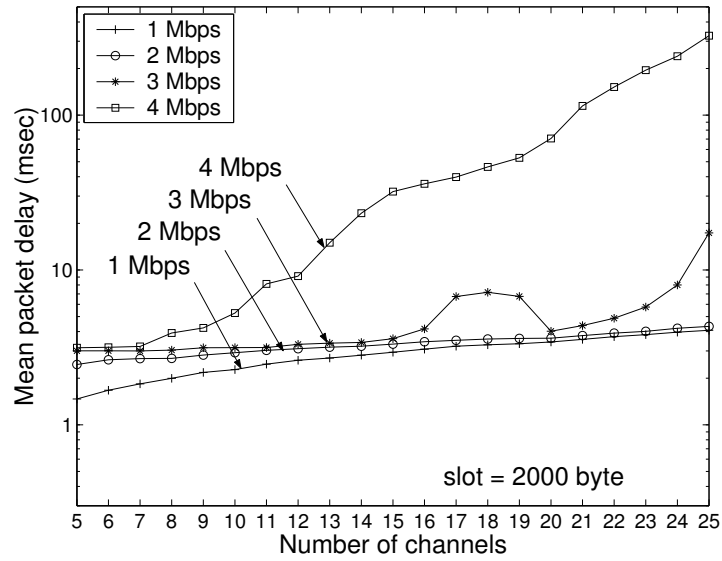


Figure 4.25: Mean packet delay of MAC A3 when slot size is 2000 byte.

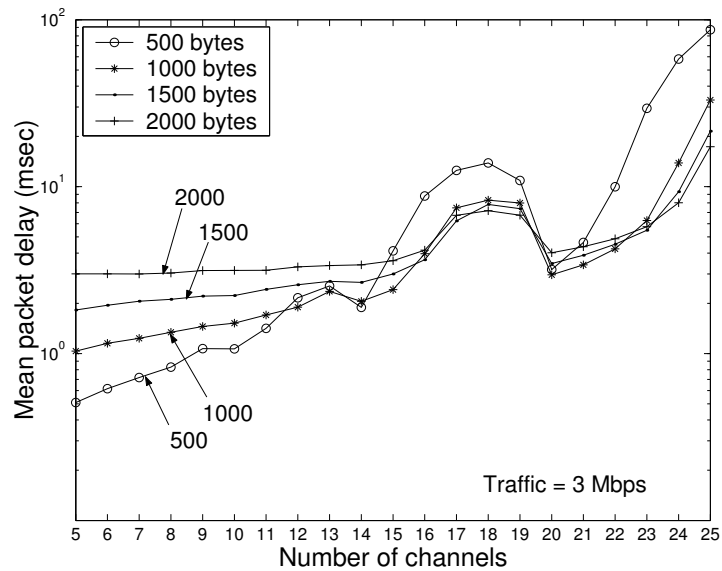


Figure 4.26: Mean packet delay of MAC A3 with different number of channels and slot sizes when traffic load per MH is three Mbps.

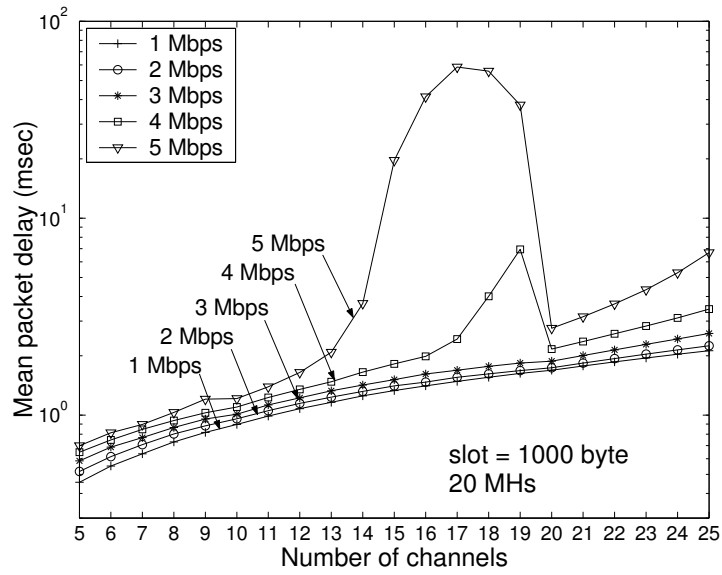


Figure 4.27: Mean packet delay of MAC A3 with different number of channels when there are 20 MHz in the cluster.

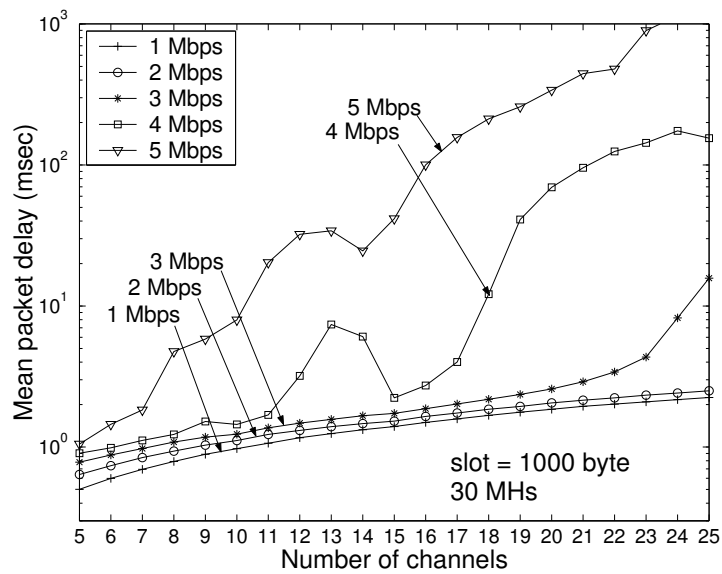


Figure 4.28: Mean packet delay of MAC A3 with different number of channels when there are 30 MHz in the cluster.

MHs with four Mbps traffic load come together in the same picocell, their total traffic load becomes 16 Mbps, which is greater than the channel bandwidth. This accounts for the large mean packet delay when the traffic load is four Mbps. The same situation may take place when C is five; however, in this case the probability that eight MHs with four Mbps traffic aggregate in a picocell is very low. Therefore, Fig. 4.29 shows relatively small mean packet delay. Similar arguments can be applied to the case where C is 15 as shown in Fig. 4.31. In this case each of the five channels is shared by two MHs, and each of the remaining ten channels is used by three MHs, respectively, and the channel bandwidth is about 10 Mbps. If the three MHs with a traffic load of four Mbps using the same channel come together in a picocell, their total traffic load is 12 Mbps that is greater than the channel bandwidth leading to larger packet delay.

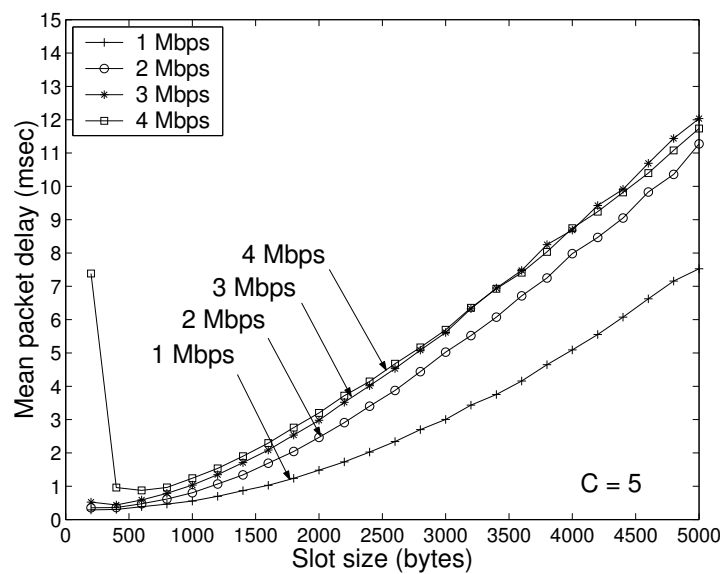


Figure 4.29: Mean packet delay of MAC A3 when C is five.

Buffer length vs. the number of channels is given in Fig. 4.32. We can still see “nonuniform channel distribution effect” in the figure when the traffic load is three Mbps. Except some points buffer length increases with the number of channels. Mean packet delay performance with heavy traffic load is illustrated in Fig. 4.33. It looks similar to the figure for buffer length (Fig. 4.32) because the buffer length is closely related to the mean packet delay. However, mean packet delay grows with the number of channels except some points.

4.6.5 Delay Performance of Group B MAC Protocols

Due to the capability of channel change of MH group B MAC protocols show quite different properties as compared to group A MACs. Channel change ability of MHs allows for more efficient resource management. In this study, three simple schemes described in Table 4.3 are considered, where channel

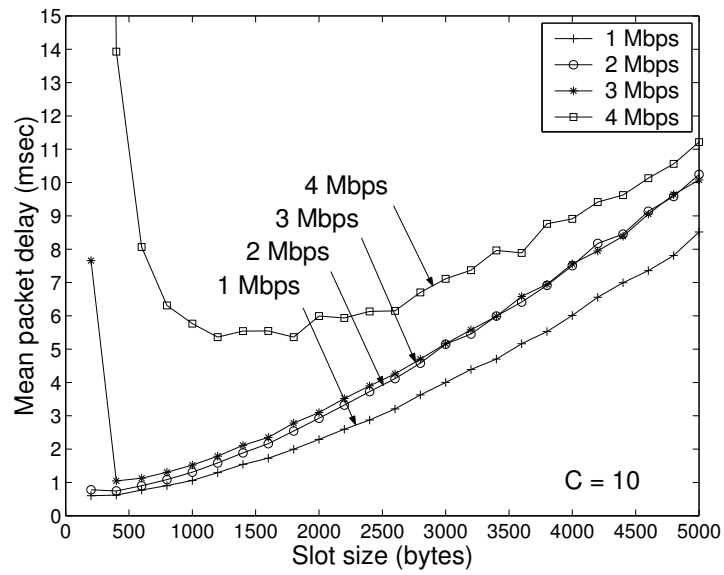


Figure 4.30: Mean packet delay of MAC A3 when C is ten.

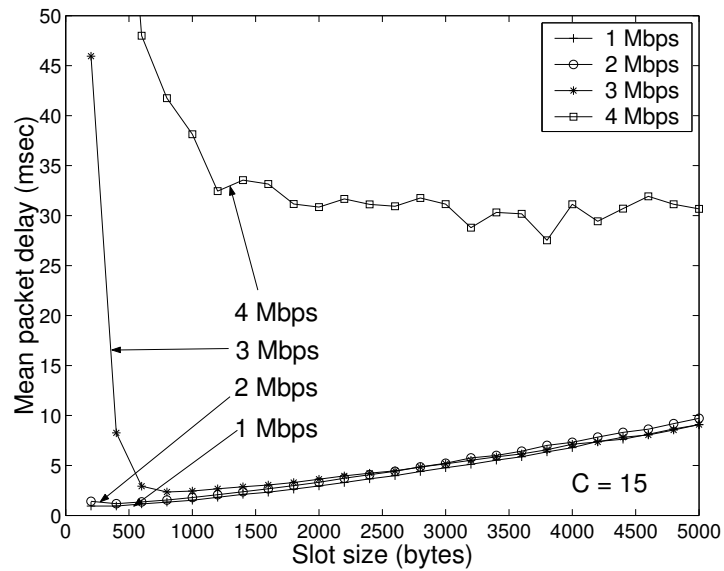


Figure 4.31: Mean packet delay of MAC A3 when C is 15.

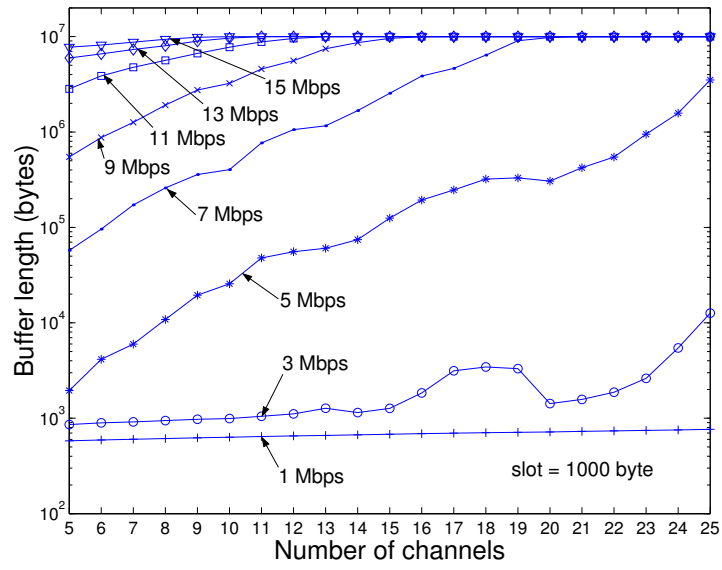


Figure 4.32: Buffer length of MAC A3.

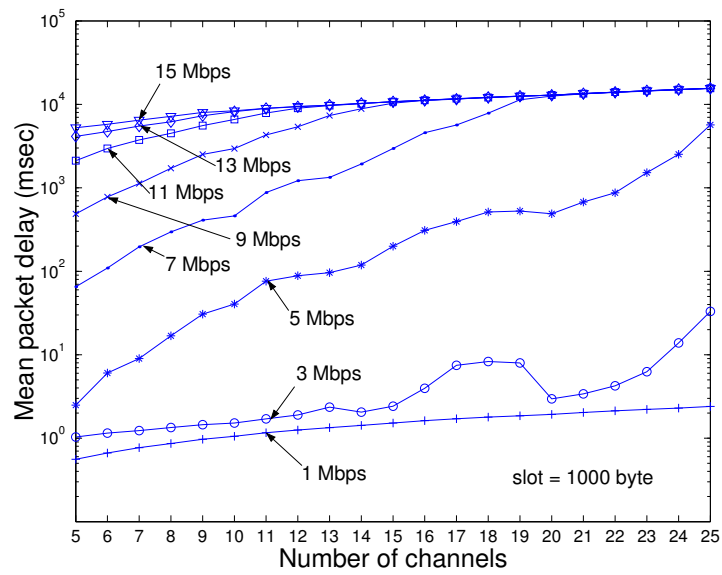


Figure 4.33: Mean packet delay of MAC A3.

change operation of MH in group B MACs is allowed only when the CS commands it to do so.

Mean packet delay vs. traffic load when C is five and slot size is 1000 bytes is shown in Fig. 4.34. One can clearly notice that MAC B2 and B3 are better than MAC B1 in terms of mean packet delay. In addition, MAC B2 indicates similar performance to MAC B3. When C is five, each channel is shared by two MHs on the average in a picocell since the average number of MHs in a picocell is ten in our simulation scenario. The performance difference among group B MAC protocols vanishes as C grows as illustrated in Fig. 4.35 and 4.36 for which slot size is 1000 bytes and C is 10 and 15, respectively. It comes from the fact that ten MHs operate in each picocell on the average, so when C is more than or equal to ten every MH will be assigned to its own channel. However, when C is 15, some channels are unused resulting in a waste of bandwidth. From the above three figures, it is observed that with light traffic load the mean packet delay is small when C is small. That is because the mean packet delay is proportional to C when collision for reservation is rare. Another important observation is that with heavy traffic, e.g., more than six Mbps, small mean packet delay is seen when C is ten, the reason will be described later in more detail.

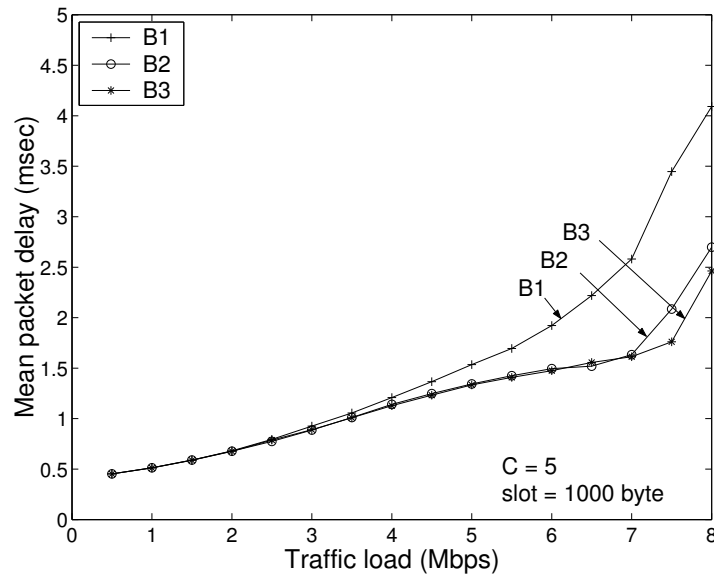


Figure 4.34: Mean packet delay of group B MACs when C is five.

Histograms of mean packet delay of MAC B1 and B2 are indicated in Fig. 4.37 , 4.38, respectively, when C is five, slot size is 1000 byte and traffic load per MH is seven Mbps. It is clear from the two figures that MAC B2 is better than MAC B1 in terms of mean packet delay. In particular, the portions of the mean packet delay over 5.25 msec are 12.8 % and 7.1 % for MAC B1 and B2, respectively. In addition, MAC B2 and B3 have comparable performance as shown in Fig. 4.38 and 4.39. From now on, we consider only MAC B3 in more detail.

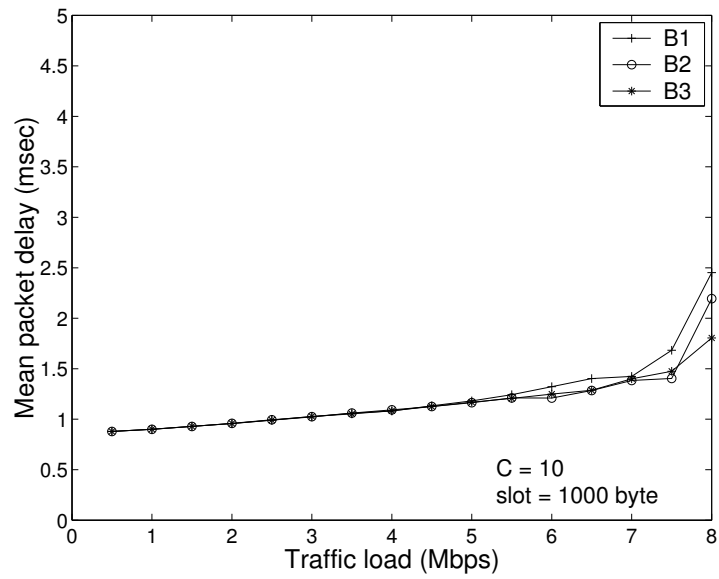


Figure 4.35: Mean packet delay of group B MACs when C is ten.

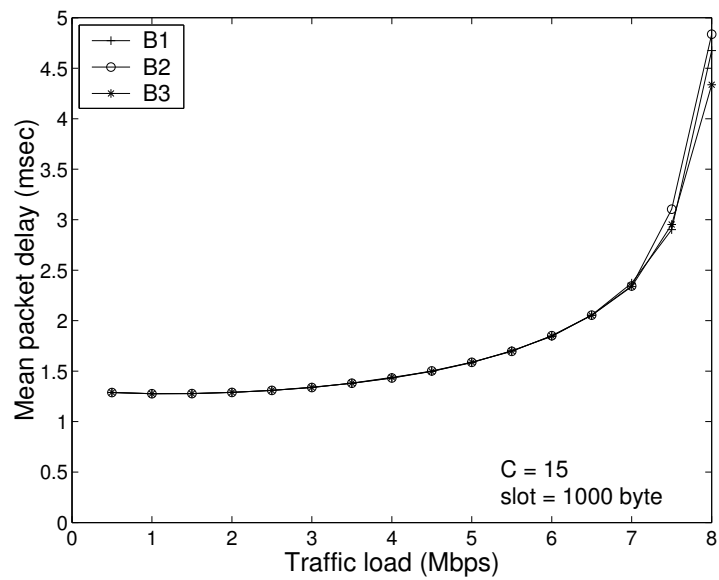


Figure 4.36: Mean packet delay of group B MACs when C is 15.

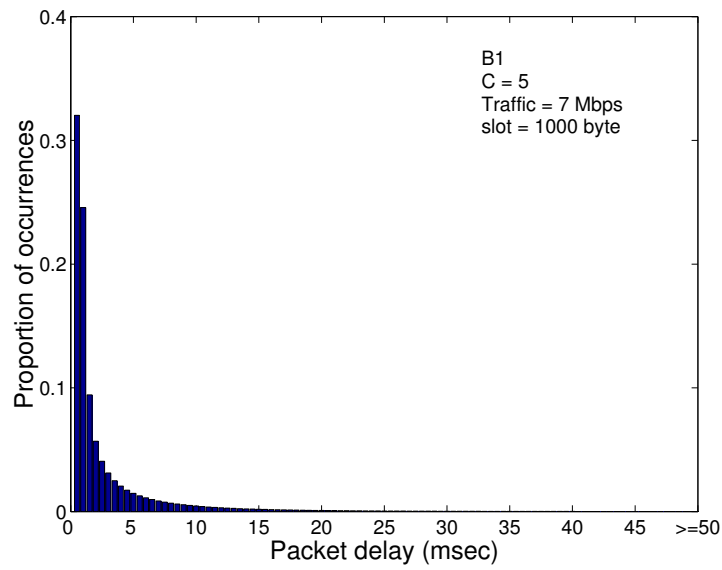


Figure 4.37: Histogram of the packet delay of MAC B1 when C is five, slot size is 1000 byte, and traffic load per MH is 7 Mbps

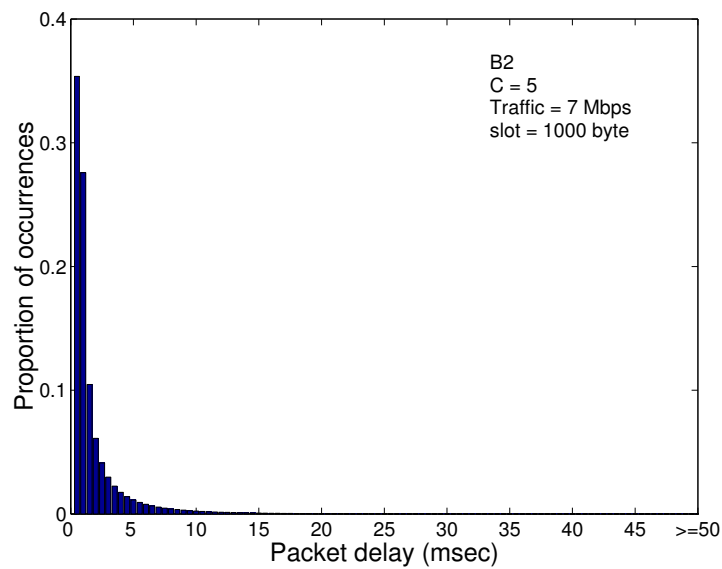


Figure 4.38: Histogram of the packet delay of MAC B2 when C is five, slot size is 1000 byte, and traffic load per MH is 7 Mbps

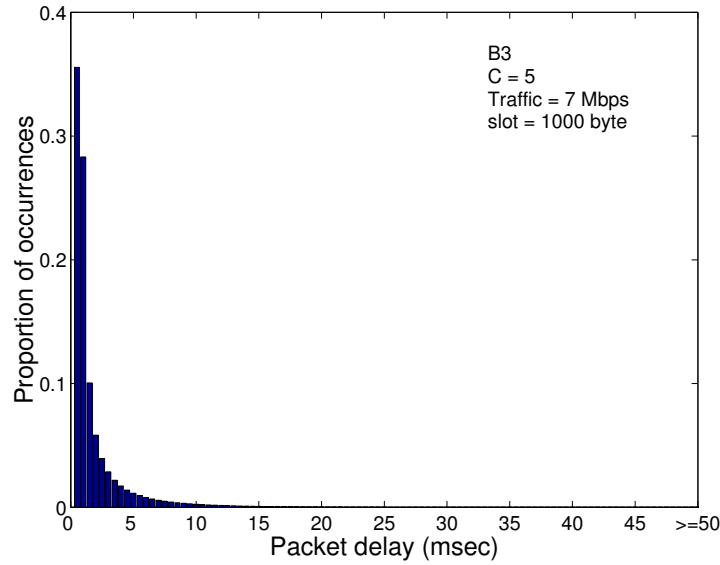


Figure 4.39: Histogram of the packet delay of MAC B3 when C is five, slot size is 1000 byte, and traffic load per MH is 7 Mbps

4.6.6 Delay Performance of MAC B3

The effect of the number of channels on packet delay is shown in Fig. 4.40. With light traffic load, delay grows along with C since frame time is proportional to it. As traffic load increases, delay has a minimum when C is around ten. Note that in our simulation scenario the average number of MHs in a picocell is ten. Thus, when C is 10, each MH is assigned on average its own channel resulting in rare collision and minimum reservation delay. If C is over ten, the system has more channels than MHs on the average, thereby increasing frame time and wasting of bandwidth. However, since the number of MHs in a picocell varies dynamically, more channels than ten will be needed to accommodate traffic variance caused by nonuniform distribution of MHs.

Fig. 4.41 indicates the effect of the number of channels on the mean packet delay when slot size is 500 bytes. Compared to the previous figure, we can see in this figure that 1) packet delay is smaller with smaller C when the traffic load is light, 2) unlike the previous case packet delay increases with traffic load, and 3) due to the fixed-size overhead larger packet size is advantageous when both C is high and traffic load is heavy. Indeed, from the next two figures (Fig. 4.42, 4.43) for which slot size is 1500 and 2000 bytes, respectively, the minimum mean packet delays when the traffic load is seven Mbps are observed with $C = 11$. Fig. 4.44 illustrates how the slot size influences the packet delay when the traffic load per MH is five Mbps. When slot size is 500 bytes, no minimum point is observed. However, the minimum point moves towards higher number of channels with increase in slot size. For instance, when the slot sizes are 1000, 1500, 2000 bytes, the minimum delay are found at $C = 10, 12, 13$, respectively.

The impact of slot size of MAC B3 is shown in Fig. 4.45. Just as in MAC A3 smaller slot size is advantageous in terms of delay performance but due to the fixed-size overhead, small slot is not

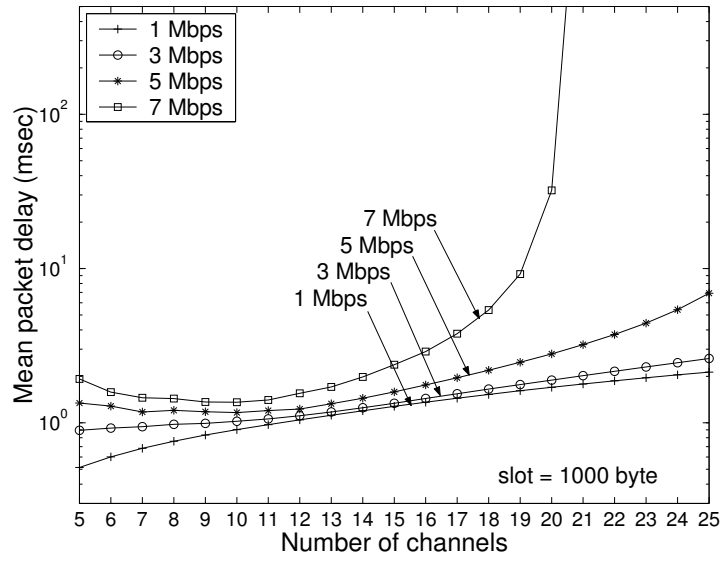


Figure 4.40: Mean packet delay of B3 when the slot size is 1000 bytes.

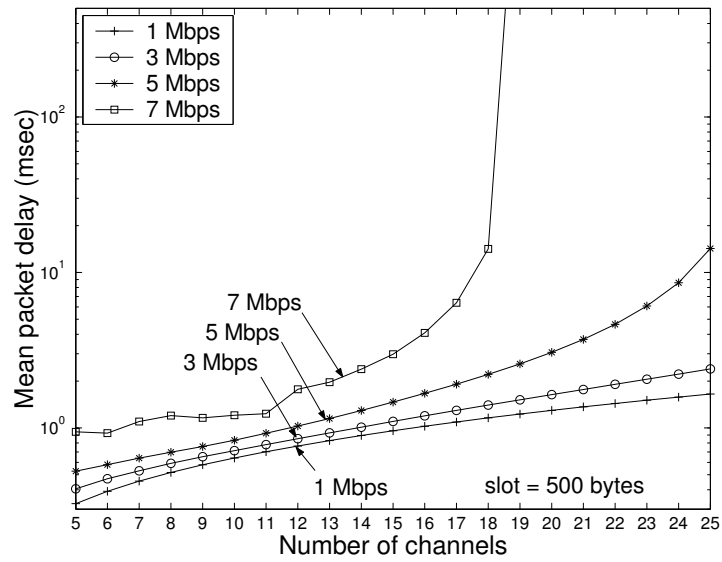


Figure 4.41: Mean packet delay of B3 when the slot size is 500 bytes.

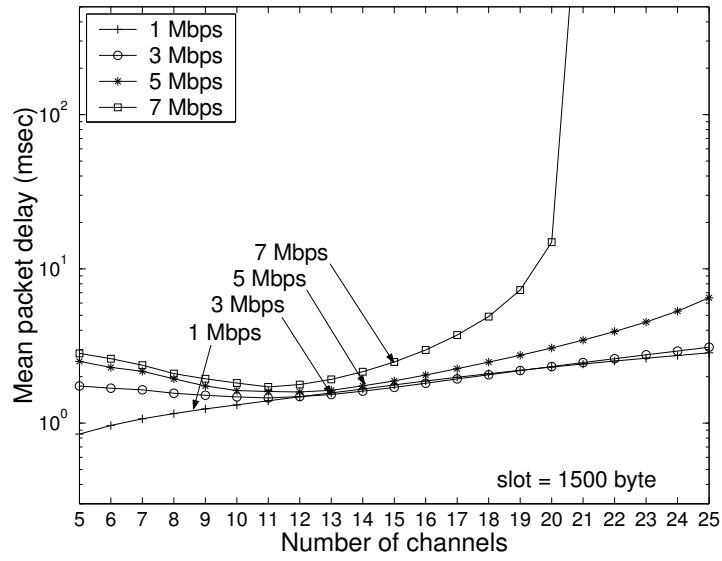


Figure 4.42: Mean packet delay of B3 when the slot size is 1500 bytes.

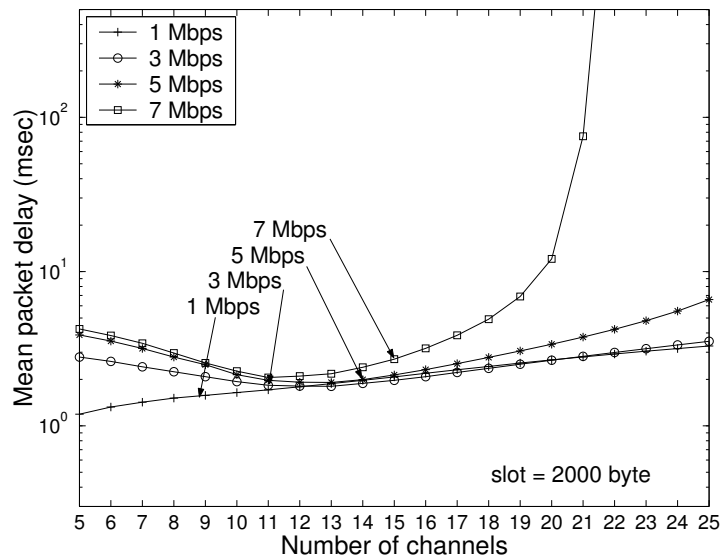


Figure 4.43: Mean packet delay of B3 when the slot size is 2000 bytes.

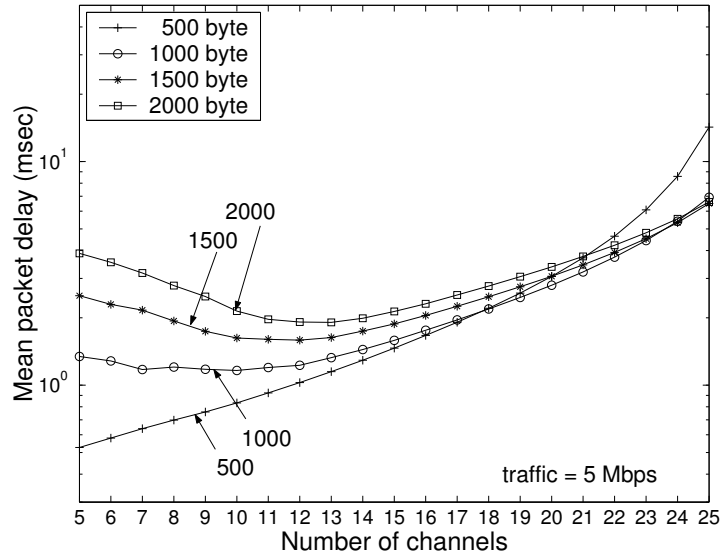


Figure 4.44: Mean packet delay of B3 with different number of channels and slot sizes when traffic load per MH is five Mbps.

always beneficial. When slot size is large (> 3000 bytes) and traffic load is high (five or seven Mbps), several packets can be packed into one slot. The delay performance with different slot sizes when C is ten is illustrated in Fig. 4.46. As compared to Fig. 4.45, small packet delay is observed as the slot size increases. As described earlier, in this case each MH is allocated its own channel on the average since the number of MHs in a picocell on average is equal to the number of channels. When C is 15 mean packet delay vs. slot size is shown in Fig. 4.47. It indicates similar performance to the previous figure. However, since the channel bandwidth is inversely proportional to C as traffic load per MH approaches it, mean packet delay will grow exponentially or packet loss rate increases.

From the above three figures, we can see for the mean packet delay of MAC B3 that 1) when the traffic load is light small number of channels and small slot size is beneficial, and 2) as traffic load increases best result can be expected when the number of channels is approximately equal to (or slightly more than) the number of MHs in a picocell on the average, and 3) small slot size is not appropriate due to the overhead. If the RoF WLAN system considered in this study had the capability to change both the number of channels and slot size during operation, dynamic optimization would be an interesting topic for future research.

Buffer length vs. the number of channels with traffic loads is shown in Fig. 4.48. Compared with Fig. 4.32 for MAC A3 it is seen that with heavy traffic load buffer length suddenly jumps to its maximum value at some channel numbers. For instance, with a traffic load of seven Mbps it goes to its maximum when C is 21. In this case, the channel bandwidth is 7.38 Mbps ($= 155/21$), but due to overhead it is not enough to transport 7 Mbps traffic load. This is the reason for the sudden jumps in the figure. The corresponding mean packet delay performance is depicted in Fig. 4.49, indicating similar

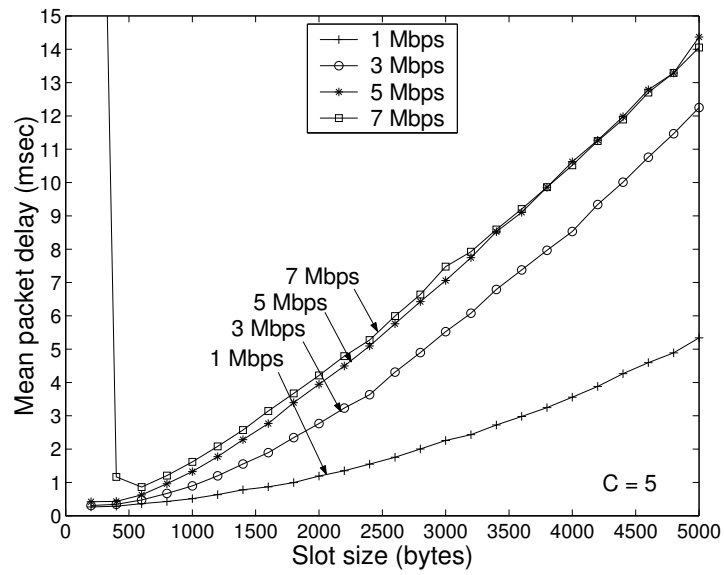


Figure 4.45: Mean packet delay of MAC B3 with different slot sizes when C is 5.

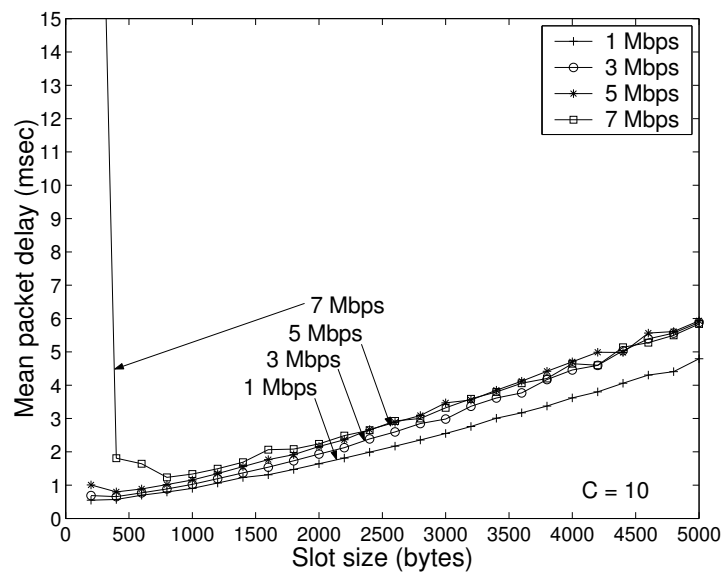


Figure 4.46: Mean packet delay of MAC B3 with different slot sizes when C is 10.

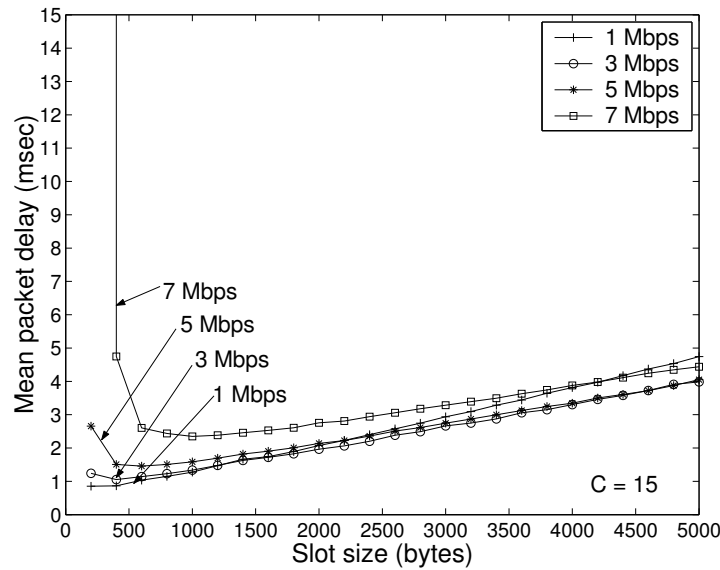


Figure 4.47: Mean packet delay of MAC B3 with different slot sizes when C is 15.

curves to the previous one except that because there is no maximum value in the mean packet delay, it continues to increase after buffer length approaches its maximum.

4.6.7 Throughput Performance

In this section throughput performance of MAC A3 and B3 is investigated. Throughput (normalized) is defined in this study as the ratio between aggregate traffic transferred from 40 MHs to four BSs to the total system capacity ($= 155 \times 4$ Mbps). As for the previous case for mean packet delay the influence of both the number of channels and slot size on throughput is considered. First, we see how the number of channels impacts on it. As described earlier, in Chess Board protocol throughput is affected by the channel data rate since the maximum bandwidth an MH can use is limited by it. Throughput vs. the number of channels of MAC A3 is shown in Fig. 4.50. It is clear from the figure that in terms of throughput performance small number of channels is better. In words, Chess Board protocol is not efficient from the bandwidth point of view. Rather, its design emphasis is placed on handover efficiency. Fig. 4.51 depicts throughput performance for MAC B3. Comparing the above two figures MAC B3 highly outperforms MAC A3 in terms of throughput.

In Fig. 4.52 and 4.53 slot size effect on throughput is shown for MAC A3 and B3, respectively. The capability of channel change makes a difference in performance in the two figures. In case of MAC B3, when $C = 5$ throughput is limited largely by MH's traffic load as each channel is shared by multiple MHs (two MHs on the average) and the channel data rate is about 30 Mbps ($\approx 155/5$). On the other hand when $C = 15$ throughput is restricted mainly by channel data rate, which is about 10 Mbps in this case. Furthermore, larger slot size is favorable in terms of throughput although the effect is not noticeable.

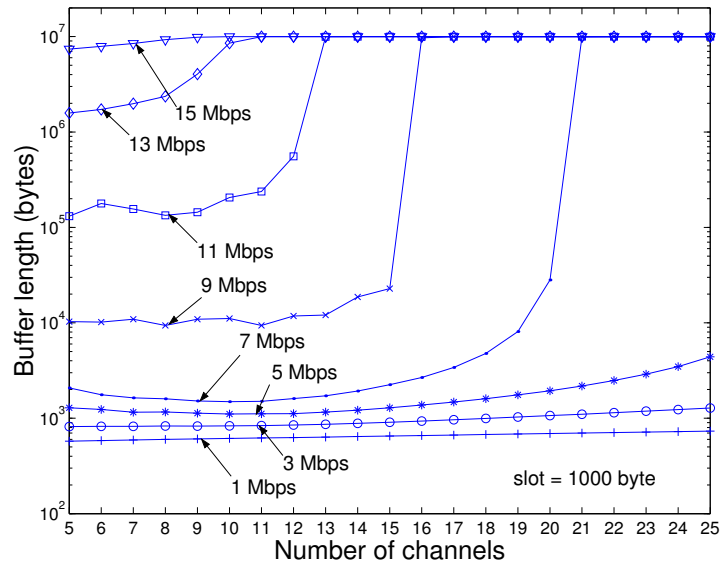


Figure 4.48: Buffer length of MAC B3.

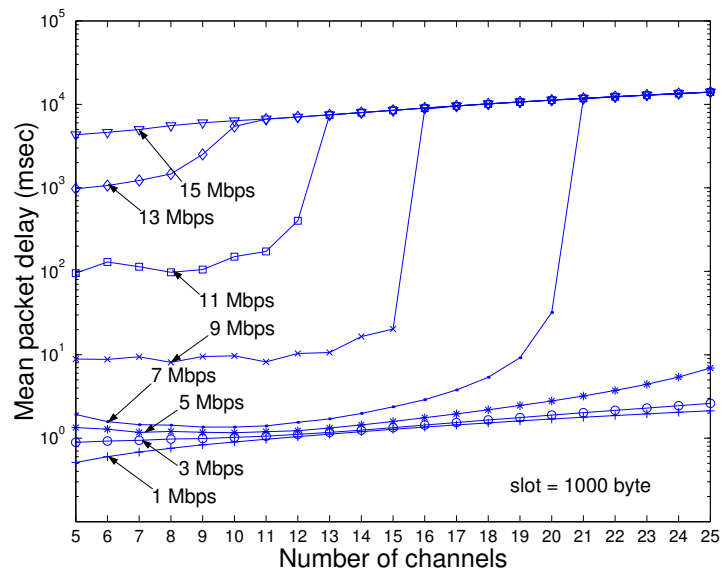


Figure 4.49: Mean packet delay of MAC B3.

From the point the line is no longer linear great packet loss begins to occur.

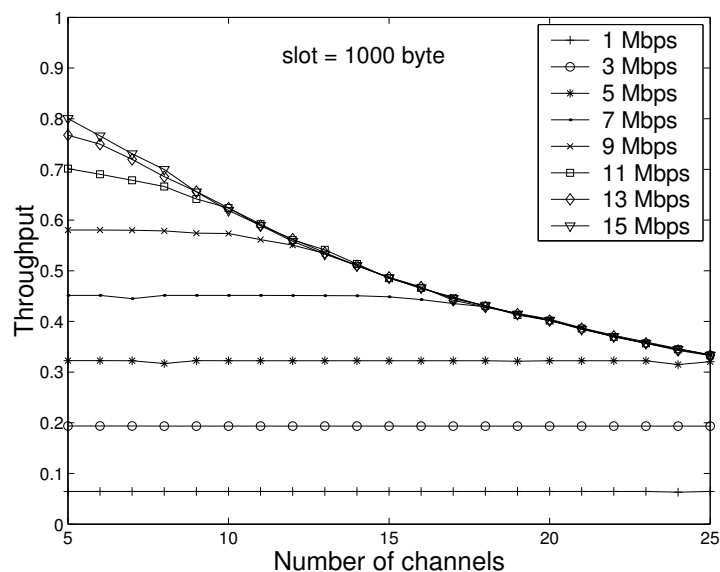


Figure 4.50: Throughput of MAC A3 with different number of channels when slot size is 1000 bytes.

4.7 Conclusion

The wireless LAN system using RoF technology operating in the mm-wave bands imposes quite different requirements on the system design as compared to the conventional WLANs. Since the high penetration loss of mm-wave signal, many BSs should be employed to cover indoor areas. In such network with high number of small cells, the issue of mobility management has a very special significance. An MAC protocol, called Chess Board protocol, featuring fast and easy handover and QoS support has been proposed in this study. The protocol is based on frequency switching (FS) codes and adjacent cells employ orthogonal FS codes to avoid possible co-channel interference as well as fast and easy handover. Important parameters of the protocol were analyzed and simple analysis using Markov chain has been performed. To investigate properties of the protocol in more realistic environments, six variants of the Chess Board protocol were considered and their performance has been evaluated by a simulation study.

Simulation results have shown that group B MAC protocols, which are assumed to have a capacity to change channels during operation, highly outperform group A MAC protocols where a fixed channel is assumed for each MH. Delay performance of both of them depends on the slot size and the number of channels; moreover, in group A MAC protocols, it relies also on channel distribution of MHs. Smaller slot size and smaller number of channels are beneficial in delay performance with light traffic load; however, that is not always true as traffic load grows. On the other hand, larger slot size and smaller number of channels are in favor of throughput performance. To exploit bandwidth resources effectively, MH's capability to change channels during operation is required in a highly dense mobile environment.

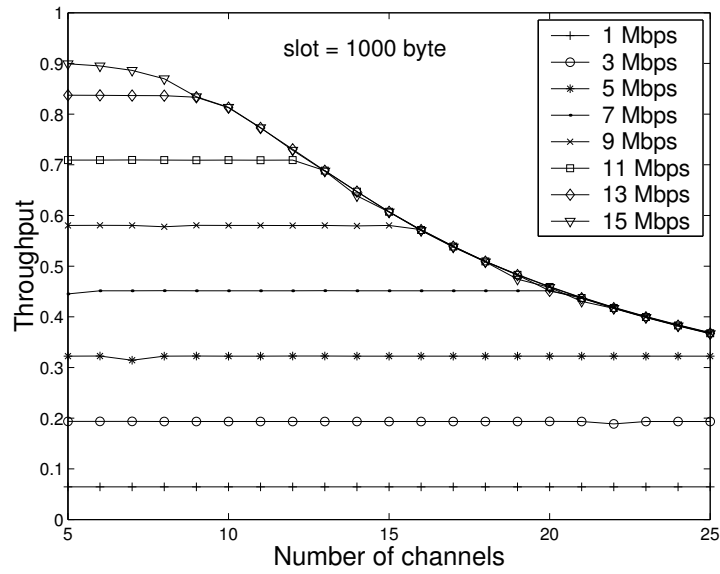


Figure 4.51: Throughput of MAC B3 with different number of channels when slot size is 1000 bytes.

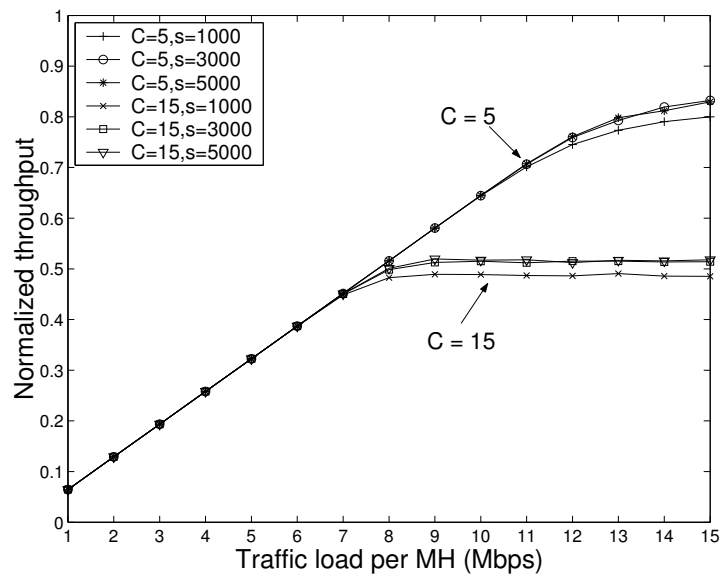


Figure 4.52: Throughput of MAC A3 with different number of channels and slot sizes.

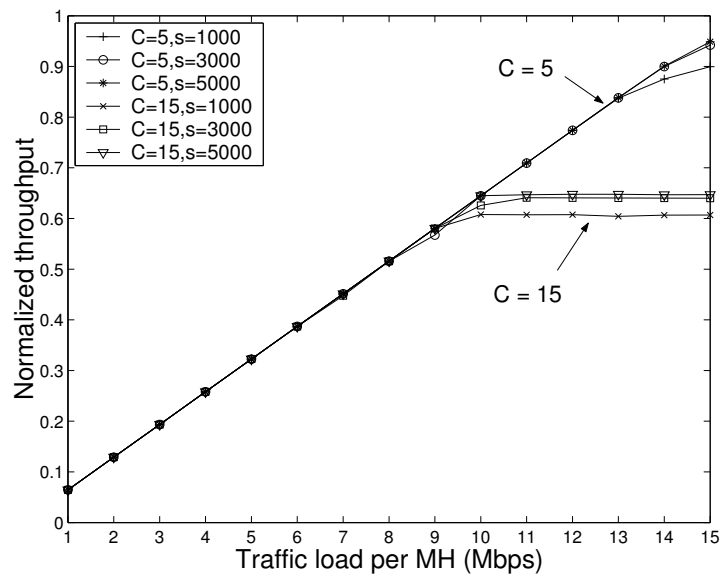


Figure 4.53: Throughput of MAC B3 with different number of channels and slot sizes.

Chapter 5

Radio over Fiber based Road Vehicle Communication System

5.1 Introduction

The demand for intelligent transportation systems (ITSs) using the latest mobile communication technologies continuously increase to exchange traffic information and achieve safe, smooth, and comfortable driving. These systems can be categorized into road vehicle communication (RVC) systems and inter-vehicle communication (IVC) systems. The RVC system is an infrastructure network for ITS, which will be deployed along the road. The design requirements discussed in [78] for future RVC systems indicate that the data rate of about 2–10 Mbps per MH will be required. In particular, the system supports not only voice, data but also multimedia services such as realtime video under high mobility conditions. Since current and upcoming mobile cellular systems (e.g., GSM, UMTS) at microwave bands cannot supply a high-speed user with such high data rate traffic [79],[80], mm-wave bands such as 36 or 60 GHz have been considered [72],[78],[81]. Although these bands have higher bandwidth, it leads to very small cell size (up to tens of meters) due to its higher free space propagation loss as compared to conventional microwave bands. Thus, this system is characterized by very small cell that means numerous BSs are required to cover long roads and high user mobility. We see two challenging issues here: (1) the system should be cost-effective and (2) it must support a fast and simple handover procedure.

One promising alternative to the first issue is an RoF based network as mentioned in chapter 1. However, the second issue, i.e., fast handover procedure, still remains challenging and more difficulty than indoor environment due to high speed users. In order to consider the requirements, the system imposes on handover management, imagine a highway where a vehicle with an ongoing communication session is running at a speed of 100 km/h and the cell size is 100 m , then it will request handover every 3.6 sec. In addition, if the overlapping area between two adjacent cells is 10 m , handover must be done within 0.36 sec. This example suggests that a fast and simple handover procedure is indispensable in

contrast to conventional mobile cellular networks, where cell size as well as overlapping region is so large that there is enough time to treat handover. In this chapter we propose an MAC protocol for RoF RVC systems featuring fast handover and dynamic bandwidth allocation. It utilizes centralized control ability of RoF networks for efficient mobility management.

This chapter is organized as follows. In section 5.2, we briefly mention related works and in the following section the proposed RoF network architecture is described. An MAC protocol is presented in section 5.4, which is followed by a description of mobility support in section 5.5. Resource allocation issues are discussed in section 5.6. We also propose bandwidth management schemes for enhanced handover quality and bandwidth utilization in section 5.7. Performance evaluation of the schemes is reported in section 5.8, and finally we conclude the chapter in section 5.9.

5.2 Related Works

In [72], an RoF network at mm-wave bands for future RVC system based on CDMA has been proposed and implemented. To facilitate handover management, all the BSs connected to a CS simulcast the same signal to communicate with MHs. A drawback of the system is that the data cannot be properly received in the overlapping region between cells because of co-channel interference. An MAC protocol for RoF RVC system has been proposed in [81], which is based on reservation slotted ALOHA and dynamic slot assignment. This architecture also assumed simulcasting from all the BSs connected to a CS, having co-channel interference problem in overlapping areas. In contrast, the proposed architecture in this chapter avoids co-channel interference between cells, leading to seamless handover.

IEEE 802.11p is currently working on a draft standard for wireless access in vehicular environments (WAVE) using dedicated short-range communications (DSRC) operating at 5.9 GHz frequency bands [82]. However, it does not consider micro-cellular architecture deployed along the roads [83]. Combined with IEEE 802.11r for fast roaming, the system has a potential for fast handover although its handover latency would be much longer compared to our scheme and high bandwidth service considered in this chapter would not be supported.

5.3 System Description

5.3.1 Network Architecture

An RVC system based on RoF technology is shown in Fig. 5.1, where a CS is interconnected with a large number of BSs via optical fibers, and BSs are deployed along the road to support communication link to vehicles. In this chapter, we consider only one-dimensional road, and assume that the direction of MH's movement is known to the CS as it is easily determined while the MH moves. A CS is in turn connected to backbone networks such as public switched telephone network (PSTN) or the Internet. Each BS covers an area called "*cell*" and we assume that there is small overlapping area between two adjacent cells. In this study we focus on mm-wave band, e.g., 36 GHz or 60 GHz; therefore, the cell size

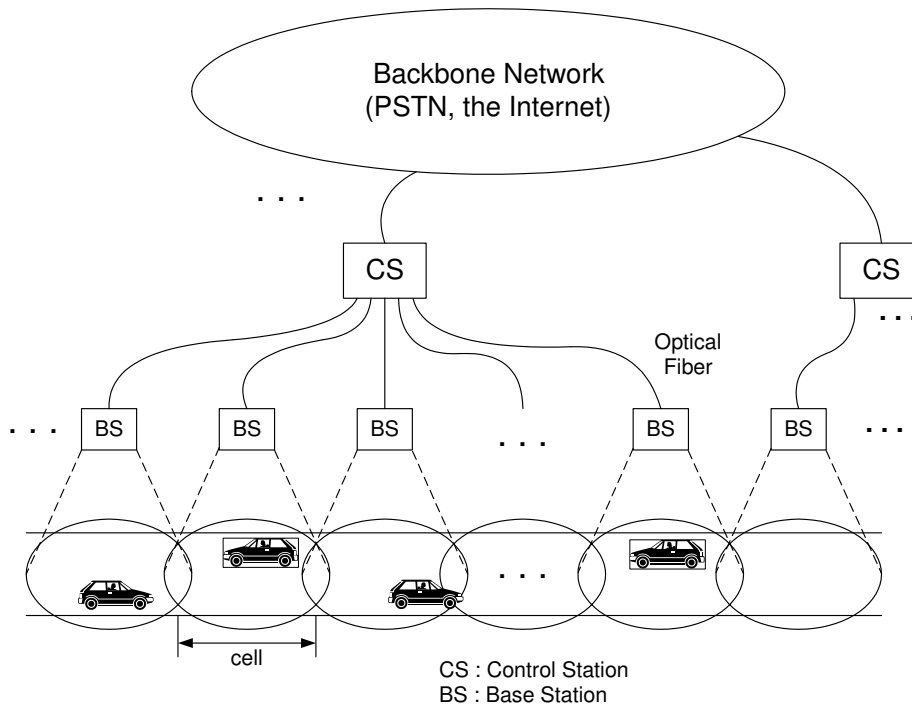


Figure 5.1: Road vehicle communication system based on radio over fiber technology.

could be very small up to a few tens of meters. As a result, a large number of BSs are required to cover a long road.

Several RoF technologies have been proposed to develop simple BS and transport mm-wave signals over an optical fiber. In this chapter, an RoF architecture is assumed, where TDMA/TDD operation is possible. Though there exist several possible options to implement such a system using different technologies, we present for explanation purpose an example of RoF architecture based on external modulation as shown in Fig. 5.2.

For downlink transmission (from CS to MH) user data first modulates RF source, which, in turn, modulates optical light source using an external optical modulator (EOM). This signal is carried over the downlink optical fiber to a BS, where the optical signal is converted into wireless signal and emitted from the BS. For uplink transmission (from MH to CS), the wireless signal received at the BS is changed into optical signal by modulating light source. It is then transported over uplink optical fiber to the CS, where a PD first demodulates optical signal to obtain electrical signal, which is again demodulated using oscillator to acquire user data. In this architecture, the CS has as many transceivers (TRXs) as BSs, and each TRX constitutes a light source such as laser diode (LD) for downlink transmission, a PD for uplink reception, and a modem to transmit and receive user data in the RF domain. The BS is basically composed of a PD, an LD, an EOM and amplifiers, and it has no processing functions. Each TRX can be equipped either with fixed RF oscillator or tunable RF oscillator. With tunable RF oscillator, the system has flexibility in resource allocation as will be seen in section 5.7.

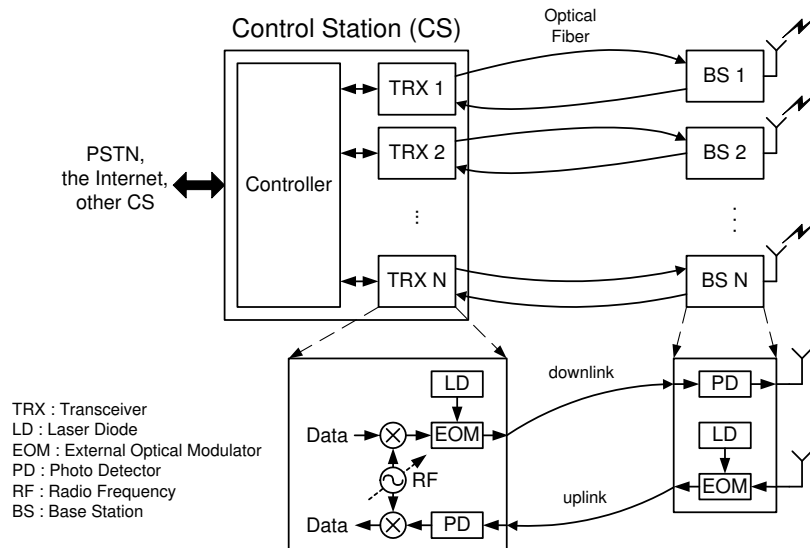


Figure 5.2: An access network architecture for road vehicle communication system based on radio over fiber technology.

5.3.2 Basic Operations

Suppose a CS is connected to N BSs based on the RoF architecture shown in Fig. 5.2, and the BSs are deployed along one-dimensional road. The N BSs are subdivided into S groups, $1 \leq S \leq N$, where a set of BSs in the same group must be contiguously deployed, and the area covered by a group is called “*virtual cellular zone (VCZ)*”. TDMA is utilized in the system for which a fixed-size super-frame consisting of M slots is defined for each VCZ with each slot fitted into the minimum size data packet. The RF channel in a VCZ is the same, and adjacent VCZs must not use the same RF channel to avoid co-channel interference. Therefore, while a vehicle is running within a VCZ it does not have to change RF channels. It must change RF channels only when it enters a new VCZ. A super-frame for a VCZ is subdivided into frames for the cells in the VCZ, and a frame is composed of downlink and uplink portion (detailed description of frame structure will be given in section 5.4). The size of a frame for a cell can be made proportional to the traffic demand of the cell.

Fig. 5.3 depicts a single VCZ constituting three cells and how three frames are allocated to each cell in the time domain while using the same RF channel. It should be emphasized here that during a time period for frame i only the corresponding BS i is activated by the CS; that is, BSs in a VCZ are supported by the CS in disjoint time periods (i.e., frames). Therefore, although one RF channel is employed there is no co-channel interference between cells within a VCZ. If a vehicle is in non-overlapping area, it will receive only one frame that corresponds to the cell where it is located. While if it is in overlapping area, it will listen to two frames within a super-frame time. For instance, in Fig. 5.3 vehicle 1 (V1) receives only frame 1, while vehicle 2 receives frame 1 and 2 since it is in the overlapping area between cell 1 and 2. Moreover, the figure also indicates the fact that a frame can support multiple vehicles as described in cell 3. Note that if a CS has multiple VCZs, as many super-frames as VCZs are served simultaneously.

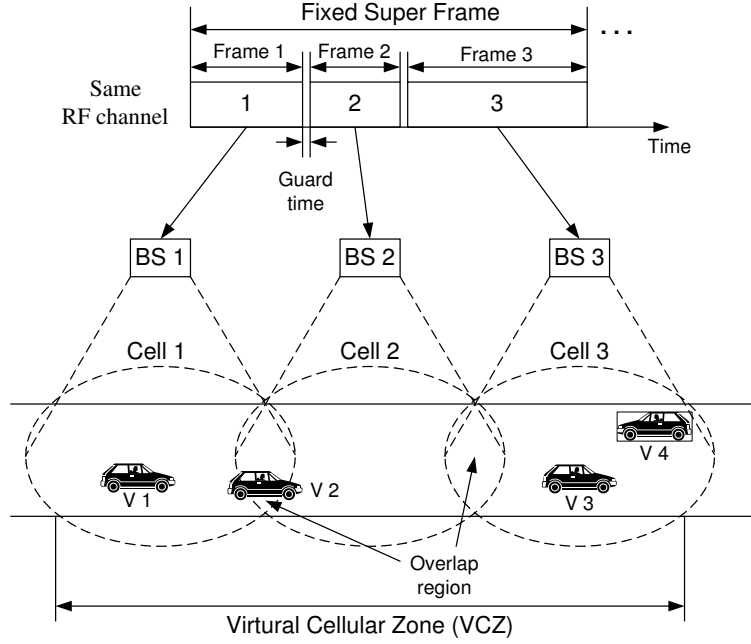


Figure 5.3: Frame allocation example.

5.4 Medium Access Control

In this section, we propose an MAC protocol for the system. Design goals of the MAC include a support of fast handover and capability of adaptive resource allocation for high throughput based on dynamic TDMA.

5.4.1 Frame Structure

The proposed architecture assumes a centralized MAC entity located at the CS offering a reservation-based, collision-free medium access. For each VCZ, the MAC regulates the medium access employing a super-frame-based slotted access (Fig. 5.4). The super-frame structure determines the “air-time” given to each BS within the VCZ, i.e., the time period each BS uniquely uses to communicate with MHs located in its coverage area. Even though the length of the super-frame is fixed to t_{SF} seconds, the duration of the frame assigned to each BS (t_{F_j} with respect to $BS j$) may be variable as long as

$$\sum_{j=1}^n t_{F_j} \leq t_{SF}$$

where n denotes the number of BSs accommodated in the current VCZ.

Each frame belonging to a certain BS begins with “*beacon*” field generated at the CS that consists of BS identification (ID) number and slot assignment map specifying the start slot position and length for each MH. The following field is “*reservation minislots*” which is accessed by MHs that have not yet reserved any slots but have the data to transmit. This field has a fixed size minislots and is

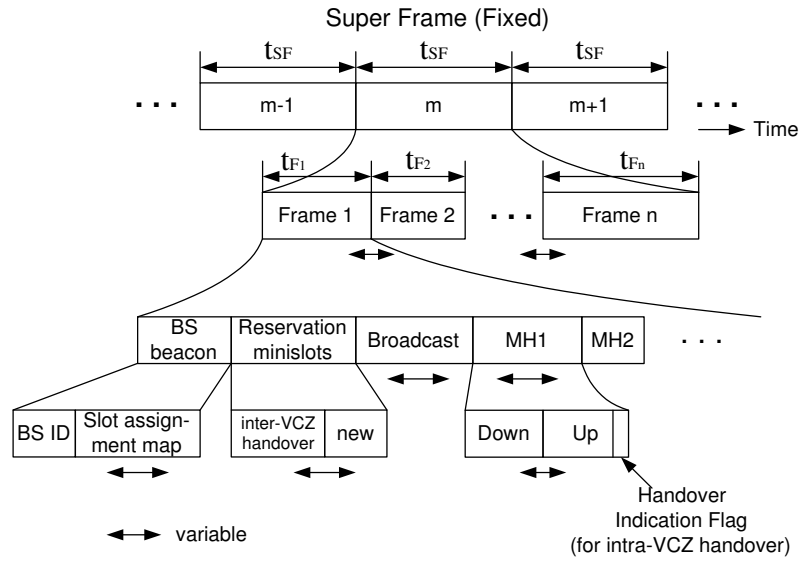


Figure 5.4: Frame structure. For simplicity, guard time is not represented.

accessed in contention-based way. In addition, it subdivides into minislots for inter-VCZ/inter-CS handover request (which will be described in section 5.5), and those for new connection request. The CS can change the portion of the minislots so that handover latency could be smaller than new connection requests. For contention resolution, conventional method such as p -persistent can be utilized. The results of reservation trial in the previous super-frame is broadcast in the “broadcast” field, which is followed by downlink and uplink slots assigned to each MHs as specified in the slot assignment map. In the uplink slot, there is a one-bit field called “handover indication flag” for fast intra-VCZ handover as explained later.

5.4.2 Initialization

When an MH wants to initiate communication with the system, it must first scan RF channels. After having identified the RF channel used in the cell, it must send a request for bandwidth to the CS using one of the reservation mini-slots. If the request is successful and the system has enough bandwidth to accommodate the requested bandwidth, the vehicle will be assigned the bandwidth in the next super-frame.

5.5 Mobility Support

5.5.1 Types of handovers

Within the proposed system architecture, we have three kinds of handovers:

- handover between two BSs belonging to the same VCZ (intra-VCZ handover),
- handover between two BSs belonging to different VCZs (inter-VCZ handover),

- handover between two BSs which are controlled by two different CSs (inter-CS handover).

In the following, the handover procedure for each of the three types is described. For all cases, an overlapping area between two adjacent BSs is assumed to be large enough to complete the handover procedure. For example, if an MH is running at 100 km/h the time it takes to run 1 m is 36 ms . Thus, when the super-frame time is small (say, $1\text{--}5 \text{ ms}$) a few meters of overlapping area would be enough for most practical cases.

5.5.2 Intra-VCZ Handover

As all BSs of a VCZ utilize the same RF channel, an MH entering the overlapping region between BSs begins to receive two beacons, each containing a different BS-ID during a super-frame time (t_{SF}). The MH sends in turn the CS a handover request by setting the “*handover indication flag*” then the CS reserves bandwidth for it in the next cell and releases bandwidth used by the MH in the old cell. It should be noted that resources to handover a connection from one BS to its successor BS are always available as the centralized MAC may adjust (i.e. shorten) the frame length of the BS the MH is leaving and hence can increase the frame duration of the successor BS in order to provide the MH with the required resources. As a result, in intra-VCZ handover, zero handover latency and zero handover dropping are possible; moreover, bandwidth is allocated along the MH’s movement. This is a main feature of the proposed architecture.

5.5.3 Inter-VCZ Handover

In this case, the MH cannot listen to a beacon from the new VCZ because adjacent VCZs must not use identical RF channel to avoid co-channel interference. Similar to conventional procedure, the MH may scan RF channels in the next VCZ, corresponding to the so-called hard handover. However, since the CS knows the direction of the MH, it can inform the MHs running in the last cell of the VCZ about the RF channel in the next VCZ. In this approach as soon as the MH is informed about the new RF channel, it begins to scan the new RF channel in a period during which it is not assigned bandwidth. If it receives the new RF channel, it sends a handover request using one of the reservation minislots for inter-VCZ handover. If the request to the new VCZ is successful and there is enough bandwidth in the new VCZ, the MH can continue its communication session; otherwise, the request is dropped. Thus, unlike intra-VCZ handover successful inter-VCZ handover involves not only changing RF channels but also bandwidth management. The CS may give the MH requesting handover higher priority than new connection requests. The issue is closely related to the so-called bandwidth reservation and connection admission control problem in mobile cellular networks, which will be discussed in section 5.6.

5.5.4 Inter-CS Handover

The handover between two CSs, i.e., between two VCZs controlled by two mutually different centralized MAC entities, is the most critical in terms of guaranteeing quality of service (QoS) parameters to any

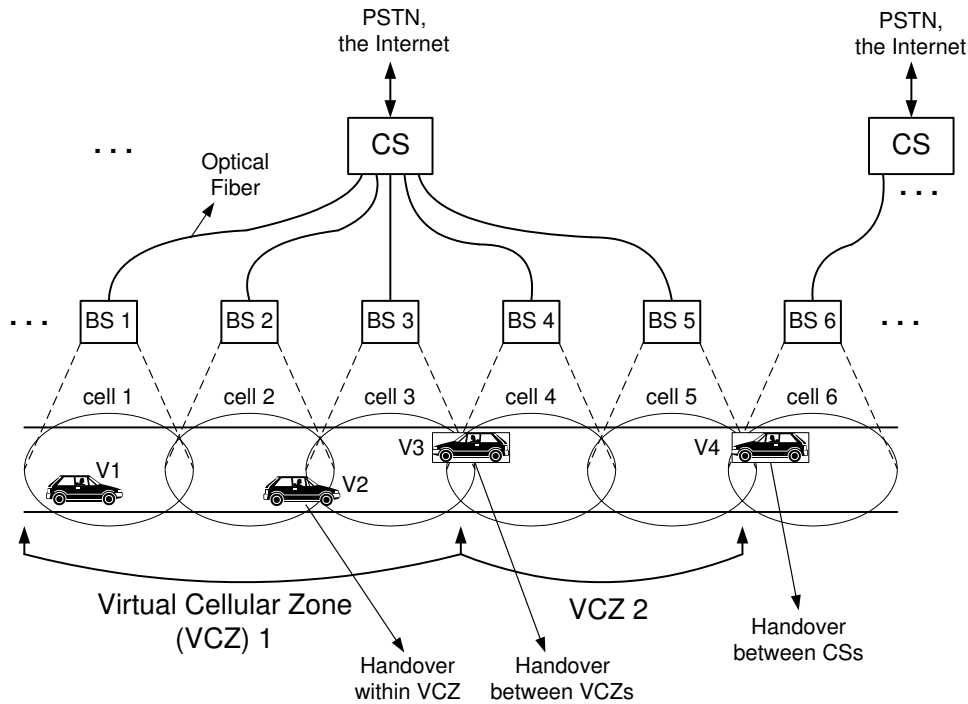


Figure 5.5: An example of the proposed architecture where cell 1,2,3 and 4,5 constitute two VCZs, respectively.

ongoing connection. The handover procedure is similar to inter-VCZ handover except that the two VCZs associated with it are controlled by two different CSs. Therefore, the same handover procedure for inter-VCZ handover can be applied. But, it requires the CSs to exchange control traffic for handover and if the traffic is based on internet protocol (IP), the problem becomes significant as handover involves change of routing path. This issue will not be discussed any more in this chapter.

5.5.5 Operation Example

Fig. 5.5 shows a simple example where a CS connected with five BSs. It consists of two VCZs, each of which has three and two BSs, respectively. The figure depicts that vehicle 2, 3, and 4 request intra-VCZ handover, inter-VCZ handover, and inter-CS handover, respectively. The corresponding two super-frames and their frame allocations before and after handover are indicated in Fig. 5.6.

5.6 Resource Allocation Issues

The network architecture raises an interesting issue, i.e., the number of VCZs as well as the number of cells of each VCZ can be dynamically changed if the system provides flexibility for such operation. If the total traffic load can be supported by one super-frame, all the BSs form a single VCZ. From handover point of view, such case would produce the best performance as inter-VCZ handover is not involved while a vehicle crosses the area covered by the CS. On the other hand, if traffic load of each

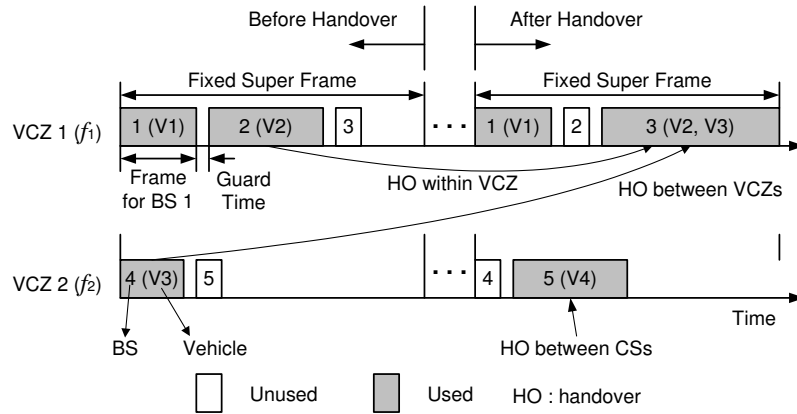


Figure 5.6: Frame allocation example for Fig. 5.5.

cell is high and the CS's capacity is enough that it can support as many VCZs as BSs, then each cell may become a VCZ. In such case whenever an MH crosses a cell boundary, it requires inter-VCZ handover, resulting in possibly poor handover performance in terms of handover dropping. An interesting issue can be described as follows. Given traffic load, what is the minimum number of VCZs and the optimal number of cells in each VCZ? Moreover, these two quantities can be changed dynamically according to traffic load. However, when a cell belonging to a VCZ changes to other VCZ, the MHs in the cell must change RF channels accordingly, resulting in an overhead. In this study, we consider only the case when the number of VCZs is fixed, while the number of cells, called *VCZ-size*, of each VCZ can be variable, which will be referred to as "*VCZ-resizing*".

"Guard channel concept" in conventional mobile cellular networks can be applied to inter-VCZ (and -CS) handover with some modification; that is, each VCZ (not each cell) reserves some bandwidth for handover connection. A challenging open issue here is how much bandwidth should be reserved. To improve the QoS as perceived by the users, various methods have been devised to prioritize handover requests over connection initiation requests when allocating bandwidth. Recently, schemes that try to limit handover dropping probability to prespecified target value in multimedia wireless environment have been proposed [57],[58],[85]. In this study, we adopt one of them for our inter-VCZ handover and propose an algorithm that allows VCZs to resize while maintaining handover dropping probability below a prespecified target value.

5.7 Bandwidth Management Schemes

In this section, we propose bandwidth management schemes for inter-VCZ handover assuming that intra-VCZ handover is perfect, the number of VCZs is fixed while the number of cells of each VCZ can be changed. In addition, we also assume each VCZ reserves a portion of its bandwidth to prioritize handover connection. In particular, we consider a CS connected with fixed number of cells and focus

Table 5.1: Bandwidth Management Schemes

		BW reservation	
		fixed	adaptive
VCZ size	fixed	FA1	FA2
	variable	VA1	VA2

on the case when the number of VCZs is fixed but the number of cells of each VCZ, called “VCZ-size”, can either be fixed or variable. The objective of the schemes is to enhance handover performance while achieving high bandwidth utilization. Concerning handover quality two performance measures are relevant, that is, the probability (P_{HD}) of inter-VCZ handover dropping and the probability (P_{CB}) of new connection blocking. And bandwidth utilization (B_U) and reserved bandwidth for handover (B_H) are two performance measures regarding bandwidth usage.

It is to be noted that we have two parameters by which bandwidth management schemes proposed are differentiated: (1) VCZ-size and (2) bandwidth reservation algorithm for handover. According to the capability to dynamically change each of the two parameters four schemes are considered, which are summarized in table 5.1. In **FA1** both VCZ-size and B_H are fixed, while in **FA2** VCZ-size is fixed, but B_H is adaptively changed according to traffic load and a target handover dropping probability. For an adaptive bandwidth reservation algorithm for handover, we adopt a recently proposed scheme for mobile cellular networks [85]. It is suitable for our purpose since it has the ability to adaptively change B_H so that P_{HD} is limited to a prespecified target value regardless of traffic load. Since it was originally proposed for mobile cellular networks, it should be modified appropriately so that it can be utilized for inter-VCZ handover. In **VA1** VCZ-size is variable (i.e. resizing VCZ) with fixed B_H , while in **VA2** both are variable. Basic idea of the resizing procedure of VCZ is as follows. When a VCZ has no enough bandwidth to accommodate a new or handover request, the CS investigates if the leftmost (or rightmost) cell of the VCZ can be taken over to adjacent VCZ to secure bandwidth for the request (a generalized version will be given below). If so, the cell is taken over to the adjacent VCZ and the request is accepted. It is expected that by changing VCZ-size bandwidth utilization is improved. However, it will incur overhead since the MHs in the cell must change RF channels when a cell belonging to a VCZ is taken over to another VCZ. In addition, since there is a trade-off between handover quality and bandwidth utilization, it should carefully be designed so that it makes no great effect on handover quality. The proposed scheme in this study works together with adaptive bandwidth algorithm to accomplish high bandwidth usage and handover quality. Each of the schemes is described in more detail in the following sections.

5.7.1 Fixed-VCZ Schemes

In these schemes (**FA1**, **FA2**) VCZ size, i.e., the number of cells covered by each VCZ, remains the same. Therefore, a fixed-tuned radio modem can be employed at the CS, leading to a simple RF modem.

We consider two schemes that are different in terms of bandwidth management for handover connection. In the first scheme, called **FA1**, a fixed amount of bandwidth is reserved for handover in each VCZ. One drawback of the scheme is that blocking probabilities (P_{CB}, P_{HD}) increase with traffic load. Furthermore, bandwidth is not efficiently used when too large bandwidth is reserved.

For a handover connection request with bandwidth B_{hand} in a VCZ i a simple admission control is used. That is, it is admitted when the following relation, called **AC0**, is satisfied.

$$B_U^i + B_{hand} \leq C \quad (\mathbf{AC0})$$

where B_U^i is the bandwidth being employed in VCZ i by ongoing connections and C is the VCZ capacity.

For a new connection request with bandwidth B_{new} admission control (**AC1**) is

$$B_U^i + B_{new} \leq C - B_H^i \quad (\mathbf{AC1})$$

where B_H^i is the reserved bandwidth for inter-VCZ handover of VCZ i . Only when the above test is satisfied the new connection request is accepted.

In **FA1** B_H in **AC1** is fixed, while in **FA2** it is adaptively changed according to the scheme proposed in [85]. The scheme is designed to limit P_{HD} to a prespecified target handover dropping probability (P_t) regardless of traffic load in multimedia mobile cellular networks. After a modification, the algorithm is rewritten in Fig. 5.7. When a handover request arrives the CS examines whether there is available bandwidth or not in the VCZ. If it is dropped due to insufficient bandwidth, the VCZ must promptly respond to it by increasing B_H for inter-VCZ handover by one bandwidth unit (BU) (in our case, BU corresponds to one data slot). When the handover request is successful, the number of successful requests (R_q) is increased by one. If R_q is greater than the inverse of P_t , B_H is decreased by one BU and R_q is set to zero. So the algorithm simply says that for a given P_t , it counts the number of handover failures and successes such that P_{HD} is maintained below P_t .

The following admission control for new connection request is applied along with the above algorithm.

$$(i) \quad B_U^i + B_{new} \leq C - B_H^i \quad (\mathbf{AC2})$$

$$(ii) \quad B_U^j + B_H^j \leq C$$

for the next adjacent VCZ j

The first line examines if there is enough bandwidth for the request in the current VCZ, while the second line investigates whether the next adjacent VCZ j is likely to be overloaded or not. Note that direction information of a MH is known to the CS so that only the next VCZ is examined instead of all adjacent VCZs. Not satisfying the second condition suggests the possibility that the VCZ might be overloaded, so if the new connection request is accepted, it will be likely to be dropped when it is handed over to the VCZ. The new connection is accepted only when the two conditions are satisfied .

```

1 :  $R_q := 0; B_H := 0;$ 
2 : WHILE (time increases)
3 :   IF (handover into the current VCZ happens) THEN
4 :     /* examine available bandwidth in the VCZ */
5 :     IF ( FA2 ) THEN run AC0
6 :     IF ( VA2 ) THEN run AC4
7 :     IF (handover request drops) THEN
8 :        $B_H := B_H + BU;$ 
9 :     ELSE
10:       $R_q := R_q + 1;$ 
11:      IF ( $R_q > \lceil 1/P_t \rceil$ ) THEN
12:         $B_H := B_H - BU;$ 
13:         $R_q := 0;$ 
14:      END IF
15:    END IF
16:    IF ( $B_H < 0$ ) THEN  $B_H := 0;$  END IF
17:    IF ( $B_H > C$ ) THEN  $B_H := C;$  END IF
18:  END IF
19: END WHILE

```

Figure 5.7: Pseudo code of bandwidth reservation scheme for inter-VCZ handover. R_q and B_H are initialized to zero from the beginning of the scheme. $\lceil x \rceil$ indicates the smallest integer greater than or equal to x .

The second condition (*ii*) plays an important role for proper operation at heavy traffic load as indicated in [85]. The reason can be explained as follows. Suppose two adjacent cells A and B , each of which has a BS, and at some time instant handover traffic from cell B to cell A is dropped due to insufficient bandwidth in cell A . Then, cell A increases B_H to reduce its P_{HD} , which will suppress newly generated traffic in cell A . That, in turn, reduces handover traffic from cell A to cell B so that cell B could allow more new traffic. This will cause more handover traffic from cell B to cell A . The circulation continues until it reaches an equilibrium point. In an extreme case with heavy traffic, cell A will serve only handed-over traffic from cell B , while cell B will see few handed-over traffic from cell A . This explanation can be extended to a more general case with many cells. That is, with heavy traffic load some cells reject almost all new connection requests while serving only handed-over connections. On the other hand, the opposite occurs in others. This is an undesirable situation into which an adaptive bandwidth reservation schemes may fall unless they are carefully designed considering the above condition. This phenomenon was found in [58],[85]. To solve the problem, admission control **AC2** has been proposed in [58].

5.7.2 Variable-VCZ Schemes

In these schemes the number of cells of each VCZ varies (i.e., resizing VCZs) while the number of VCZs remains the same. Resizing of VCZs requires that radio modem for each BS in the CS must have the capability to change RF channels; furthermore, a mechanism is needed for the CS to send the MHs

commands so that they can change RF channels accordingly. This is the cost to be paid for variable-VCZ schemes. Basic operation of resizing of VCZs is in the following. When a VCZ has no enough bandwidth to accommodate a new or handover request, the CS investigates whether a set of contiguous cells S_{left} starting from the leftmost cell of the VCZ can be taken over to left adjacent VCZ to secure bandwidth for the request. Similarly, the CS also obtains a set of cells S_{right} starting from the rightmost cell. It then compares the two sets and chooses one of them that has enough bandwidth for the request and more available bandwidth if the set were taken over. When there are no such cells, the request is blocked; otherwise, the cells in the chosen set are taken over to the corresponding adjacent VCZ, and the request is accepted.

The scheme can be more efficient in system resource management at the cost of overhead. The first scheme, called **VA1**, employs this VCZ resizing procedure with fixed B_H , while the second scheme, called **VA2**, combines this procedure with adaptive bandwidth reservation described in Fig. 5.7 to maintain handover quality regardless of traffic load.

When a request arrives at a VCZ the following procedure is conducted for resizing VCZs.

- C1)** If the request with bandwidth B_{req} is of new (handover) connection type, the CS investigates whether it passes **AC1** (**AC0**). If so, the request is admitted and finishes the procedure, otherwise go to step **C2**.
- C2)** Let $\{B_{cell,1}, B_{cell,2}, \dots, B_{cell,K}\}$ denotes a set of bandwidth usage of cells in the VCZ starting from the leftmost cell, where K is the total number of cells in the VCZ. At first, obtain a set of cells S_{left} starting from the leftmost cell that could be taken over to the left VCZ as described in Fig. 5.8. The algorithm identifies the left set S_{left} , and informs how much bandwidth would be left $B_{empty,left}$ in the left adjacent VCZ if the set of cells were taken over to the left VCZ. Similarly, for the right cells obtain S_{right} and $B_{empty,right}$ as shown in Fig. 5.9 and go to step **C3**
- C3)** In this step, select either S_{left} or S_{right} based on the criterion that a set having larger empty bandwidth (B_{empty}) is chosen and give it over to the chosen VCZ according to the procedure described in Fig. 5.10. If the condition in the code is not satisfied, the request is blocked.

Note that there is a possibility that at a certain traffic load, frequent takeover of cells could occur between VCZs, resulting in great overhead. In order to mitigate such phenomenon, a threshold Th is introduced in step **C3** as shown in Fig. 5.10. Its range covers from 0 to C and when it is C , **VA1** becomes **FA1**. In this sense **VA1** is a generalized scheme of **FA1**. Since the above procedure can be regarded as a kind of admission control for new and handover connections, it is called **AC3**.

The second scheme **VA2** combines the above VCZ resizing procedure with adaptive bandwidth reservation in Fig 5.7. Specifically, this performs almost the same as **VA1** with an exception that **AC1** is replaced with **AC2** in step **C1**. Then, this scheme for **VA2** is referred to as **AC4**. It should be emphasized that in this case B_H in the adaptive bandwidth reservation is adaptively changed according to the handover admission result of **AC4**, which is specified in Fig. 5.7. That is, in **VA2** for every

```

1 :  $B_{take,left} := 0;$ 
2 :  $i := 1;$ 
3 : WHILE ( $i \leq K - 1$ )
4 :    $B_{take,left} := B_{take,left} + B_{cell,i};$ 
5 :   include cell  $i$  in  $S_{left};$ 
6 :   IF (request occurs in cell  $i$ ) THEN
7 :      $B_{take,left} := B_{take,left} + B_{req};$ 
8 :     BREAK WHILE
9 :   END IF
10 :  IF ( $B_{take,left} \geq B_{req}$ ) THEN
11 :    BREAK WHILE
12 :  END IF
13 :   $i := i + 1;$ 
14 : END WHILE
15 :  $B_{empty,left} := C - B_{U,left} - B_{take,left};$ 

```

Figure 5.8: Pseudo code for part of step **C2** to obtain the left set S_{left} and left empty bandwidth $B_{empty,left}$ for variable-VCZ scheme. $B_{take,left}$ and i are initialized to 0 and 1, respectively, and $B_{U,left}$ is the bandwidth being used in the left VCZ.

```

1 :  $B_{take,right} := 0;$ 
2 :  $i := K;$ 
3 : WHILE ( $i \geq 2$ )
4 :    $B_{take,right} := B_{take,right} + B_{cell,i};$ 
5 :   include cell  $i$  in  $S_{right};$ 
6 :   IF (request occurs in cell  $i$ ) THEN
7 :      $B_{take,right} := B_{take,right} + B_{req};$ 
8 :     BREAK WHILE
9 :   END IF
10 :  IF ( $B_{take,right} \geq B_{req}$ ) THEN
11 :    BREAK WHILE
12 :  END IF
13 :   $i := i - 1;$ 
14 : END WHILE
15 :  $B_{empty,right} := C - B_{U,right} - B_{take,right};$ 

```

Figure 5.9: Pseudo code for part of step **C2** to obtain the right set S_{right} and right empty bandwidth $B_{empty,right}$ for variable-VCZ scheme. $B_{take,right}$ and i are initialized to 0 and K , respectively, and $B_{U,right}$ is the bandwidth being used in the right VCZ.

```

1:  $B_{empty} = -1; direction = -1;$ 
2: IF ( $B_{empty,left} \geq Th$  AND  $B_{empty,right} \geq Th$ ) THEN
3:   IF ( $B_{empty,left} \geq B_{empty,right}$ ) THEN
4:      $B_{empty} := B_{empty,left}; direction := left;$ 
5:   ELSE
6:      $B_{empty} := B_{empty,right}; direction := right;$ 
7:   END IF
8: ELSE IF ( $B_{empty,left} < Th$  AND  $B_{empty,right} \geq Th$ ) THEN
9:    $B_{empty} = B_{empty,right}; direction := right;$ 
10: ELSE IF ( $B_{empty,left} \geq Th$  AND  $B_{empty,right} < Th$ ) THEN
11:    $B_{empty} = B_{empty,left}; direction := left;$ 
12: END IF
13: IF ( $B_{empty} \neq -1$  AND  $direction \neq -1$ )
14:   IF ( $direction = right$ ) THEN
15:     right VCZ takes over the cells in  $S_{right}$ ;
16:   ELSE
17:     left VCZ takes over the cells in  $S_{left}$ ;
18:   END IF
19: END IF

```

Figure 5.10: Pseudo code for step **C3** to give a set of cells over to an adjacent VCZ. $B_{empty}, direction$ are initialized to -1, respectively. Th is introduced to mitigate frequent takeover of cells between VCZs.

handover request **AC4** is run, and the result is used to change B_H in the adaptive bandwidth reservation, which is specified in line 6 of Fig. 5.7. Notice again that if the parameter Th in step **C3** is too small frequent takeover of cells between VCZs can take place that might affect B_U and B_H in Fig. 5.7 and **AC2**, leading to improper operation. Thus, it should be chosen in such a way that it leads to stable operation as well as system improvement. On the other hand, when Th grows high **VA2** becomes **FA2**; therefore, **VA2** can be considered as a generalization of **FA2**.

5.7.3 Inter-CS Handover Management

For inter-CS handover, **FA1** can easily be applied without any modification, while variable-VCZ schemes cannot be utilized. However, inter-CS handover dropping probability can also be limited to a prespecified value using the adaptive bandwidth reservation algorithm described in Fig. 5.7, but it requires overhead. In particular, admission control **AC2** for the algorithm requires bandwidth being used in the next adjacent VCZ. That is, the two CSs must exchange information on bandwidth utilization of the corresponding two VCZs in the border between the CSs whenever a new connection request is made. The overhead that will increase with traffic load can greatly be reduced by the introduction of a margin in the second line of **AC2** as shown in [85] at the cost of small portion of bandwidth.

5.8 Performance Evaluation

In this section, a simulation study for the proposed bandwidth management schemes in Table 5.1 for inter-VCZ handover is described.

5.8.1 Simulation Assumptions and Parameters

We consider a one-dimensional road, a typical highway environment, where MHs travel along a straight road. The following assumptions are made for this model:

- A1) Fig. 5.11 shows a simulation model, where a CS covers 5 km area with 50 BSs, and the cell size is 100 m. The cells are numbered from 1 to 50, with wraparound to avoid edge effect.
- A2) Five VCZs, i.e., five super-frames, are supported. Each VCZ is initialized to cover ten contiguously deployed cells (Fig. 5.11).
- A3) Connection requests are generated according to a Poisson process with rate λ (connections/second) in the system. A newly generated connection can appear anywhere in the VCZ with an equal probability.
- A4) A connection is either for voice (requiring 1 BU) or for video (requiring 4 BU) with probabilities R_v and $1 - R_v$, respectively, where the voice ratio $R_v \leq 1$.
- A5) An MH can travel in either of two directions with an equal probability with a speed chosen at random between 80 and 120 (km/h). Each MH will run straight through the road with the chosen speed and never turn around.
- A6) Each connection's life time is exponentially distributed with mean 120 seconds.
- A7) Each super-frame has a fixed channel capacity (C) of 100 BUs.
- A8) Intra-VCZ handover is perfect, so only the inter-VCZ handover is considered.

Unless otherwise specified, the above parameter values are assumed. For a measure of traffic, we use the *offered load* (L), which is defined as connection generation rate \times connections' bandwidth \times average connection life time. That is, L is represented by

$$L = \lambda \cdot (1 \cdot R_v + 4 \cdot (1 - R_v)) \cdot 120 \quad (5.1)$$

with the assumptions described above. The physical meaning of the offered load is the total bandwidth required on the average to support all the existing connections in the system.

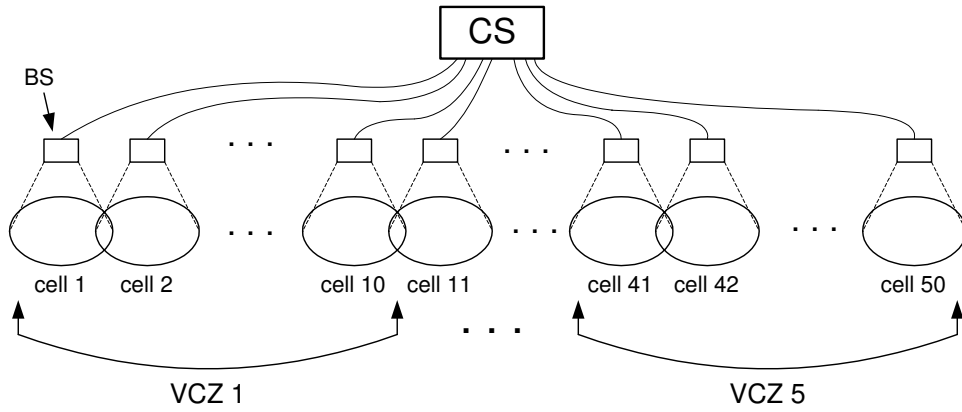


Figure 5.11: Simulation model comprises 50 cells and five VCZs that cover 5 km road. Each VCZ is initialized to cover ten contiguous cells and the cell size is 100 m. In fixed-VCZ schemes the configuration remains the same, while in the variable-VCZ schemes the number of cells covered by each VCZ can change with time.

5.8.2 Numerical Results

5.8.2.1 Blocking Probabilities

Blocking probabilities (P_{HD} , P_{CB}) versus offered load when $R_v = 0.5$ for **FA1** is shown in Fig. 5.12. It is observed that P_{HD} and P_{CB} increase with traffic load, and by setting B_H to 10 BU's P_{HD} can be greatly reduced at the cost of P_{CB} . Fig. 5.13 indicates P_{HD} , P_{CB} of **FA2** when $R_v = 0.5$. In contrast to **FA1**, P_{HD} is maintained below P_t regardless of traffic load. The effects of R_v in **FA2** is shown in Fig. 5.14, suggesting that as traffic tends to be voice-oriented smaller blocking probabilities are observed even if offered load remains the same. The three figures we have seen so far for fixed-VCZ schemes will be compared to those of variable-VCZ schemes in the following.

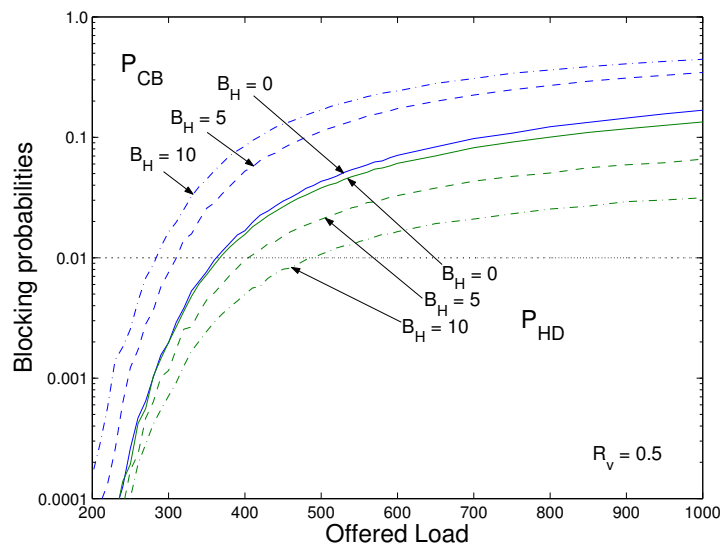


Figure 5.12: P_{CB} and P_{HD} vs. offered load for **FA1** when $R_v = 0.5$.

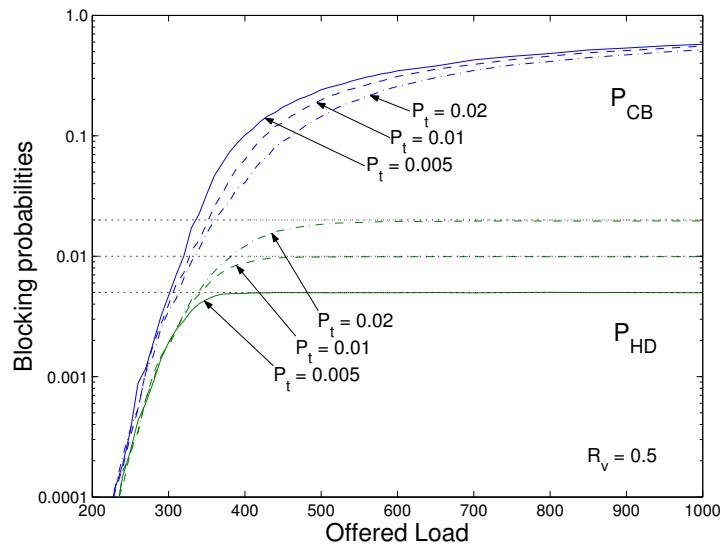


Figure 5.13: P_{CB} and P_{HD} vs. offered load for **FA2** when $R_v = 0.5$.

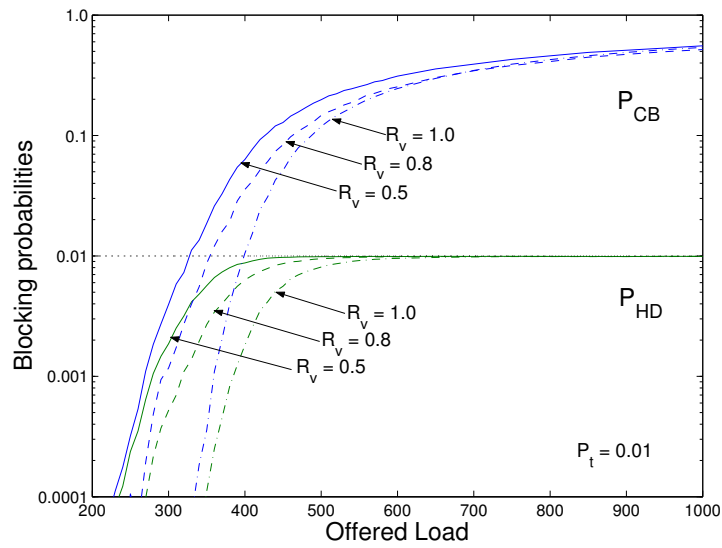


Figure 5.14: P_{CB} and P_{HD} vs. offered load for **FA2** when P_t is 0.01.

Blocking probabilities of **VA1** with $R_v = 0.5$ is represented in Fig. 5.15, where four cases are considered, i.e., $(B_H = 0, Th = 0)$, $(B_H = 0, Th = 10)$, $(B_H = 10, Th = 0)$, $(B_H = 10, Th = 10)$. Notice that B_H is introduced for giving priority to handover requests in admission control, while Th mainly for mitigating frequent takeover of cells between VCZs in variable VCZ-size algorithm. When B_H is zero, no preference is given to handover requests over new requests, and when Th is zero most frequent cell exchange between VCZs is expected. In the first case $(B_H = 0, Th = 0)$, much better performance at low and medium traffic load is observed in terms of blocking probabilities as compared to the case when B_H is zero in **FA1**. In the second case $(B_H = 0, Th = 10)$, on a request arrival **VA1** tries to find capacity within the VCZ rather than in adjacent VCZs. As will be clear later, no noticeable improvement is seen in terms of blocking probabilities and bandwidth utilization, but cell takeover rate is greatly reduced. P_{HD} is to a large extent decreased in the third case $(B_H = 10, Th = 0)$ at the cost of increased P_{CB} . Of all the four cases, the lowest P_{HD} is obtained in the fourth case $(B_H = 10, Th = 10)$.

P_{HD} is kept below P_t in **VA2** irrespective of offered load as shown in Fig. 5.16 with $R_v = 0.5$ and $Th = 20$. Our simulation study has shown that when both Th and P_t are small (e.g., $Th = 10$ and $P_t = 0.005$) P_{HD} is no longer maintained below P_t in **VA2**. The reason is as follows. In such a case whenever a handover drop occurs B_H will increase, which then decreases admission probability of new connections in **AC1**. However, new connection requests have still possibility to be admitted by VCZ-resizing procedure. In other words, high B_H does not always prevent new connection requests from being admitted, which, in turn, leads to P_{HD} higher than P_t . In case when P_t is greater than 0.005 **VA2** works very well when Th is greater than or equal to 15 $BU's$. As compared to Fig. 5.13, it shows smaller blocking probabilities, implying **VA2** manages bandwidth more efficiently than **FA2**. The effect of R_v is illustrated in Fig. 5.17 when P_t is 0.01 and Th is 20. It depicts that regardless of the voice ratio P_{HD} is limited below P_t , and **VA2** is far better than **FA2** in terms of blocking probabilities especially when traffic load is below system capacity.

5.8.2.2 Bandwidth Utilization

In this subsection, we will see bandwidth utilization (B_U, B_H) that correspond to the above six figures (Fig. 5.12 – Fig. 5.17). Fig. 5.18 indicates B_U and B_H of **FA1** when R_v is 0.5. In conjunction with Fig. 5.12, we observe nonzero B_H contributes to reducing handover dropping probability at the cost of bandwidth utilization. In other words, there is a trade-off between handover quality and bandwidth utilization. In **FA2** smaller P_t requires larger bandwidth to be reserved, resulting in smaller bandwidth utilization as shown in Fig. 5.19. Although we consider only two types of connections in this study Fig. 5.20 suggests this heterogeneity in traffic might have a great impact on bandwidth usage in **FA2**.

Bandwidth usage of **VA1** that corresponds to Fig. 5.15 is illustrated in Fig. 5.21 when R_v is 0.5. It achieves higher bandwidth utilization as compared to **FA1**. Of the four cases considered for **VA1**, the first case $(B_H = 0, Th = 0)$ exhibits the highest B_U , while the other parameters remain the same. That is because in this case there is no constraint on takeover of cells between VCZs and there is no

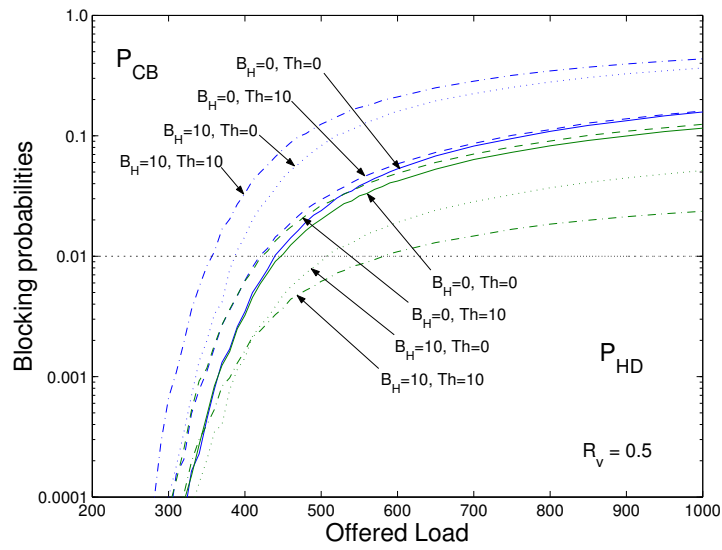


Figure 5.15: P_{CB} and P_{HD} vs. offered load for **VA1** with $R_v = 0.5$.

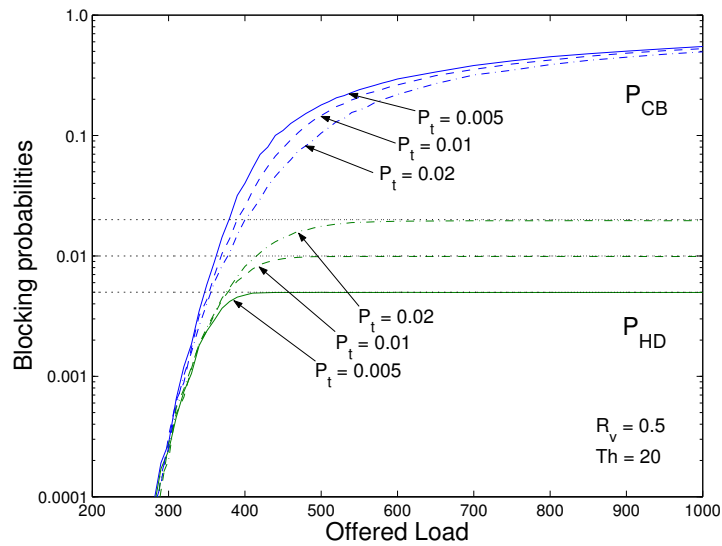


Figure 5.16: P_{CB} and P_{HD} vs. offered load for **VA2** for different P_t values with $R_v = 0.5$ and $Th = 20$.

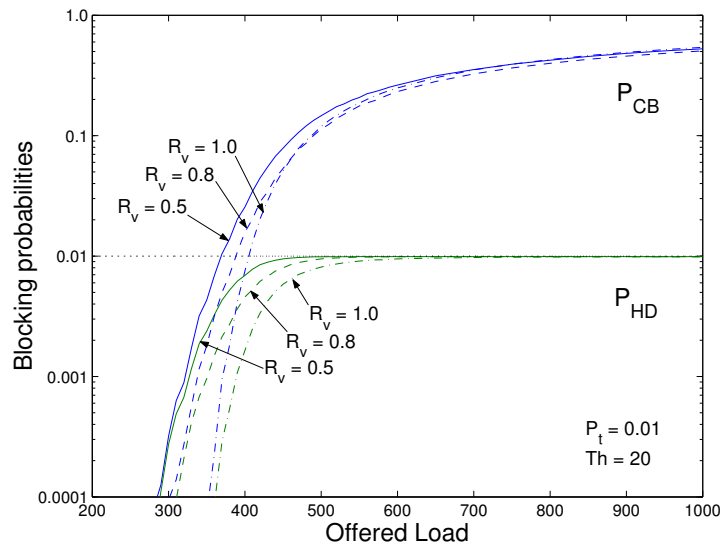


Figure 5.17: P_{CB} and P_{HD} vs. offered load for **VA2** for different R_v values when P_t is 0.01 and Th is 20.

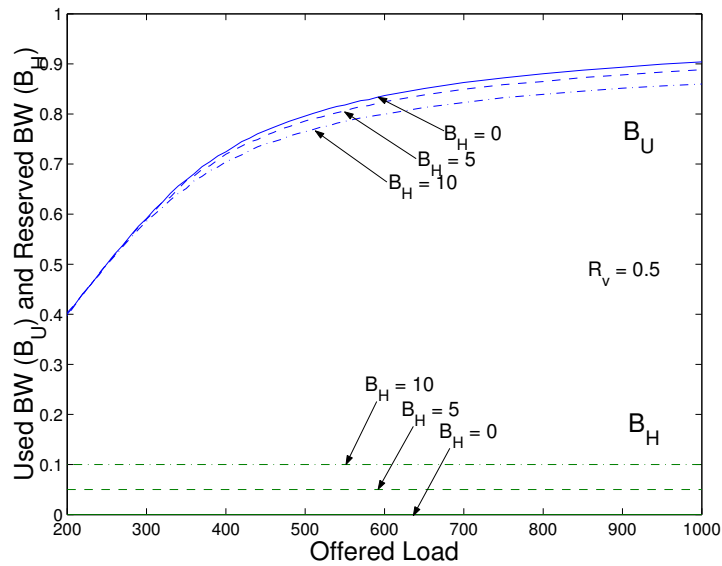


Figure 5.18: B_U and B_H vs. offered load for **FA1** when R_v is 0.5.

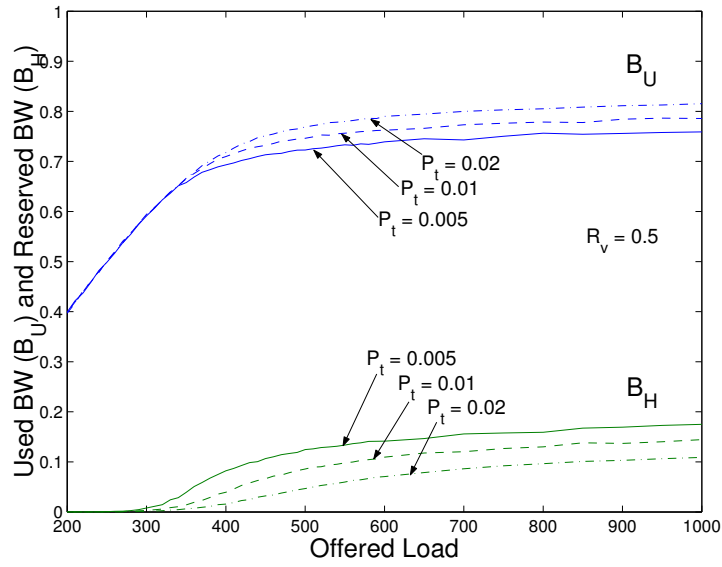


Figure 5.19: B_U and B_H vs. offered load for **FA2** when R_v is 0.5.

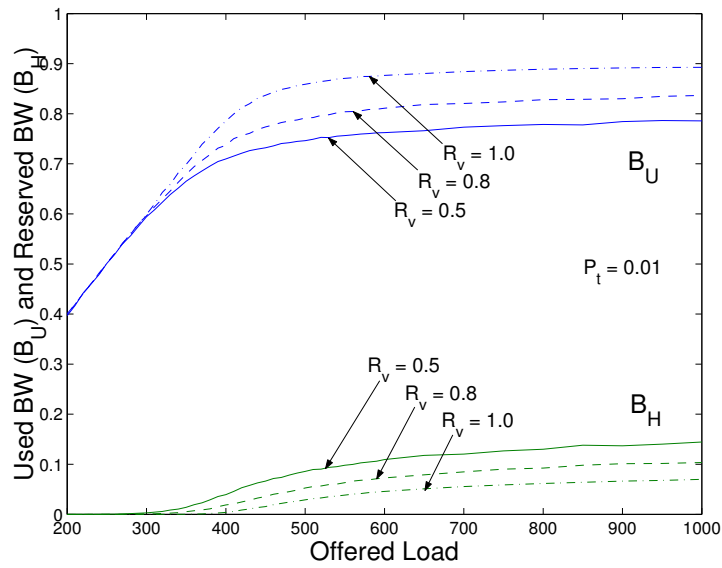


Figure 5.20: B_U and B_H vs. offered load for **FA2** when P_t is 0.01.

bandwidth reserved for handover. However, it has poor performance in blocking probabilities as shown in Fig. 5.15. The fourth case ($B_H = 10, Th = 10$) shows lowest bandwidth utilization at the price of lower P_{HD} .

Fig. 5.22 shows bandwidth utilization of **VA2** when R_v is 0.5 and Th is 20. As compared to **FA2** (Fig. 5.19), a remarkable increase is seen. That is, in comparison with **FA2**, **VA2** requires smaller B_H and achieves higher B_U while maintaining P_{HD} below P_t . The effect of R_v of **VA2** is indicated in Fig. 5.23, showing R_v has smaller impact on bandwidth utilization than in **FA2**. These results suggest that **VA2** is much better than **FA2** in terms of both blocking probabilities and bandwidth usage. This performance enhancement comes from the fact that the system resources are effectively utilized in variable-VCZ schemes by exchanging cells between VCZs.

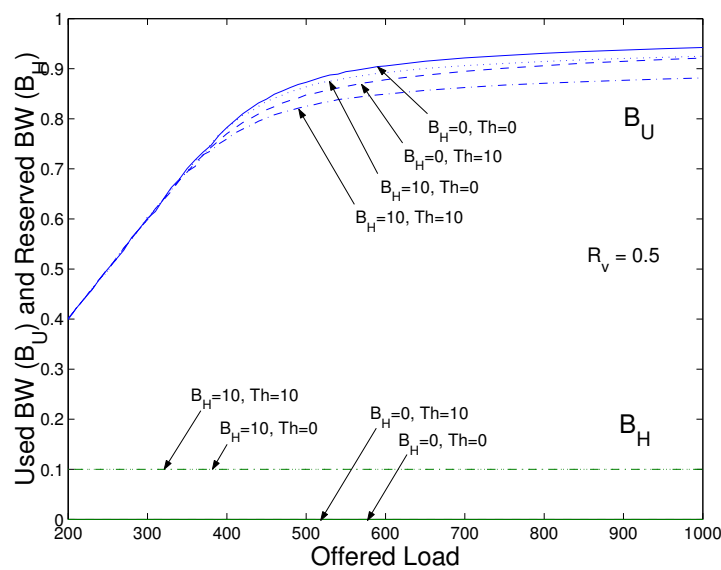


Figure 5.21: B_U and B_H vs. offered load for **VA1** when R_v is 0.5.

5.8.2.3 Cell Takeover Rate

The cost to be paid for enhanced performance of variable-VCZ schemes are shown in this subsection. Fig. 5.24 depicts mean cell takeover rate (cells/sec/VCZ) and the corresponding mean traffic takeover rate ($BUs/sec/VCZ$) of **VA1** when R_v is 0.5 and Th is 20. Of the four cases, with $B_H = 10$ and $Th = 0$, maximum takeover rate is seen. This is because in this case when a new connection request arrives in a VCZ **VA1** attempts to find capacity in adjacent VCZs whenever the bandwidth being used in the VCZ is over $C - B_H$. On the other hand, when B_H is zero and Th is 10, the smallest takeover rate is observed with poor blocking probabilities as shown in Fig. 5.15. In the case when B_H is 10 and Th is 10 a desirable performance is obtained in terms of blocking probabilities, bandwidth utilization, and cell takeover rate. The figure also shows that the takeover rate is influenced by not only B_H but also Th . Furthermore, for offered load between 300 and 550, takeover rate continuously increases, while at high traffic load takeover rate slightly grows (or decreases) since it is hard for the CS to find a VCZ that

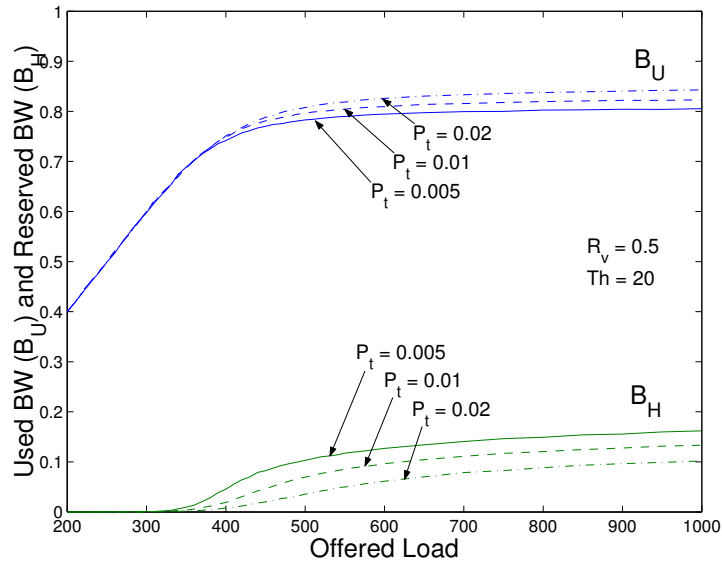


Figure 5.22: B_U and B_H vs. offered load for **VA2** when R_v is 0.5 and Th is 20.

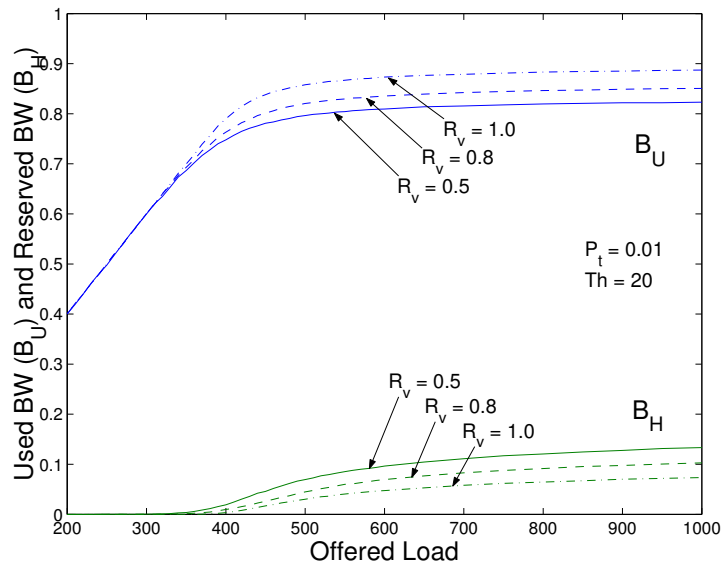


Figure 5.23: B_U and B_H vs. offered load for **VA2** when P_t is 0.01 and Th is 20.

can take over cells.

The influence of P_t on takeover rate in **VA2** is depicted in Fig. 5.25 with $R_v = 0.5$ and $Th = 20$, indicating small P_t incurs high takeover rate with heavy traffic load. Fig. 5.26 shows how the voice ratio affects takeover rate in **VA2** when P_t is 0.01 and Th is 20. It suggests that heterogeneity in traffic might have a great impact on takeover rate in **VA2**.

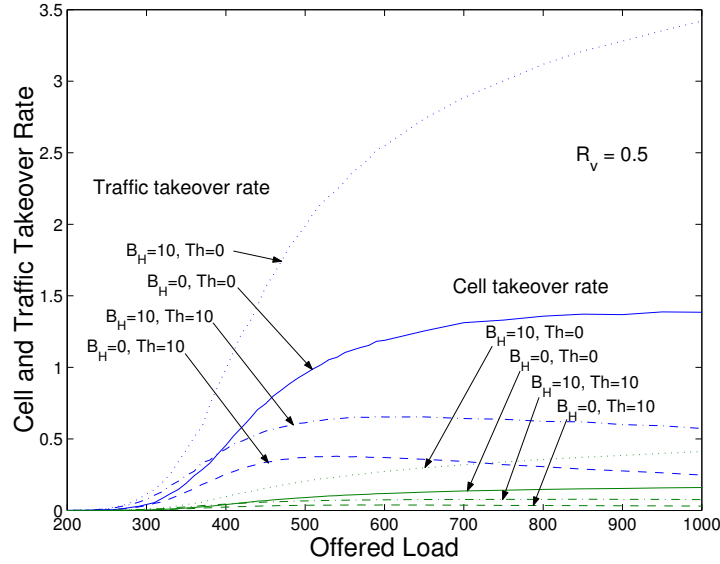


Figure 5.24: Mean cell takeover rate (cells/sec/VCZ) and mean traffic takeover rate ($BU/s/sec/VCZ$) for **VA1** when R_v is 0.5.

5.8.2.4 The Effect of Speed

In order to investigate the influence of MH's speed on performance in **VA2**, MH's speed was chosen at random between 40 and 60 km/h (called "low speed"), instead of 80 and 120 km/h (referred to as "high speed"). Fig. 5.27 shows blocking probabilities vs. offered load for different R_v values when P_t is 0.01 and Th is 20. As compared with the high speed case (Fig. 5.17), there is no big difference, implying MH's speed has no great effect on blocking probabilities. On the other hand, bandwidth usage is better in low speed case as indicated in Fig. 5.28 in comparison with high speed case (Fig. 5.23). Moreover, traffic and cell takeover rates are much lower than high speed case as shown in Fig. 5.29. The three figures suggest that in **VA2** bandwidth management becomes more efficient with slow speed users than high speed users.

5.8.2.5 The Effect of Cell Size

The impact of cell size in **VA2** is shown in the following three figures, where cell size was set to 50 m instead of 100 m , i.e., the number of cells becomes 100 while maintaining the same number of VCZs, and MH's speed was chosen at random between 80 and 120 km/h . Notice that in variable VCZ-size schemes, small cell size means that the CS has higher probability to shift cells between VCZs given the

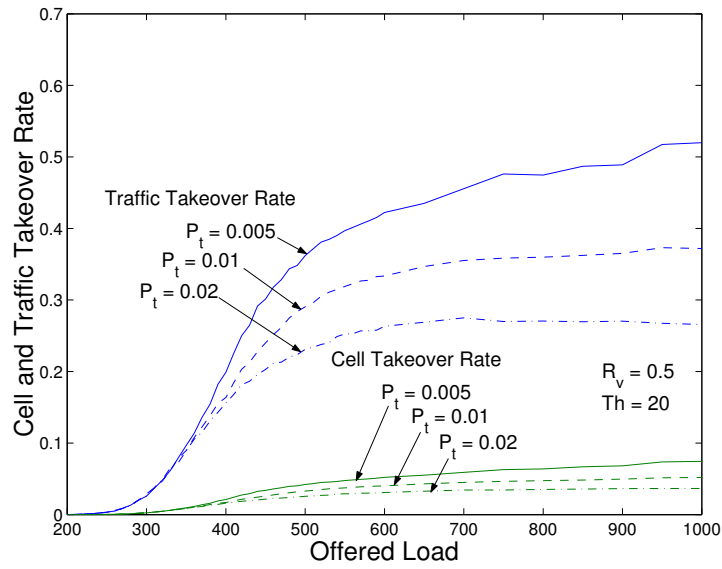


Figure 5.25: Mean cell takeover rate (cells/sec/VCZ) and mean traffic takeover rate ($BU s/sec/VCZ$) for **VA2** when R_v is 0.5 and Th is 20.

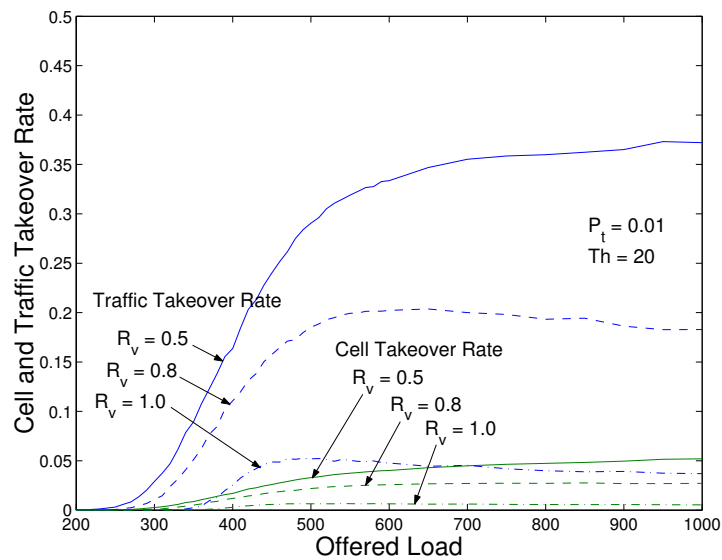


Figure 5.26: Mean cell takeover rate (cells/sec/VCZ) and mean traffic takeover rate ($BU s/sec/VCZ$) for **VA2** when P_t is 0.01 and Th is 20.

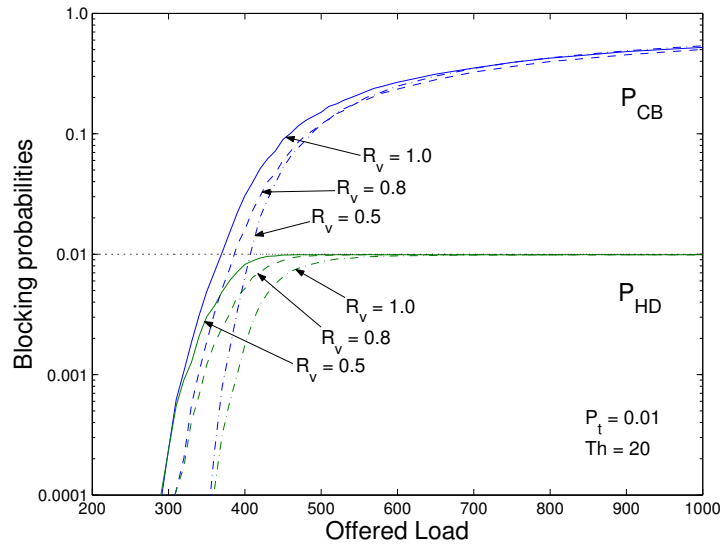


Figure 5.27: P_{CB} and P_{HD} vs. offered load for **VA2** when P_t is 0.01, Th is 20 and MH's speed is uniformly distributed between 40 and 60 km/h.

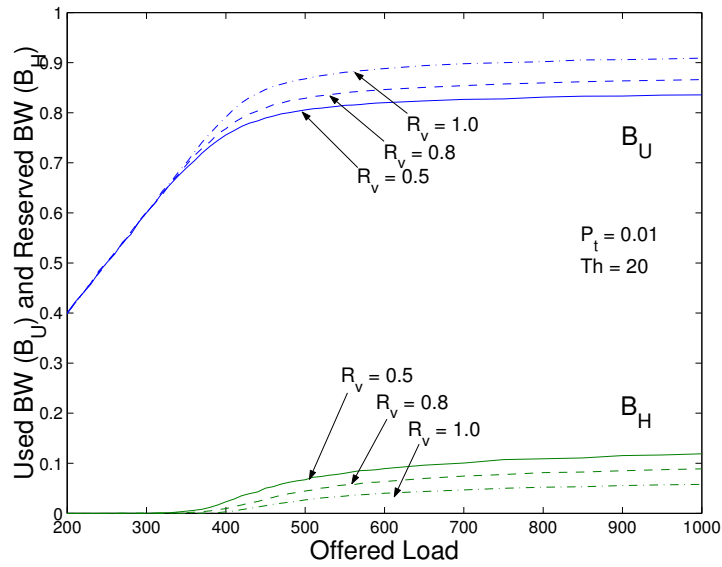


Figure 5.28: B_U and B_H vs. offered load for **VA2** when P_t is 0.01, Th is 20 and MH's speed is uniformly distributed between 40 and 60 km/h.

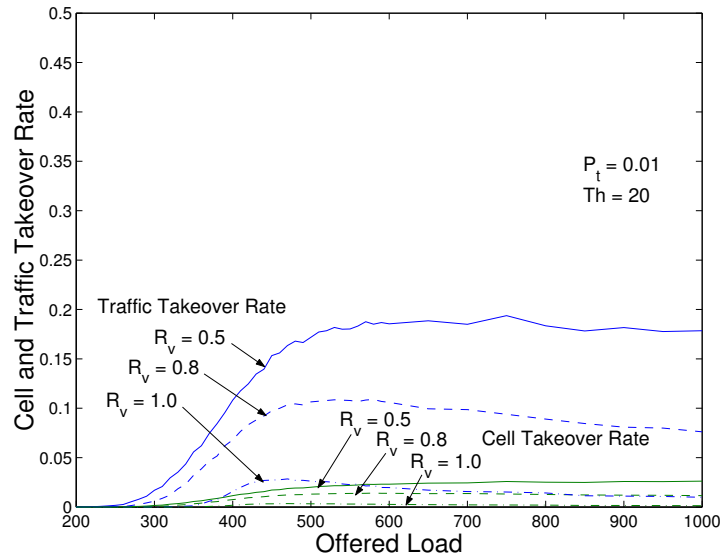


Figure 5.29: Mean cell takeover rate (cells/sec/VCZ) and mean traffic takeover rate ($BU/s/sec/VCZ$) for **VA2** when P_t is 0.01, Th is 20 and MH's speed is uniformly distributed between 40 and 60 km/h .

same traffic load. Blocking probabilities of small cell case is depicted in Fig. 5.30 when P_t is 0.01 and Th is 20, showing better performance as compared with Fig. 5.17. Bandwidth utilization and takeover rate are represented in Fig. 5.31 and 5.32, respectively. Due to more frequent takeover shown in the latter figure, bandwidth usage and blocking probabilities slightly improve. That is, system performance becomes better with the smaller cell size at the cost of more frequent takeover of cells in **VA2**.

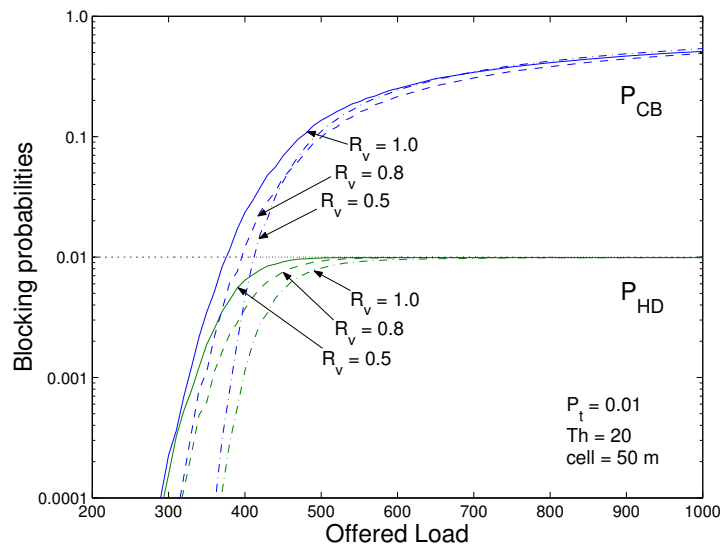


Figure 5.30: P_{CB} and P_{HD} vs. offered load for **VA2** when P_t is 0.01, Th is 20 and cell size is 50 m .

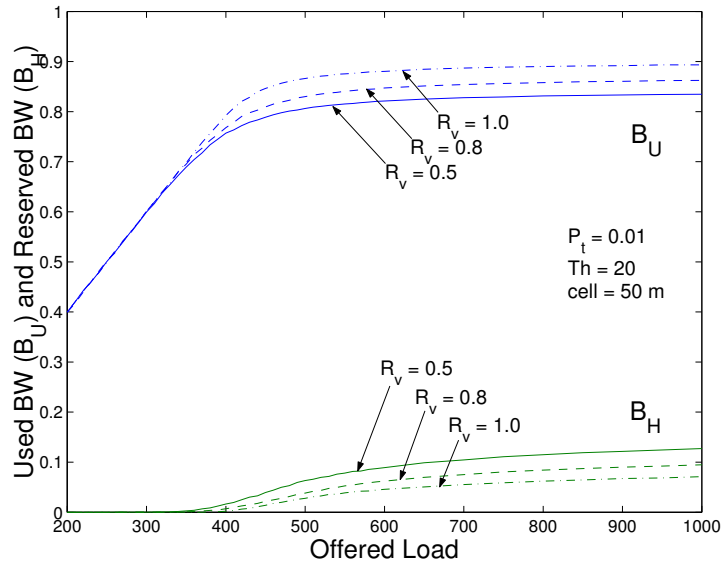


Figure 5.31: B_U and B_H vs. offered load for **VA2** when P_t is 0.01, Th is 20 and cell size is 50 m.

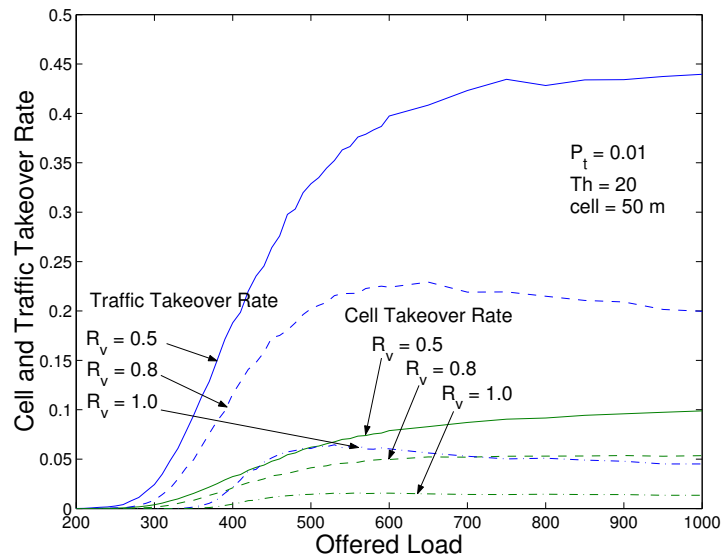


Figure 5.32: Mean cell takeover rate (cells/sec/VCZ) and mean traffic takeover rate (BU s/sec/VCZ) for **VA2** when P_t is 0.01, Th is 20 and cell size is 50 m.

5.8.2.6 The Influence of Threshold (Th) Parameter

The influence of Th in **VA2** on blocking probabilities, bandwidth utilization, and mean cell takeover rate are depicted for $P_t = 0.01$ and $R_v = 0.5$ in Fig. 5.33, 5.34 and 5.35, respectively. It is obvious that smaller Th is better in terms of blocking probabilities and bandwidth utilization at the cost of higher takeover rate. However, when Th is too small, **VA2** may fall into improper operation in which P_{HD} is not limited to P_t any more and hence B_H becomes higher. Therefore, Th must be carefully chosen in such a way that it leads to a proper operation as well as performance enhancement. In our simulation study, when Th is more than 20, **VA2** works well in most cases.

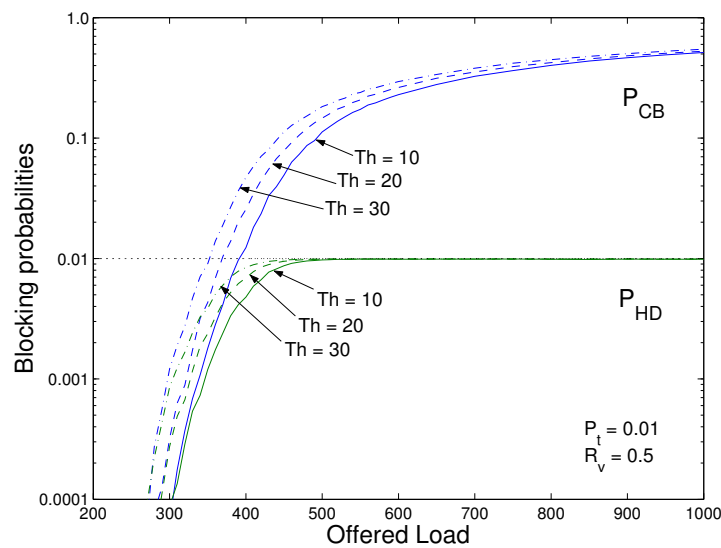


Figure 5.33: P_{CB} and P_{HD} vs. offered load for **VA2** when P_t is 0.01 and R_v is 0.5.

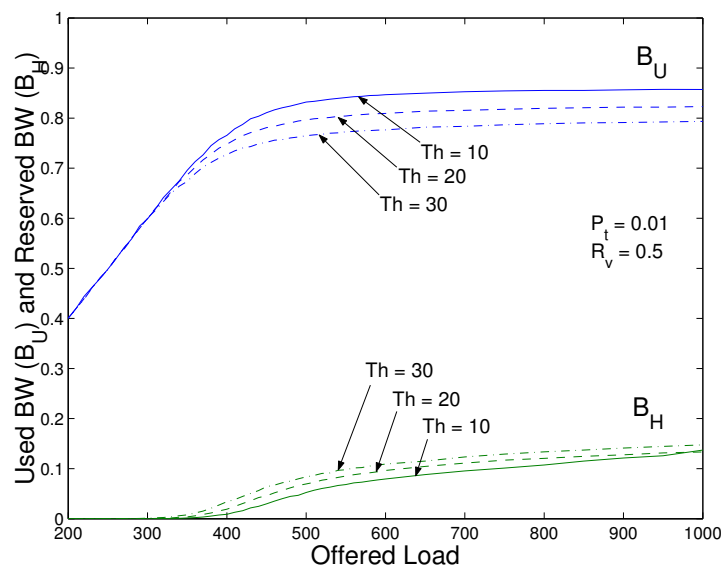


Figure 5.34: B_U and B_H vs. offered load for **VA2** when P_t is 0.01 and R_v is 0.5.

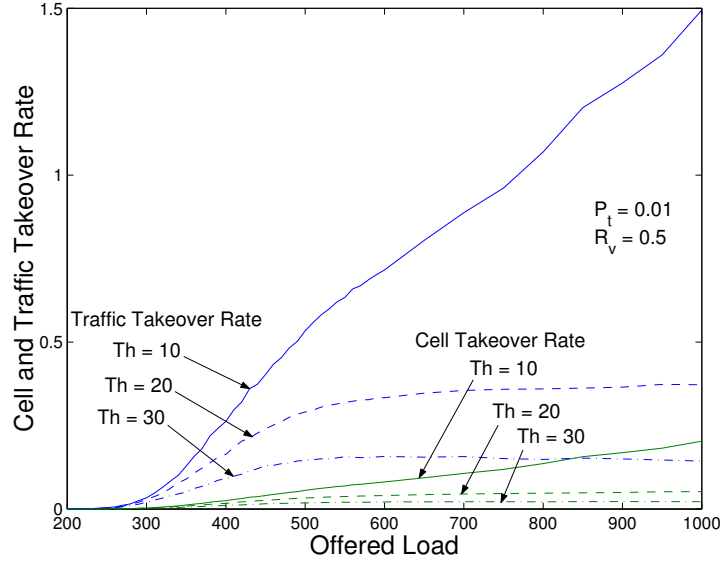


Figure 5.35: Mean cell takeover rate (cells/sec/VCZ) and mean traffic takeover rate ($BU\text{s}/\text{sec}/\text{VCZ}$) for VA2 when P_t is 0.01 and R_v is 0.5.

5.8.2.7 Performance Evaluation Summary

In summary, the following observations are made based on the results shown in this section: (1) there is a trade-off between handover quality and bandwidth utilization, (2) the proposed variable-VCZ scheme can provide better performance in terms of handover quality as well as bandwidth usage when parameters (B_H, Th) are appropriately chosen as compared to fixed-VCZ schemes, (3) when the VCZ resizing procedure is combined with an adaptive bandwidth reservation, P_{HD} can be maintained below P_t regardless of traffic load and the voice ratio, and high bandwidth utilization is achieved.

5.9 Conclusions

Future road vehicle communication systems will operate at mm-wave bands to support the high data rate traffic (2–10 Mbps per user). The system is characterized by a small cell size due to high propagation loss of mm-wave band signal and high user mobility. Thus, handover management becomes a very significant and challenging issue. In the present study, we have proposed an MAC protocol for RoF based RVC systems featuring a support of fast handover and dynamic bandwidth allocation according to the movement of MHs using a centralized control capability of RoF networks. Bandwidth management schemes have also been proposed that are differentiated in accordance with their capability to change VCZ size (i.e. the number of cells covered by the VCZ) and/or to adaptively change the bandwidth reserved for handover requests. A simulation study has been performed suggesting that the schemes with the ability to change VCZ size is efficient in bandwidth usage. In addition, when it is combined with a conventional adaptive bandwidth reservation algorithm, handover quality has been improved at the cost of bandwidth.

Chapter 6

Radio over Fiber based Wireless Access Network Architecture for Rural and Remote Areas

6.1 Introduction

The demand for broadband access has grown steadily as users experience the convenience of high-speed response combined with “*always-on*” connectivity. A broadband wireless access network (BWAN) is a cost-effective alternative to provide users with such broadband services as it requires much less infrastructure compared to wireline access networks such as xDSL and cable modem networks [86]. Thus, these days the so-called “*wireless last mile*” has attracted much attention. However, it has been concerned mainly with densely populated urban areas. Recent survey reveals that although penetration of personal computers in rural areas is significant in some countries, most of the users still use low-speed dial-up modem for the Internet access [87][88]. Since in such case broadband services based on wireline networks are prohibitively expensive, wireless access network might be the best solution. In the present investigation, we are concerned with a BWAN for sparsely populated rural and remote areas where a large number of base stations (BSs) are required, while the traffic demand per BS is much lower compared to densely populated urban areas.

On the other hand, an RoF based wireless access network has been proposed as a promising alternative to BWANs due to its cost-effective network architecture [12]. Moreover, in order to support the broadband services, mm-wave bands such as 36 or 60 GHz have been considered for BWANs. In particular, considerable attention has been paid to RoF system at mm-wave bands for BWANs to overcome spectral congestion in the lower microwave frequency regions and achieve cost-effectiveness [30],[33], [34],[38],[40],[42].

In most conventional RoF architectures, the CS has a laser diode (LD) and photo detector (PD) pair and a modem for each BS, leading to a complicated CS structure [29][40] (in this study an optical

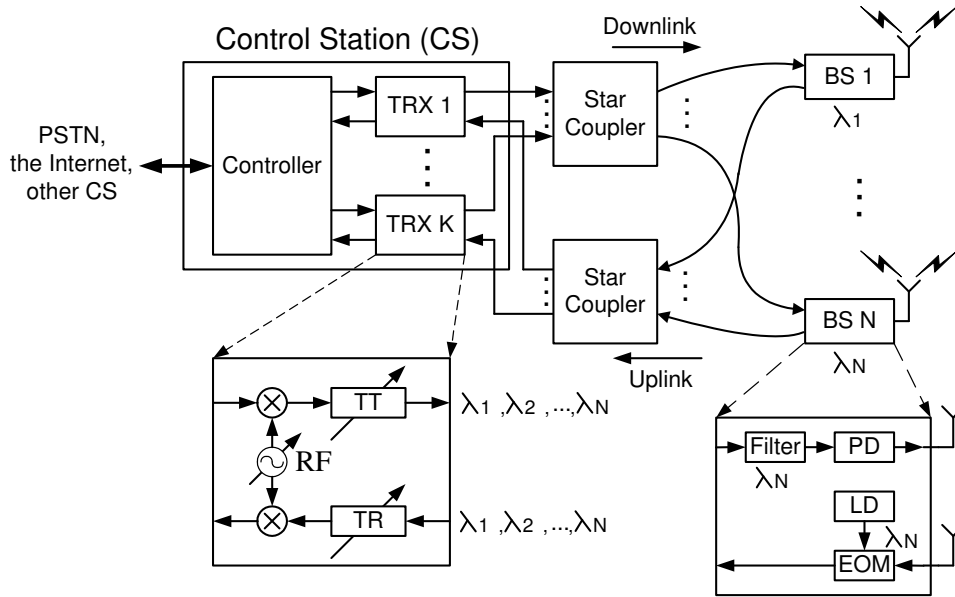


Figure 6.1: A proposed radio over fiber access network architecture consisting of K transceivers (TRXs) and N base stations (BSs).

transmitter-receiver pair with a modem is called a transceiver (TRX)). In addition, though wavelength division multiplexing (WDM) is widely employed in RoF systems, its usage is limited to simplifying connection between the CS and BSs [9],[29]. In this study, we propose an RoF architecture for BWANs using WDM for efficient bandwidth allocation. Specifically, the CS has the smaller number of TRXs than the number of BSs, where a TRX consists of optical tunable transmitter (TT) and tunable receiver (TR) pairs and a modem, resulting in simpler CS structure. The CS is interconnected to BSs, each of which is fixed-tuned to one of the available wavelengths, through a broadcast-and-select type optical passive device. Although system capacity is limited by the number of TRXs, it has simpler a CS structure and flexibility in terms of bandwidth allocation. Thus, this system is suitable for BWANs where a number of BSs are required but the average traffic load is small, satisfying the requirements for rural and remote areas.

The chapter is organized as follows. Section 6.2 describes the proposed network architecture. An MAC protocol together with scheduling issue is described in section 6.3. Section 6.4 deals with the capacity analysis, which is followed by numerical results in section 6.5. We discuss further study topic, multiplexing techniques for choosing BSs and draw conclusions in section 6.6.

6.2 Network Architecture

6.2.1 Architecture Description

The network comprises one CS with K TRXs, N BSs and many fixed subscriber stations (SSs), and each BS is connected to the CS via two optical fibers for uplink and downlink communication, respectively, as

shown in Fig. 6.1. In order to interconnect the CS and BSs, optical passive device is used such as optical star coupler or optical combiner/splitter that are insensitive to wavelength. The latter is especially better when the distance between the CS and BSs is large. The BS serves as an access point for an area called “cell”. The only function of a BS is to convert optical signal into wireless signal and vice versa. In this study, an RoF architecture is assumed so that TDMA/TDD operation is possible. Though there exist several possible options to implement such a system using different technologies (for more information refer to [11]), we present for illustration purposes an example of RoF network in Fig. 6.1. Each TRX in the CS include a modem and a TT-TR pair, tuning range of which covers wavelengths $\lambda_i, 1 \leq i \leq N$. In addition, tuning time is assumed to be negligible, which is a realistic assumption for TRXs with a tuning time of less than tens of nanoseconds [89]. The modem in each TRX has the capability to change RF channels. On the other hand, BS i is fixed-tuned to the wavelengths $\lambda_i, 1 \leq i \leq N$ that could be accomplished using an optical filter. One wavelength is used as a carrier for downlink and uplink data transmission. As a result, the network is of broadcast-and-select type where any TRX at the CS can access any BS by tuning optical wavelength unless wavelength collision occurs. In this architecture, we assume $K < N$.

Note that the architecture has a possibility that if multiple BSs are tuned to the same wavelength the total number of BSs could far exceed the number of wavelengths. In this case, the areas covered by the BSs tuned to the same wavelength are considered as a single cell. For proper operation, they should be spaced apart so that there is no co-channel interference between them, and propagation delay over optical fiber between the CS and the BSs has to be identical. Using this approach a broader area can be covered with small number of wavelengths. From now onwards, we however consider only the case where the number of BSs equals the number of wavelengths.

6.2.2 Basic Operations

The system operates in TDMA/TDD mode. In order for a TRX to support a BS it must know the wavelength and the RF channel used by the BS. Regarding RF channel we assume that RF channels are predetermined and fixed for each BS based on frequency reuse technique. The CS maintains a table listing BS identification (ID) number, its wavelength and RF channel.

For downlink transmission from CS to BS i user data first modulates RF source which, in turn, modulates optical light source that is tuned to λ_i . This signal is carried over the downlink optical fiber to the BS i , where the optical signal is converted into wireless signal and emitted from the BS. For uplink transmission, the wireless signal received by BS i is changed into optical signal by modulating light source, which is fixed-tuned to λ_i . It is then transported over uplink optical fiber to a TRX, where its TR tuned to λ_i first demodulates optical signal to obtain electrical signal, which is again demodulated in the RF domain to acquire user data.

The time period during which TT (TR) stays tuned to a certain wavelength corresponds to the bandwidth allocated for downlink (uplink) communication for the BS, suggesting flexible bandwidth management is possible. Note that more than one TRX is not allowed to support the same BS at the

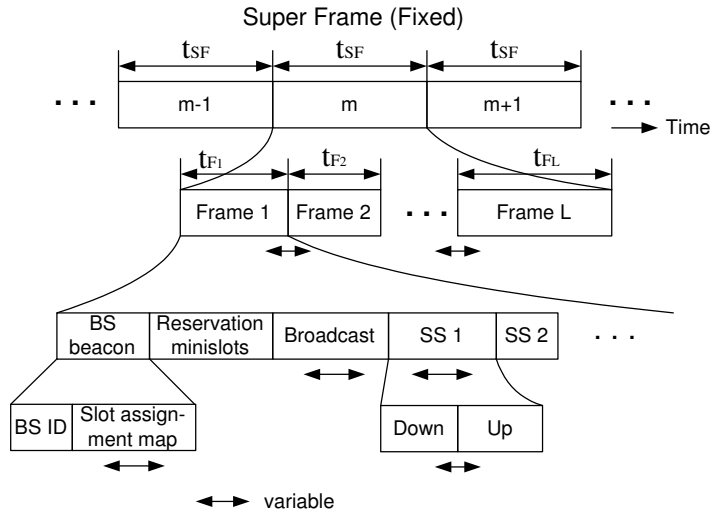


Figure 6.2: Frame structure. For simplicity, guard time is not shown.

same time due to wavelength collision. So, the maximum bandwidth that can be allocated to a BS is confined to the TRX capacity while the system capacity is K times the TRX capacity. Notice that it is easy to extend system capacity by adding more TRXs to the CS. Considering modern dense WDM technology hundreds of BSs can be supported by a CS. In addition, recent progress in RoF systems at mm-wave bands suggests a TRX capacity could amount to a few hundreds Mbps. Therefore, in most cases K TRXs that is much smaller than N will be sufficient enough to serve sparsely populated areas if user bandwidth is limited to a few Mbps. In summary, the architecture has two salient features: (1) efficient and flexible bandwidth allocation and (2) simple extension of system capacity.

6.3 Medium Access Protocol

Since propagation delay between the CS and BSs in the RoF networks under consideration could be large compared to packet transmission time, CSMA-like MAC protocol is not appropriate. As a result, the proposed architecture assumes a centralized MAC entity located at the CS offering a reservation-based, collision-free medium access.

6.3.1 Frame Structure

For each TRX a fixed-size super-frame is defined, which determines the “air-time” given to each BS (defined as a frame), i.e., the time period each BS uniquely uses to communicate with SSs located in its cell (Fig. 6.2). The super-frame provides users with data slots, each of which fits a minimum data packet. Even though the length of the super-frame is fixed to t_{SF} seconds, the duration of the frame assigned to each BS (t_{F_j} with respect to $BS j$) may be variable as long as

$$\sum_{j=1}^L t_{F_j} \leq t_{SF}$$

where L denotes the number of BSs supported by a TRX. Note that depending on traffic demands from BSs each TRX could have different L values.

Each frame belonging to a certain BS begins with “*beacon*” field that consists of BS ID and “*slot assignment map*” specifying the start slot position and the length for each SS. The following field is “*reservation minislots*”, which is accessed by SSs in a contention-based way that have not yet reserved any slots but have data to transmit. It is up to the CS to decide on the number of the minislots for each BS. An uplink reservation minislot contains the SS ID and quality of service (QoS) parameters for the traffic. For contention resolution, conventional method such as p -persistence can be utilized. The results of reservation trial in the previous super-frame is broadcast in the “*broadcast*” field, which is followed by downlink and uplink slots assigned to each SSs as specified in the slot assignment map. A minislot is attached to each uplink slot from an SS. Using this minislot the SS can request more bandwidth if necessary, which makes it unnecessary for the SS to send a request in a contention-based way.

Note that since the CS has K TRXs, up to K super-frames can be supported simultaneously. In order for a TRX to access a BS, it must have appropriate information; that is, the wavelength of the BS, tuning instant for TT and TR, and RF channel of the BS. A scheduler at the CS provides the information and controls each TRX.

6.3.2 Scheduling

Since scheduling issue in broadband wireless networks is beyond the scope of the study, we confine our discussion to the requirements of scheduling algorithm for the proposed architecture. In particular, we consider only a simple case where each TRX has a fixed-size capacity of C data slots and connection-oriented traffic requesting constant bandwidth during its lifetime. That is necessary to justify capacity analysis in the next section. The main task of a scheduler is to allocate frames to TRXs such that it should be efficient in bandwidth usage and avoid wavelength collision. The output of it provides each TRX with such information as wavelengths to which it has to tune, tuning instant and duration for each of them, and the corresponding RF channels for BSs. It also prepares downlink data blocks for each BS and associates them with the corresponding TRX every frame time. As BWANs considered in this study might have hundreds of BSs connected with one CS, scheduling algorithm should be fast and simple.

The scheduling problem can be translated into how to pack N frames belonging to N BSs into K super-frames. If fragmentation of a frame is allowed (i.e., multiple TRXs support a BS in distinct time periods within a super-frame time), bandwidth usage will be more efficient although it requires overhead. Fig. 6.3 shows an example indicating how to pack five frames into two super-frames where frame three is fragmented. The algorithm must keep fragmented frames from causing wavelength collision.

For a new request requiring B_{new} (in units of data slots) in every super-frame in BS i two conditions are checked out for admission control

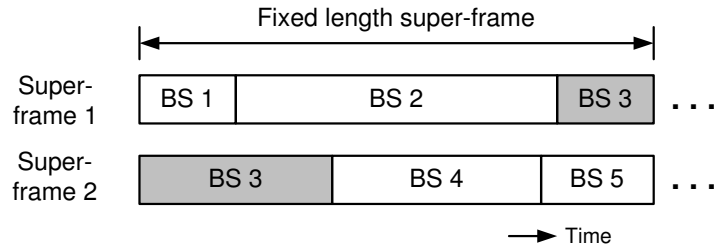


Figure 6.3: Packing of five frames into two super-frames where frame three is fragmented in such a way that no wavelength collision occurs.

$$\begin{aligned}
 (i) \quad & B_U^i + B_{new} \leq C \\
 (ii) \quad & \sum_{j=1}^N B_U^j + B_{new} \leq K \cdot C
 \end{aligned} \tag{6.1}$$

where B_U^j is the bandwidth being used in BS j . The first line is required to avoid wavelength collision, while the second line says total traffic load must be less than or equal to the CS capacity.

6.4 Capacity Analysis

In this section, assuming overhead associated with fragmentation in scheduling is negligible a capacity analysis of the system based on multitraffic loss system is performed [90][91]. With the assumption that call arrival processes are Poisson, the original version of multitraffic loss system provides state distribution in steady state in a closed-form equation. It is so general that it holds for arbitrary resource sharing policies [90].

The basic idea behind our analysis comes from the fact that the traffic intensity from BS i can be modeled as a Poisson process, if traffic from an SS is a Poisson process because a sum of Poisson processes is also a Poisson process. So, we don't consider individual traffic from a SS; instead, an aggregate traffic load to a BS is taken into account. In addition, traffic from BS i can be considered as belonging to class i traffic. Here, the constraints on wavelength collision and system capacity of Eq. (6.1) are integrated into resource sharing policy as described later. We make the following assumptions for the analysis.

- A1) A connection arrival to BS i is a Poisson process with the mean arrival rate being a_i , and the bandwidth demand of it is one slot.
- A2) A connection of BS i has a connection life time with mean $1/\mu_i$.
- A3) A connection which cannot be accepted by the system is blocked and cleared.

Let $A_i = a_i/\mu_i$ be the traffic intensity from BS i . Under these assumptions, we consider the state description $\mathbf{n} = (n_1, \dots, n_N)$ where n_i is the number of connections of BS i connected. The set of allowable set Ω of \mathbf{n} is determined by the number of transceivers K , transceiver's capacity C and wavelength collision constraint. Any \mathbf{n} of the allowable set should satisfy:

$$\mathbf{n} \in \Omega \Rightarrow 0 \leq n_i \leq C, \quad i = 1, \dots, N \quad (6.2)$$

$$\sum_{i=1}^N n_i \leq K \cdot C \quad (6.3)$$

Eq. (6.2) is necessary to avoid wavelength collision, while Eq. (6.3) says bandwidth demands cannot exceed system capacity. In other words, the two equations correspond to the first and the second line of Eq. (6.1), respectively. For any resource sharing policy, a product form solution prevails in steady state, i.e., the probability that the system is in \mathbf{n} in steady state is given by [90]

$$\mathbf{P}(\mathbf{n}) = G^{-1}(\Omega) \prod_{i=1}^N \frac{A_i^{n_i}}{n_i!} \quad \text{for } \mathbf{n} \in \Omega \quad (6.4)$$

where

$$G(\Omega) = \sum_{\mathbf{n} \in \Omega} \left(\prod_{i=1}^N \frac{A_i^{n_i}}{n_i!} \right) \quad (6.5)$$

Suppose a test BS i , then the blocking probability of a connection that requests a bandwidth through the BS is given by

$$\mathbf{P}_b = \sum_{\mathbf{n} \in \Omega_i^+} \mathbf{P}(\mathbf{n}) \quad (6.6)$$

where

$$\Omega_i^+ = \left\{ \mathbf{n} \in \Omega \mid n_i = C \text{ or } \sum_{k=1}^N n_k = K \cdot C \right\} \quad (6.7)$$

That is, the connection request is blocked either when (1) the bandwidth used at the BS is C or (2) the total bandwidth of all connections is system capacity $K \cdot C$. Given $\mathbf{P}(\mathbf{n})$ bandwidth utilization is simply calculated by

$$\mathbf{U} = \sum_{\mathbf{n} \in \Omega} |\mathbf{n}| \cdot \mathbf{P}(\mathbf{n}) \quad (6.8)$$

6.5 Numerical Results

One problem with Eq. (6.4) in calculating $\mathbf{P}(\mathbf{n})$ is that computational burden greatly increases as C or N grows, so we consider only the cases where C and N are computationally tractable for analysis. Fig. 6.4 indicates blocking probabilities versus traffic load to the system with different K values when

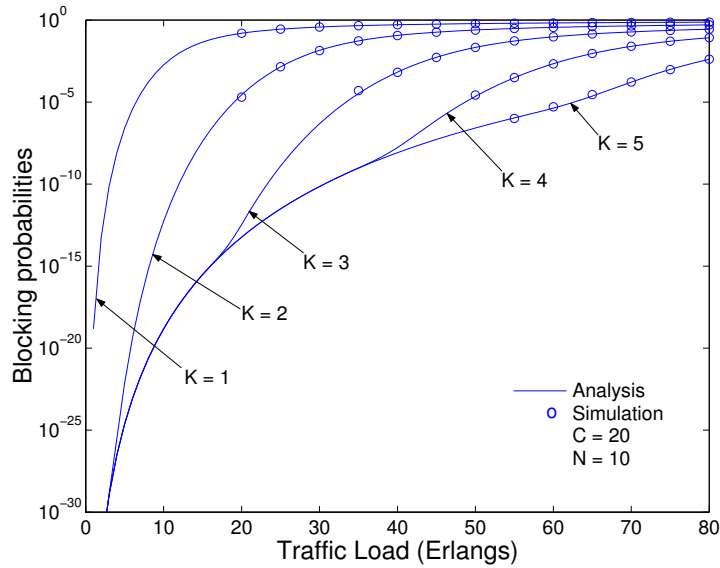


Figure 6.4: Blocking probabilities when $N = 10$ and $C = 20$.

N is 10 and C is 20. With $K = 1$ Eq. (6.4) reduces to the Erlang-B formula for $M/M/m/m$ queueing system. In such case blocking probability is simply given by $\mathbf{P}_b = \sum_{|n|=C} \mathbf{P}(n)$. In case when K is more than one an interesting point is observed. Blocking probabilities are not different regardless of K up to some traffic load. After that point (called a “critical point”) a distinguishable difference is observed. For example, the blocking probabilities for $K = 3, 4$ are the same up to a traffic intensity of 18 Erlangs. However, after that point the difference becomes large as traffic increases.

To explain it more clearly, refer to Fig. 6.5 that indicates blocking probabilities versus traffic load when $K = 3$, $C = 20$ and $N = 10$ (solid line) together with cases when $K = 1$, $C = 60$ (dotted line) and $K = 5$, $C = 20$ (dashed line). When the traffic load is smaller than the critical point connection blocking is governed mainly by Eq. (6.2) (i.e., wavelength collision constraint) because the probability that the total bandwidth demand is greater than the CS capacity is very small. That is, when $K > 1$, connection blocking is constrained by wavelength collision regardless of K until traffic load reaches the critical point. On the other hand, as traffic load grows Eq. (6.3) plays a dominant role in determining connection blocking. In this case the system behaves as if it had a single server with the same capacity as the CS in terms of blocking probabilities. That is, after the critical point blocking probabilities follow those of single server with the same total aggregate capacity (see the dotted line for $K = 1$, $C = 60$).

The figure also shows that for a given K TRXs, the critical point can be determined as a cross point between the line of blocking probabilities for a single server with the same total capacity (i.e., $K = 1$, $C = 60$) and that for a larger number of TRXs (e.g., $K = 5$, $C = 20$). Using discrete-event simulation, blocking probabilities of Eq. (6.6) can be easily calculated, however, critical points cannot be simply observed since they have very small values. In Fig. 6.4 simulation results are depicted as small circles. It implies the analytical model developed in the last section can be utilized to get an insight into how the number of TRXs impacts on system performance.

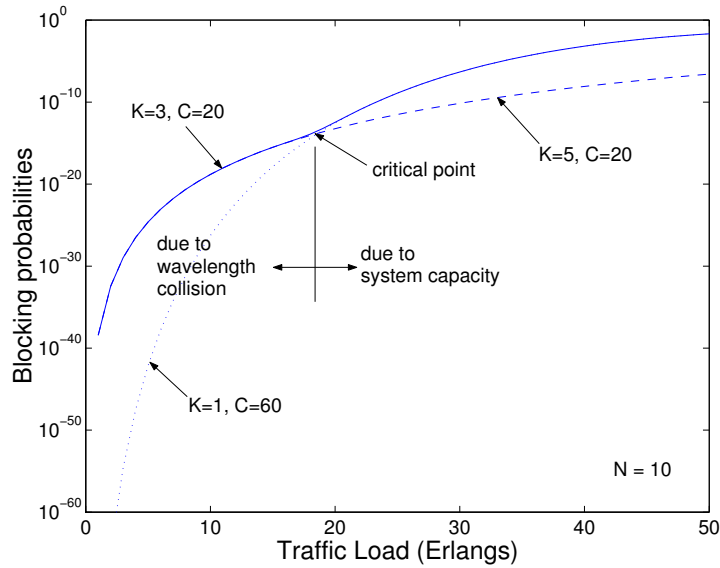


Figure 6.5: Blocking probabilities when $K = 3$, $N = 10$ and $C = 20$.

6.6 Discussion and Conclusion

Although we assume in this study frequency bands for each BS are predetermined, if it could be dynamically changed by the CS the proposed architecture leads to an interesting problem. Essentially, it then has two-degree of freedom in the time and frequency domain, respectively. In such case, at any given time the CS changes time periods and frequency bands for each cell, where not only bandwidth allocation but also interference among cells can be taken into account for better system performance. Since adjacent cells must not utilize the same frequency band at the same time, it is closely related to graph coloring problem that is an interesting topic for our future course of study.

In our architecture, we exploit only optical wavelength for choosing BS, however, when the number of BSs to be independently selected is larger than the number of available wavelengths, we could rely on an extra degree of freedom (in addition to the wavelength) at the cost of increased hardware complexity. That is, another multiplexing technique (e.g., time, space, signal polarization, codes, sub-carriers) can be utilized over WDM. For instance, a popular electrical multiplexing scheme is subcarrier multiplexing, whereby multiple electrical signals are multiplexed in the RF domain and then modulate a single optical source. Though the necessary enabling technologies have yet to mature, they provide a way to increase the number of BSs that should be independently accessed by the CS while achieving simple network configuration, which has been discussed in [92].

Chapter 7

Conclusions and Future Works

RoF is a very effective technology for integrating wireless and optical access. It combines the two media; fiber optics and radio, and is a way to easily distribute radio frequency as a broadband or baseband signal over fiber. It utilizes analog fiber optic links to transmit and distribute radio signals between a central CS and numerous BSs. Since it was first proposed and demonstrated by Cooper [5] in 1990 a lot of research efforts has been made to investigate physical limitations and develop simple BSs. It now accounts for a significant market size and this relatively *niche* market is expected to grow significantly in the future as new RoF technologies emerge and their applications become more diverse and less costly. It has three conspicuous features that make it quite different from conventional wireless networks: (1) it is transparent to bandwidth, modulation of RF signals and protocol, (2) simple and small BSs, and (3) centralized network architecture. In contrast to research efforts devoted to physical layer in this area, little attention has been paid to upper layer network architecture and system resource management issues using its centralized architecture. For instance, the CS in an RoF network has global knowledge of current network status and can dynamically control network resources. In this dissertation, we are concerned with how to use such features to address mobility management and bandwidth allocation issues. Specifically, the dissertation is composed of three studies, each of which takes different network environment into account. Two of them consider wireless networks with very small cell and mobile users, leading to a very challenging and significant issue of handover management. We have proposed RoF based network architecture together with MAC protocols that support fast and simple handover using centralized network architecture. Furthermore, in the third study we have proposed access network architecture based on RoF for rural and remote areas that provides an efficient bandwidth management, which also depends on centralized network architecture. As a consequence, the studies suggest that RoF based networks could address difficult issues that are hard to solve with the conventional approaches originated from distributed wireless network architecture. Thus, RoF based wireless networks could be much more efficient in terms of system resource management as compared to conventional wireless networks. In this sense RoF is a promising technology for future high-capacity and broadband multimedia wireless services.

7.1 Research Contributions

In this dissertation, we have proposed RoF based network architecture and MAC protocols that make efficient use of centralized control capability of RoF networks for fast and simple handover and effective bandwidth allocation. One should notice that the dissertation did not consider general solutions to resource management issues in RoF networks, but only proposed possible solutions for the network environments under consideration in each study. This means there is an ample scope for further study as to how to utilize centralized architecture of RoF networks for resource management issues in wireless networks.

- We have developed an MAC protocol for RoF based WLAN operating in the 60 GHz band in chapter 4. This system imposes quite different requirements on system design in comparison with the conventional WLANs due to high propagation and penetration loss of the band. That is, each room in a building should be supported by at least one BS. Thus, in such network with numerous small cells, the issue of mobility management becomes very significant. The proposed MAC protocol, called Chess Board protocol, features fast and easy handover and QoS support. It is based on frequency switching (FS) codes and adjacent cells employ orthogonal FS codes to avoid possible co-channel interference as well as allow fast and easy handover. Important parameters of the protocol have been analyzed, and to investigate the properties, six variants of the protocol were considered. A simulation study has been performed to evaluate them.
- For future RVC system at mm-wave bands an RoF based network architecture along with mobility and bandwidth management schemes has been proposed in chapter 5. In this case, due to high user mobility, e.g., vehicles running in a highway, mobility management becomes even more difficult. Using the centralized control capability of RoF networks and dynamic TDMA we proposed an RoF based network architecture that allows simple and fast handover and additionally developed bandwidth management schemes to enhance handover quality and bandwidth utilization. They were evaluated in detail by a simulation study considering a typical highway environment.
- An RoF based broadband wireless access network architecture has been proposed for sparsely populated rural and remote areas in chapter 6. In the architecture a CS has optical tunable-transmitter (TT) and tunable-receiver (TR) pairs and utilizes WDM to access numerous antenna BSs, each of which is fixed-tuned to a wavelength, for efficient and flexible bandwidth allocation. Although its capacity is limited by the number of TT/TR pairs, it has simpler CS structure while maintaining trunking efficiency. Characteristics of the architecture, access protocol, and scheduling have been discussed; furthermore, capacity analysis based on multitraffic loss system was performed to show some properties of the proposed architecture.

7.2 Future Research Directions

- Only simple six variants of Chess Board protocol have been considered and evaluated in this dissertation. Bandwidth management scheme prioritizing handover connection over new connection and scheduling for QoS support are possible research topics.
- We have developed bandwidth management schemes for RoF based RVC system based on adaptive bandwidth reservation scheme for mobile cellular networks proposed in [85], but there are other interesting schemes able to limit handover dropping probability to a prespecified value [57][58]. Interesting future research topics include how to combine such schemes with VCZ-resizing procedure and a comparison study of these schemes.
- Centralized network architecture of RoF networks suggests a new possibility for efficient resource management. Resource management issues in wireless networks based on cellular architecture involve dynamic channel assignment, dynamic transmit power control, load balancing, mobility management and so on. Resource management techniques in such networks require access to information that must be gathered across a number of BSs, and the techniques involve control decisions that apply to a number of BSs, not just one. Thus, some centralized decision making is appropriate. In this sense, RoF networks have great potential for efficient resource management that might be hard to achieve in conventional distributed wireless architecture, implying so many open issues.

Appendix A

Acronyms

AP Access Point

BER Bit Error Rate

BLER Block Error Rate

BS Base Station

CBR Constant Bit Rate

CDMA Code Division Multiple Access

CIR Carrier-to-Interference Ratio

CS Control Station

CSMA Carrier Sense Multiple Access

DFB Decision Feedback

DSB Double Side Band

DWDM Dense Wave Division Multiplexing

EDFA Erbium-doped Fiber Amplifier

EOM External Optical Modulator

EAT Electroabsorption Transceiver

EMI Electromagnetic Interference

FCC Federal Communications Commission

FDD Frequency Division Duplex

FDMA Frequency Division Multiple Access

GSM Global System for Mobile Communications

IAPP Inter-access-point Protocol

IF Intermediate Frequency

IP Internet Protocol

ITS Intelligent Transportation System

ITU International Telecommunication Union The former CCITT.

LED Light Emitting Diode

LD Laser Diode

LO Local Oscillator

LOS Line of Sight

MAC Medium Access Control

MAHO Mobile-Assisted Handover

MCHO Mobile-Controlled Handover

MH Mobile Host

NA Numerical Aperture

NCHO Network-Controlled Handover

NLOS Non-Line of Sight

OADM Optical Add/Drop Multiplexer

PD Photodetector

PSC Passive Star Coupler

QoS Quality of Service

RF Radio Frequency

ROF Radio over Fiber

RSS Received Signal Strength

RVC Road Vehicle Communication

SDH Synchronous Digital Hierachy

SER Symbol Error Rate

SIR Signal-to-Interference Ratio

SONET Synchronous Optical Network

SRP Spatial Reuse Protocol

SSB Single Side Band

TDD Time Division Duplex

TDMA Time Division Multiple Access

TIM Traffic Indication Map

UMTS Universal Mobile Telecommunications System

WDM Wave Division Multiplexing

WLAN Wireless Local Area Network

Appendix B

Selected Publications

- H. B. Kim and A. Wolisz, “Radio over Fiber based Wireless Access Network Architecture for Rural Areas,” in *Proc. 14th IST Mobile & Wireless Commun. Summit*, June 2005, Dresden, Germany.
- H. B. Kim, M. Emmelmann, B. Rathke, and A. Wolisz, “A Radio over Fiber Network Architecture for Road Vehicle Communication Systems,” in *Proc. IEEE VTC 2005 Spring*, May. 2005, Stockholm, Sweden.
- H. B. Kim, “An Adaptive Bandwidth Reservation Scheme for Multimedia Mobile Cellular Networks,” in *Proc. IEEE ICC 2005.*, May. 2005, Seoul, Korea.
- H. B. Kim and A. Wolisz, “Performance Evaluation of a MAC Protocol for Radio over Fiber Wireless LAN operating in the 60-GHz Band,” in *Proc. IEEE Globecom 2003*, vol. 22, no. 1, pp. 2659–2665, Dec. 2003.
- H. B. Kim, H. Woesner and A. Wolisz, “A Medium Access Control Protocol for Radio over Fiber Wireless LAN operating in the 60-GHz Band,” in *Proc. 5th European Personal Mobile Commun. Conf. (EPMCC)*, pp. 204–208, Apr. 2003.

Bibliography

- [1] O. Andrisano, V. Tralli, and R. Verdone, "Millimeter Waves for Short-Range Multimedia Communication Systems," *Proc. IEEE*, vol. 86, no. 7, pp. 1383–1401, July 1998.
- [2] P. Smulders, "Exploiting the 60 GHz Band for Local Wireless Multimedia Access: Prospects and Future Directions," *IEEE Commun. Mag.*, pp. 140–147, Jan. 2002.
- [3] J. R. Forrest, "Communication Networks for the New Millennium," *IEEE Trans. Microwave Theory Tech.*, vol. 47, no. 12, pp. 2195–2201, Dec. 1999.
- [4] F. Giannetti, M. Luise and R. Reggiannini, "Mobile and Personal Communications in the 60 GHz Band: A Survey," *Wireless Personal Commun.*, pp. 207–243, Oct. 1999.
- [5] A. J. Cooper, "Fiber/Radio for the provision of cordless/mobile telephony services in the access network," *Electron. Lett.*, vol. 26, no. 24, pp. 2054–2056, Nov. 1990.
- [6] T.-S. Chu and M. J. Gans, "Fiber Optic Microcellular Radio," *IEEE Trans. Veh. Technol.*, vol. 40, no. 3, pp. 599–606, Aug. 1991.
- [7] H. Kim, J. M. Cheong, C. Lee, and Y. C. Chung, "Passive Optical Network for Microcellular CDMA Personal Communication Service," *IEEE Photonics Tech. Lett.*, vol. 10, no. 11, pp. 1641–1643, Nov. 1998.
- [8] J. S. Yoon, M. H. Song, S. H. Seo, Y. S. Son, J. M. Cheong and Y. K. Jhee, "A High-Performance Fiber-Optic Link for cdma2000 Cellular Network," *IEEE Photon. Technol. Lett.*, vol. 14, no. 10, pp. 1475–1477, Oct. 2002.
- [9] K. Kojucharow, M. Sauer, H. Kaluzni, D. Sommer, F. Poegel, W. Nowak, and D. Ferling, "Simultaneous Electrooptical Upconversion, Remote Oscillator Generation, and Air Transmission of Multiple Optical WDM Channels for a 60-GHz High-Capacity Indoor System," *IEEE Trans. Microwave Theory Tech.*, vol. 47, no. 12, pp. 2249–2255, Dec. 1999.
- [10] E. I. Ackerman and C. H. Cox, "RF Fiber-Optic Link Performance," *IEEE Microwave*, pp. 50–58, Dec. 2001.

- [11] K. Kitayama, "Architectural considerations of radio-on-fiber millimeter-wave wireless access systems," *Signals, Systems, and Electron., 1998 URSI International Symposium*, pp. 378–383, 1998.
- [12] Implementation frameworks for integrated wireless-optical access networks Deliverable 4, Eurcom, P816-PF, Feb. 2000.
- [13] H. Al-Raweshidy and S. Komaki, editors, *Radio over Fiber Technologies for Mobile Communications Networks*, Norwood: Artech House, 2002.
- [14] H. Ogawa, D. Polifko and S. Banba, "Millimeter-Wave Fiber Optics Systems for Personal Radio Communication," *IEEE Trans. Microwave Theory Tech.*, vol. 40, no. 12, pp. 2285–2293, Dec. 1992.
- [15] U. Gliese, S. Norskow, and T. N. Nielsen, "Chromatic Dispersion in Fiber-Optic Microwave and Millimeter-Wave Links," *IEEE Trans. Microwave Theory Tech.*, vol. 44, no. 10, pp. 1716–1724, Oct. 1996.
- [16] R. Hofstetter, H. Schmuck, and R. Heidemann, "Dispersion Effects in Optical Millimeter-Wave Systems Using Self-Heterodyne Method for Transport and Generation," *IEEE Trans. Microwave Theory Tech.*, vol. 43, no. 9, pp. 2263–2269, Sep. 1995.
- [17] J. J. O'Reilly, P. M. Lane, R. Heidemann, and R. Hofstetter, "Optical generation of very narrow linewidth millimeter wave signals," *Electron. Lett.*, vol. 28, pp. 2309–2311, 1995.
- [18] D. Novak, Z. Ahmed, R. B. Waterhouse, and R. S. Tucker, "Signal generation using pulsed semiconductor lasers for application in millimeter-wave wireless links," *IEEE Trans. Microwave Theory Tech.*, vol. 43, pp. 2257–2262, 1995.
- [19] K. Kitayama, T. Kuri, H. Yokoyama, and M. Okuno, "60 GHz millimeter-wave generation and transport using stabilized mode-locked laser diode with optical frequency DEMUX switch," in *Proc. Conf. IEEE Globecom'96*, Nov. 1996, pp. 2162–2169.
- [20] R. Braun, G. Grosskopf, D. Rohde, and F. Schmidt, "Low-Phase-Noise Millimeter-Wave Generation at 64 GHz and Data Transmission Using Optical Sideband Injection Locking," *IEEE Photon. Technol. Lett.*, vol. 10, no. 5, pp. 728–730, May. 1998.
- [21] T. Kuri, K. Kitayama, "Optical Heterodyne Detection Technique for Densely Multiplexed Millimeter-Wave-Band Radio-on-Fiber Systems," *J. Lightwave Technol.*, vol. 21, no. 12, pp. 3167–3179, Dec 2003.
- [22] T. Kuri, K. Kitayama, and Y. Ogawa, "Fiber-Optic Millimeter-Wave Uplink System Incorporating Remotely Fed 60-GHz-Band Optical Pilot Tone," *IEEE Trans. Microwave Theory Tech.*, vol. 47, no. 7, pp. 1332–1337, Jul. 1999.

- [23] T. Kuri, K. Kitayama, A. Stöhr, and Y. Ogawa, "Fiber-Optic Millimeter-Wave Downlink System Using 60 GHz-Band External Modulation," *J. Lightwave Technol.*, vol. 17, no. 5, pp. 799–806, May 1999.
- [24] G. H. Smith, D. Nowak, and Z. Ahmed, "Technique for optical SSB generation to overcome dispersion penalties in fibre-radio systems," *Electron. Lett.*, vol. 33, no. 1, pp. 74–75, Jan. 1997.
- [25] J. Park, W. V. Sorin, and K. Y. Lau, "Elimination of the fibre chromatic dispersion penalty on 1550 nm millimeter-wave optical transmission," *Electron. Lett.*, vol. 33, no. 6, pp. 512–513, Mar. 1997.
- [26] K. J. Williams, and R. D. Esman, "Optically Amplified Downconverting Link with Shot-Noise-Limited Performance," *IEEE Photon. Technol. Lett.*, vol. 8, no. 1, pp. 148–150, Jan. 1996.
- [27] C. K. Sun, R. J. Orazi, and S. A. Pappert, "Efficient Microwave Frequency Conversion Using Photonic Link Signal Mixing," *IEEE Photon. Technol. Lett.*, vol. 8, no. 1, pp. 154–156, Jan. 1996.
- [28] R. Helkey, J. C. Twichell, and C. Cox, "A Down-Conversion Optical Link with RF Gain," *J. Lightwave Technol.*, vol. 15, no. 6, pp. 956–961, Jun. 1997.
- [29] G. H. Smith and D. Novak, "Broadband millimeter-wave fiber-radio network incorporating remote up/down conversion," *Microwave Symposium Digest, IEEE MTT-S*, vol. 3, pp. 1509–1512, Jun. 1998.
- [30] K. Kitayama and R. A. Griffin, "Optical Downconversion from Millimeter-Wave to IF-Band Over 50-km-Long Optical Fiber Link Using an Electroabsorption Modulator," *IEEE Photon. Technol. Lett.*, vol. 11, no. 2, pp. 287–289, Feb. 1999.
- [31] L. Noël, D. Wake, D. G. Moodie, D. D. Marcenac, L. D. Westbrook, and D. Nasset, "Novel Techniques for High-Capacity 60-GHz Fiber-Radio Transmission Systems," *IEEE Trans. Microwave Theory Tech.*, vol. 45, no. 8, pp. 1416–1423, Aug. 1997.
- [32] A. Stöhr, K. Kitayama, and D. Jäger, "Full-Duplex Fiber-Optic RF Subcarrier Transmission Using a Dual-Function Modulator/Photodetector," *IEEE Trans. Microwave Theory Tech.*, vol. 47, no. 7, pp. 1338–1341, Jul. 1999.
- [33] K. Kitayama, A. Stöhr, T. Kuri, R. Heinzlmann, D. Jäger and Y. Takahashi, "An Approach to Single Optical Component Antenna Base Stations for Broad-Band Millimeter-Wave Fiber-Radio Access Systems," *IEEE Trans. Microwave Theory Tech.*, vol. 48, pp. 2588–2594, Dec. 2000.
- [34] T. Kuri, K. Kitayama, and Y. Takahashi, "60-GHz-Band Full-Duplex Radio-On-Fiber System Using Two-RF-Port Electroabsorption Transceiver," *IEEE Photon. Technol. Lett.*, vol. 12, no. 4, pp. 419–421, Apr. 2000.
- [35] M. S. Borella, J. P. Jue, D. Banerjee, B. Ramamurthy, and B. Mukherjee, "Optical Components for WDM Lightwave Networks," *Proc. IEEE*, vol. 85, no. 8, pp. 1274–1307, Aug. 1997.

- [36] R. A. Griffin, P. M. Lane, and J. J. O'Reilly, "Radio-Over-Fiber Distribution Using an Optical Millimeter-Wave/DWDM Overlay," *Proc. OFC/IOOC 99*, vol. 2, pp. 70–72, Feb. 1999.
- [37] R. A. Griffin, "DWDM Aspects of Radio-over-Fiber," *Proc. LEOS 2000 Annual Meeting*, vol. 1, pp. 76–77, Nov. 2000.
- [38] R. Heinzlmann, T. Kuri, K. Kitayama, A. Stöhr, and D. Jäger, "Optical add-drop multiplexing of 60 GHz millimeterwave signals in a WDM radio-on-fiber ring," *Proc. OFC*, vol. 1, 2000, paper FT4-1, pp. 137–139.
- [39] G. H. Smith, D. Novak, and C. Lim, "A millimeter-wave full-duplex fiber-radio star-tree architecture incorporating WDM and SCM," *IEEE Photon. Technol. Lett.*, vol. 10, pp. 1650–1652, Nov. 1998.
- [40] A. Nirmalathas, D. Novak, C. Lim and R. B. Waterhouse, "Wavelength Reuse in the WDM Optical Interface of a Millimeter-Wave Fiber-Wireless Antenna Base Station," *IEEE Trans. Microwave Theory Tech.*, vol. 49, no. 10, pp. 2006–2012, Oct. 2001.
- [41] C. G. Schäffer, M. Sauer, K. Kojucharow, and H. Kaluzni, "Increasing the channel number in WDM mm-wave systems by spectral overlap," in *Int. Topical Meeting Microwave Photonics (MWP2000)*, Oxford, Sep. 2000, WE2.4, pp. 164–167.
- [42] C. Lim, A. Nirmalathas, M. Attygalle, D. Novak, and R. Waterhouse, "On the Merging of Millimeter-Wave Fiber-Radio Backbone With 25-GHz WDM Ring Networks," *J. Lightwave Technol.*, vol. 21, no. 10, pp. 2203–2210, Oct. 2003.
- [43] H. Toda, T. Yamashita, T. Kuri, and K. Kitayama, "Demultiplexing Using an Arrayed-Waveguide Grating for Frequency-Interleaved DWDM Millimeter-Wave Radio-on-Fiber Systems," *J. Lightwave Technol.*, vol. 21, no. 8, pp. 1735–1741, Aug. 2003.
- [44] G. P. Pollini, "Trends in Handover Design," *IEEE Commun. Mag.*, pp. 82–90, Mar. 1996.
- [45] N. D. Tripathi, J. H. Reed, and H. F. Vanlandingham, "Handoff in Cellular Systems," *IEEE Pers. Commun.*, pp. 26–37, Dec. 1998.
- [46] K. Pahlavan, P. Krishnamurthy, A. Hatami, M. Ylianttila, J. Makela, R. Pichna, and J. Vallström, "Handoff in Hybrid Mobile Data Networks," *IEEE Pers. Commun.*, pp. 34–47, Apr. 2000.
- [47] G. Liodakis and P. Stravroulakis, "A Novel Approach in Handover Initiation for Microcellular Systems," *Proc. IEEE VTC 94*, Stockholm, Sweden, 1994.
- [48] R. Rezaifar, A. M. Makowski, and S. Kumar, "Optimal Control of Handoffs in Wireless Networks," *Proc. IEEE VTC 95*, 1995, pp. 887–891.

- [49] N. Tripathi, "Generic Adaptive Handoff Algorithms using Fuzzy Logic and Neural Networks," Ph.D. Thesis, VA Polytechni, Inst. and State Univ., Aug. 1997.
- [50] J. Schiller, "Mobile Communications." Addison-Wesely, 2000.
- [51] D. Hong and S. S. Rappaport, "Traffic model and performance analysis for cellular mobile radio telephone system with prioritized and non-prioritized handoff procedure," *IEEE Trans. Veh. Technol.*, vol. 35, no. 3, pp. 77–92, 1986.
- [52] E. Del Re, R. Fantacci, and G. Giambene, "Handover and Dynamic Channel Allocation Techniques in Mobile Cellular Networks," *IEEE Trans. Veh. Technol.*, vol. 44, no. 2, pp. 229–237, May 1995.
- [53] R. Ramjee, R. Nagarajan and D. Towsley, "On Optimal Call Admission Control in Cellular Networks," in *Proc. IEEE Infocom 1996*, vol. 1, pp. 43–50, Mar. 1999.
- [54] X. Luo, I. Thng, and W. Zhuang, "A Dynamic Channel Pre-reservation Scheme for Handoffs with GoS Guarantee in Mobile Networks," in *Proc. IEEE Intern. Symposium on Computers and Communications*, pp. 404–408, 1999.
- [55] L. Ortigoza-Guerrero, and A. H. Aghvami, "A Prioritized Handoff Dynamic Channal Allocation Strategy for PCS," *IEEE Trans. Veh. Technol.*, vol. 48, no. 4, pp. 1203–1215, Jul. 1999.
- [56] C. Jedrzycki and V. C.M. Leung, "Probability Distribution of Channel Holding Time in Cellular Telephony Systems," in *Proc. IEEE Veh. Technol. Conf.*, Atlanta, GA, vol. 1, pp. 247–251, 1996.
- [57] F. Yu and V. C.M. Leung, "Mobility-Based Predictive Call Admission Control and Bandwidth Reservation in Wireless Cellular Networks," *Proc. IEEE INFOCOM 2001*, pp. 518–526, 2001.
- [58] S. Choi and K. G. Shin, "Adaptive Bandwidth Reservation and Admission Control in QoS-Sensitive Cellular Networks," *IEEE Trans. Parallel Distrib. Syst.*, vol. 13, no. 9, pp. 882–897, Sep. 2002.
- [59] IEEE Recommended Practice for Multi-Vendor Access Point Interoperability via an Inter-Access Point Protocol Across Distribution Systems Supporting IEEE 802.11 Operation. *IEEE Draft 802.11f/D5*, Jan. 2003.
- [60] H. Xu, V. Kukshya, and T. S. Rappaport, "Spatial and Temporal Characteristics of 60-GHz Indoor Channels," *IEEE J. Select. Areas Commun.*, vol. 20, no. 3, pp. 620–630, Apr. 2002.
- [61] N. Moraitis, and P. Constantinou, "Indoor Channel Measurements and Characterization at 60 GHz for Wireless Local Area Network Applications," *IEEE Trans. Antennas Propagat.*, vol. 52, no. 12, pp. 3180–3189, Dec. 2004.
- [62] T. Manabe, Y. Miura, and T. Ihara, "Effects of Antenna Directivity and Polarization on Indoor Multipath Propagation Characteristics at 60 GHz," *IEEE J. Select. Areas Commun.*, vol. 14, no. 3, pp. 441–448, Apr. 1996.

- [63] K. Sato, et.al, “Measurements of Reflection and Transmission Characteristics of Interior Structures of Office Building in the 60-GHz Band,” *IEEE Trans. Antennas Propagat.*, vol. 45, no. 12, pp. 1783–1792, Dec. 1997.
- [64] G. Wu, Y. Hase, and M. Inoue, “Broadband Radio Access Integrated Network (BRAIN) in MM-Wave Band: Wireless LAN Prototype,” *Proc. IEEE PIMRC 1998*, vol. 1, pp. 23–27, 1998.
- [65] M. Inoue, G. Wu, and Y. Hase, “IP-Based High-Speed Multimedia Wireless LAN Prototype for Broadband Radio Access Integrated Network (BRAIN),” *Proc. IEEE VTC*, vol. 1, pp. 357–361, 1999.
- [66] M. Inoue, G. Wu, Y. Hase, A. Sugitani, E. Kawakami, S. Shimizu, and K. Tokuda, “An IP-Over-Ethernet-Based Ultrahigh-Speed Wireless LAN Prototype Operating in the 60-GHz Band.” *IEICE Trans. Commun.*, vol. E83-B, no. 8, pp. 1720–1730, Aug. 2000.
- [67] G. Wu, M. Inoue, H. Murakami, and Y. Hase, “156 Mbps Ultrahigh-Speed Wireless LAN Prototypes in the 38 GHz Band,” *Proc. IEEE GLOBECOM 2001*, vol. 6, pp. 3573–3578, 2001.
- [68] D. J. Skellern, et. al, “A High-Speed Wireless LAN,” *IEEE Micro*, pp. 40–47, Jan. 1997.
- [69] G. Wu, F. Watanabe, M. Inoue, and Y. Hase, “RS-ISMA with multimedia Traffic in BRAIN,” *Proc. IEEE VTC 1998*, vol. 1, pp. 96–101, 1998.
- [70] W. Szpankowski, “Analysis and Stability Consideration in a Reservation Multiaccess System,” *IEEE Trans. Commun.*, vol. 31, no. 5, pp. 684–692, May 1983.
- [71] K. Thompson, G. J. Miller and R. Wilder, “Wide-Area Internet Traffic Patterns and Characteristics,” *IEEE Network*, pp. 10–23, Nov. 1997.
- [72] H. Harada, K. Sato and M. Fujise, “A Radio-on-Fiber Based Millimeter-Wave Road-Vehicle Communication System by a Code Division Multiplexing Radio Transmission Scheme,” *IEEE Trans. Intelligent Transport. Sys.*, vol. 2, no. 4, pp. 165–179, Dec. 2001.
- [73] H. Harada, K. Sato and M. Fujise, “A Radio-on-fiber Based Millimeter-wave Road-vehicle Communication System For Future Intelligent Transport System,” in *Proc. IEEE VTC 2001 Fall.*, vol. 4, pp. 2630–2634, Oct. 2001.
- [74] Y. Okamoto, R. Miyamoto and M. Yasunaga, “Radio-On-Fiber Access Network Systems for Road-Vehicle Communication,” in *Proc. 2001 IEEE Intelligent Transportation Sys. Conf.*, pp. 1050–1055, Aug. 2001.
- [75] K. Kitayama, K. Ikeda, T. Kuri, A. Stöhr, and Y. Takahashi, “Full-duplex demonstration of single electroabsorption transceiver basestation for mm-wave fiber-radio systems,” *Microwave Photon. MWP 2001*, pp. 73-76, 2001.

- [76] G. Grosskopf, D. Rohde, and R. Eggemann, "155 Mbit/s Data Transmission at 62 GHz Using an Optically Steered Antenna," *ECOC 2000*, Muenchen, Germany, vol. 3, pp. 53–54, Sep. 2000.
- [77] A. Stöhr, R. Heinzlmann, K. Kitayama, and D. Jäger, "EA-transceiver for full-duplex WDM ring networks," *URSI International Sympo. Signals, Systems, and Electron. (ISSSE'98, Pisa)*, TM3-3, pp. 384–387, Sep. 1998.
- [78] K. Abe, T. Tobana, T. Sasamori, and H. Kolzumi, "A Study on a Road-Vehicle-Communication System," *Proc. Parallel and Distributed Sys. International Conf. on*, pp. 343–348, July 2000.
- [79] A. Furuskär, S. Mazur, F. Müller, and H. Olofsson, "EDGE: Enhanced Data Rates for GSM and TDMA/136 Evolution," *IEEE Pers. Commun.*, pp. 56–66, June 1999.
- [80] E. Dahlman, G. Gudmundson, M. Nilsson, and J. Sköld, "UMTS/IMT-2000 Based on Wideband CDMA," *IEEE Commun. Mag.*, pp. 70–80, Sep. 1998.
- [81] M. Okita, H. Harada, and M. Fujise, "A New Access Protocol in Radio-on-Fiber Based Millimeter-Wave Road-Vehicle Communication Systems," in *Proc. IEEE VTC 2001 Fall.*, vol. 4, pp. 2178–2182, Oct. 2001.
- [82] J. Zhu, and S. Roy, "MAC for Dedicated Short Range Communications in Intelligent Communication System," *IEEE Commun. Mag.*, pp. 60–67, Dec. 2003.
- [83] IEEE 802.11p Draft – Wireless Access in Vehicular Environments (WAVE), 2004.
- [84] T. S. Rappaport, *Wireless Communications*. Upper Saddle River, NJ: Prentice-Hall, 1996, pp. 34.
- [85] H. B. Kim, "An Adaptive Bandwidth Reservation Scheme for Multimedia Mobile Cellular Networks," in *Proc. IEEE ICC 2005.*, May. 2005, Seoul, Korea.
- [86] W. Webb, "Broadband Fixed Wireless Access as a Key Component of the Future Integrated Communications Environment," *IEEE Commun. Mag.*, pp. 115–121, Sep. 2001.
- [87] M. Zhang and R. S. Wolff, "Crossing the Digital Divide: Cost-Effective Broadband Wireless Access for Rural and Remote Areas," *IEEE Commun. Mag.*, pp. 99–105, Feb. 2004.
- [88] S. M. Cherry, "The Wireless Last Mile," *IEEE Spectr.*, pp. 19–22, Sep. 2003.
- [89] Y. Su, J. E. Simsarian, and L. Zhang, "Improving the Switching Performance of a Wavelength-Tunable Laser Transmitting Using a Simple and Effective Driver Circuit," *IEEE Photon. Technol. Lett.*, vol. 16, no. 9, pp. 2132–2134, Sep. 2004.
- [90] J. S. Kaufman, "Blocking in a Shared Resource Environment," *IEEE Trans. Commun.*, vol. 29, no. 10, pp. 1474–1481, Oct. 1981.

- [91] J. P. Labourdette and G. W. Hart, "Blocking Probabilities in Multitrafic Loss Systems: Insensitivity, Asymptotic Behavior and Approximations," *IEEE Trans. Commun.*, vol. 40, no. 8, pp. 1355–1366, Aug. 1992.
- [92] E. Mutafungwa, S. J. Halme, K. Kazaura, T. Wakahara, and M. Matsumoto, "Strategies for resource provisioning in optical networks supporting broadband wireless access networks," *J. Optical Networking*, vol. 2, no. 3, pp. 55–68, March 2003.